

**INVESTIGATION OF THE
ATMOSPHERIC OZONE FORMATION
POTENTIAL OF SELECTED COMPOUNDS**

Report to the
Eastman Chemical Corporation

by

William P. L. Carter, Dongmin Luo, and Irina L. Malkina

August 30, 2000

College of Engineering
Center for Environmental Research and Technology
University of California
Riverside, California 92521

ABSTRACT

A series of environmental chamber experiments and computer model calculations were carried out to assess the atmospheric ozone formation potentials of isopropyl acetate, 2-pentanone, and 2-heptanone. The experiments consisted of determining the effects the compounds on NO oxidation, ozone formation and OH radical levels when added to varying simulated model photochemical smog systems, and also included ketone - NO_x - air irradiations. Isopropyl acetate was found to enhance O₃ formation under all conditions examined, while the effects of the ketones on ozone depended on conditions. Atmospheric reaction mechanisms for the compounds were developed based on product data for isopropyl acetate and 2-pentanone and on various estimation methods, and these were evaluated by simulating the chamber experiments. The mechanism for isopropyl acetate fit the chamber data with only minor adjustment of the estimated overall nitrate yield, and the mechanisms for the ketones fit the data after adjusting the overall quantum yield for photolysis to form radicals. The best fit overall quantum yields were 0.1 for 2-pentanone and 0.02 for 2-heptanone, which are consistent with data for other compounds in indicating a monotonic decrease with the size of the molecule. The mechanisms were used to predict the ozone impacts for these compounds under simulated atmospheric conditions. Isopropyl acetate was predicted to form about 1/3 to 1/2 as much ozone on a mass basis as the average of reactive VOC emissions from all sources, but about 3-4 times more ozone than ethane, the compound used by the EPA to define "negligible" ozone reactivity. The ketones were found to have comparable ozone impacts on a mass basis as the average reactive VOC emissions, with 2-heptanone being about 10% as reactive as 2-pentanone. The data obtained in this study were used in part in the development of estimation methods for the SAPRC-99 chemical mechanism.

ACKNOWLEDGEMENTS

The authors acknowledge Mr. Dennis Fitz for assistance in administering this program, and Mr. Kurt Bumiller with assistance in carrying out the environmental chamber experiments. Helpful discussions with Dr. Roger Atkinson are also acknowledged. We also thank Eastman Chemical Company for letting us use the data from this study for the SAPRC-99 mechanism documentation prior to the submission of this report.

Although this work was funded by Eastman Chemical Company, the opinions and conclusions expressed in this report are entirely those of the primary author, Dr. William P. L. Carter. Mention of trade names or commercial products do not constitute endorsement or recommendation for use.

TABLE OF CONTENTS

INTRODUCTION.....	1
EXPERIMENTAL AND DATA ANALYSIS METHODS.....	3
Overall Experimental Approach.....	3
Environmental Chambers.....	4
Experimental Procedures.....	5
Analytical Methods.....	6
Characterization Methods.....	7
Temperature.....	7
Xenon Arc Light Source.....	7
Blacklight Light Source.....	8
Dilution.....	8
Reactivity Data Analysis Methods.....	8
CHEMICAL MECHANISMS AND MODELING METHODS.....	11
Chemical Mechanism.....	11
General Atmospheric Photooxidation Mechanism.....	11
Atmospheric Reactions of Isopropyl Acetate.....	11
Atmospheric Reactions of 2-Pentanone.....	15
Atmospheric Reactions of 2-Heptanone.....	20
Modeling Methods.....	25
Environmental Chamber Simulations.....	25
Atmospheric Reactivity Simulations.....	26
EXPERIMENTAL RESULTS AND MECHANISM EVALUATION.....	27
Summary of Experiments and Characterization Results.....	27
Isopropyl Acetate Experiments.....	27
2-Pentanone Experiments.....	32
2-Heptanone Experiments.....	35
ATMOSPHERIC REACTIVITY CALCULATIONS.....	39
Scenarios Used for Reactivity Assessment.....	39
Base Case Scenarios.....	40
Adjusted NO _x scenarios.....	42
NO _x Conditions in the Base Case Scenarios.....	42
Quantification of Atmospheric Reactivity.....	43
Results.....	44
CONCLUSIONS.....	48
REFERENCES.....	50
APPENDIX A. MECHANISM LISTING AND TABULATIONS.....	54

LIST OF TABLES

Table 1.	Detailed mechanism for the atmospheric reactions of isopropyl acetate in the presence of NO _x , showing the estimated and adjusted branching ratios. Products observed by Tuazon et al (1998) are shown in bold font.....	13
Table 2.	Measured and predicted product yields for the reactions of OH radicals with 2-pentanone.....	16
Table 3.	Detailed mechanism for the atmospheric reactions of 2-pentanone with OH radicals in the presence of NO _x , as produced by the SAPRC-99 mechanism generation system. Products observed by Atkinson et al (2000) are shown in bold font.	17
Table 4.	Measured and predicted product yields for the reactions of OH radicals with 2-heptanone.....	21
Table 5.	Detailed mechanism for the atmospheric reactions of 2-heptanone with OH radicals in the presence of NO _x , as produced by the SAPRC-99 mechanism generation system.	22
Table 6.	Chronological listing of the environmental chamber experiments carried out for this program.	28
Table 7	Summary of conditions and selected results of the environmental chamber experiments.....	31
Table 8.	Summary of the conditions of the scenarios used for atmospheric reactivity assessment.....	41
Table 9.	Atmospheric incremental calculated for the base ROG mixture, ethane, isopropyl acetate, 2-pentanone and 2-heptanone.....	45
Table 10.	Atmospheric relative calculated for the base ROG mixture, ethane, isopropyl acetate, 2-pentanone and 2-heptanone.....	46
Table A-1.	Listing of the model species in the mechanism used in the model simulations discussed in this report.....	55
Table A-2.	Listing of the reactions in the mechanism used in the model simulations discussed in this report. See Carter (2000) for documentation.	58
Table A-3.	Listing of the absorption cross sections and quantum yields for the photolysis reactions.....	68
Table A-4.	Chamber wall effect and background characterization parameters used in the environmental chamber model simulations for mechanism evaluation.....	77

LIST OF FIGURES

Figure 1.	Selected experimental and calculated results of the incremental reactivity experiments with isopropyl acetate.....	32
Figure 2.	Experimental and calculated results of selected species in the 2-pentanone - NO _x experiment.	33
Figure 3.	Selected experimental and calculated results of the incremental reactivity experiments with 2-pentanone. (Only the best fit model is shown for formaldehyde and acetaldehyde.)	34
Figure 4.	Experimental and calculated results of selected species in the 2-heptanone - NO _x experiment.	35
Figure 5.	Selected experimental and calculated results of the incremental reactivity experiments with 2-heptanone. (Only the best fit model is shown for formaldehyde and acetaldehyde.)	36

INTRODUCTION

Ozone in photochemical smog is formed from the gas-phase reactions of volatile organic compounds (VOCs) and oxides of nitrogen (NO_x) in sunlight. Although Houston and Los Angeles currently have the worst ozone problems in the United States, other areas of the country also have episodes where ozone exceeds the federal air quality standard. Ozone control strategies in the past have focused primarily on VOC controls, though the importance of NO_x control has become recognized in recent years. VOC and NO_x controls have differing effects on ozone formation. NO_x is required for ozone formation, and if the levels of NO_x are low compared to the levels of reactive VOCs, then changing VOC emissions will have relatively little effect on ozone. Since NO_x is removed from the atmosphere more rapidly than VOCs, ozone in areas far downwind from the primary sources tend to be more NO_x limited, and thus less responsive to VOC controls. VOC controls tend to reduce the rate that O_3 is formed when NO_x is present, so VOC controls are the most beneficial in reducing O_3 in the urban source areas, where NO_x is relatively plentiful, and where O_3 yields are determined primarily by how rapidly it is being formed. Because of this, any comprehensive ozone control strategy should involve reduction of emissions of both NO_x and VOCs.

Many different types of VOC compounds are emitted into the atmosphere, each reacting at different rates and having different mechanisms for their reactions. Because of this, they can differ significantly in their effects on ozone formation, or their “reactivity”. Some compounds, such as CFCs, do not react in the lower atmosphere at all, and thus make no contribution to ground-level ozone formation. Others, such as methane, react and contribute to ozone formation, but react so slowly that their practical effect on ozone formation in urban atmospheres is negligible. Obviously, it does not make sense to regulate such compounds as ozone precursors. In recognition of this, the EPA has exempted certain compounds from such regulations on the basis of having “negligible” effects on ozone formation. Although the EPA has no formal policy on what constitutes “negligible” reactivity, in practice it has used the ozone formation potential of ethane as the standard in this regard. This is because ethane is the most reactive of the compounds that the EPA has exempted to date. Therefore, the ozone formation potential of a compound relative to ethane is of particular interest when assessing whether it might be a likely candidate for exemption from regulation as an ozone precursor.

Many VOCs that would not be judged to have “negligible” reactivity under the current criterion might still have much lower ozone formation potential than average, and substituting emissions of highly reactive VOCs with such moderate-to-low reactivity VOCs would be expected to result in air quality improvements. Although the current EPA policies do not encourage such substitutions, it has been proposed to implement reactivity-based policies on a voluntary basis in consumer product regulations in California (CARB, 1999), and the EPA is currently re-evaluating its reactivity-based VOC policies (Dimitriadis, 1999, RRWG, 1999). Mc.Bride et al (1977) showed that adopting reactivity-based VOC control policies could result in significant cost savings in ozone reduction strategies, though a number of

difficult policy and enforcement issues need to be resolved (RRWG, 1999). Although regulatory approaches that appropriately deal with differences in VOC reactivity are still evolving, it is clear that producers of solvent VOCs will need to know how their VOCs might be classified under any such system, so they can appropriately adapt to reactivity-based policies once they are implemented. This requires an ability to reliably estimate the ozone impacts of the VOCs of interest.

To address the need to better understand the ozone impacts of isopropyl acetate, 2-pentanone and 2-heptanone, Eastman Chemical Company contracted the College of Engineering Center for Environmental Research and Technology (CE-CERT) to carry out an experimental and modeling study of the ozone impacts of those compounds. This involves (1) conducting environmental chamber experiments to determine the effects of the subject compounds on O₃ formation and other measures of air quality under various conditions; (2) developing chemical mechanisms for the relevant atmospheric reactions of these compounds and evaluating the predictions of these mechanisms against the environmental chamber data; (3) adjusting or modifying uncertain portions of the mechanism if needed for the predictions of the mechanism to be consistent with the chamber data; and (4) conducting model simulations of the effects of adding the compounds to emissions in various urban atmospheres to determine their ozone impacts. The mechanistic implications of data obtained in this program were also used in the development of general estimation methods for atmospheric reactions of related compounds that were implemented in the SAPRC-99 chemical mechanism of Carter (2000). The results of this program are documented in this report.

EXPERIMENTAL AND DATA ANALYSIS METHODS

Overall Experimental Approach

Most of the environmental chamber experiments for this program consisted of measurements of “incremental reactivities” of the subject VOCs under various conditions. These involve two types of irradiations of model photochemical smog mixtures. The first is a “base case” experiment where a mixture of reactive organic gases (ROGs) representing those present in polluted atmospheres (the “ROG surrogate”) is irradiated in the presence of oxides of nitrogen (NO_x) in air. The second is the “test” experiment which consists of repeating the base case irradiation except that the VOC whose reactivity is being assessed is added. The differences between the results of these experiments provide a measure of the atmospheric impact of the test compound, and the difference relative to the amount added is a measure of its reactivity.

To provide data concerning the reactivities of the test compound under varying atmospheric conditions, three types of base case experiments were carried out:

Mini-Surrogate Experiments. This base case employed a simplified ROG surrogate and relatively low ROG/NO_x ratios. Low ROG/NO_x ratios represent “maximum incremental reactivity” (MIR) conditions, which are most sensitive to VOC effects. This is useful because it provides a sensitive test for the model, and also because it is most important that the model correctly predict a VOC's reactivity under conditions where the atmosphere is most sensitive to the VOCs. The ROG mini-surrogate mixture employed consisted of ethene, n-hexane, and m-xylene. This surrogate was employed in our previous studies (Carter et al, 1993; 1995a-c, 1997, 2000), and was found to provide a more sensitive test of the mechanism than the more complex surrogates which more closely represent atmospheric conditions (Carter et al, 1995b). This high sensitivity to mechanistic differences makes the mini-surrogate experiments most useful for mechanism evaluation.

Full Surrogate Experiments. This base case employed a more complex ROG surrogate under somewhat higher, though still relatively low, ROG/NO_x conditions. While less sensitive to the mechanism employed, experiments with a more representative ROG surrogate are needed to evaluate the mechanism under conditions that more closely resembling the atmosphere. The ROG surrogate employed was the same as the 8-component “lumped molecule” surrogate as employed in our previous study (Carter et al. 1995b), and consists of n-butane, n-octane, ethene, propene, trans-2-butene, toluene, m-xylene, and formaldehyde. Calculations have indicated that use of this 8-component mixture will give essentially the same results in incremental reactivity experiments as actual ambient mixtures (Carter et al. 1995b).

Full Surrogate, low NO_x Experiments. This base case employing the same 8-component “lumped molecule” surrogate as the full surrogate experiments described above, except that lower NO_x levels (higher ROG/NO_x ratios) were employed to represent NO_x -limited conditions. Such experiments are necessary to

assess the ability of the model to properly simulate reactivities under conditions where NO_x is low. The initial ROG and NO_x reactant concentrations were comparable to those employed in our previous studies (Carter et al. 1995b, 1997, 2000).

For the ketones that were studied for this program, several ketone – NO_x – air experiments were also carried out. Such experiments provide a means to test mechanisms for VOCs with internal radical sources without the complications and uncertainties involved with modeling the reactions of the base ROG surrogate components. These experiments are not useful for evaluating mechanism of VOCs, such as isopropyl acetate, that do not have significant radical sources in their mechanisms or tend to act as radical inhibitors (Carter and Lurmann, 1991).

An appropriate set of control and characterization experiments necessary for assuring data quality and characterizing the conditions of the runs for mechanism evaluation were also carried out. These are discussed where relevant in the results or modeling methods sections (see also Carter et al, 1995c, 2000).

Environmental Chambers

Two environmental chambers were employed in this program, which differed primarily in the type of light source employed. The experiments with isopropyl acetate were carried out using the CE-CERT “Dividable Teflon Chamber” (DTC) with a blacklight light source. This consists of two ~6000-liter 2-mil heat-sealed FEP Teflon reaction bags located adjacent to each other and fitted inside an 8' x 8' x 8' framework, and which uses two diametrically opposed banks of 32 Sylvania 40-W BL black lights as the light source. The lighting system in the DTC was found to provide so much intensity that only half the lights were used for irradiation. The air conditioner for the chamber room was turned on before and during the experiments. Four air blowers that are located in the bottom of the chamber were used to help cool the chamber as well as mix the contents of the chamber. The CE-CERT DTC is very similar to the SAPRC DTC which is described in detail elsewhere (Carter et al, 1995b,c).

The blacklight light source has the advantage of being relatively inexpensive to operate and provides a reasonably good simulation of natural sunlight in the region of the spectrum that is important in affecting most photolysis reactions of importance for non-aromatic VOCs (Carter et al, 1995c,d). This is therefore appropriate for studies of reactivities of compounds, such as isopropyl acetate, which are not photoreactive or believed to form significant yields of photoreactive products whose action spectra are not well characterized. However, for photoreactive compounds such as the ketones studied in this program, it is better to use a chamber with a light source such as xenon arcs, which give a better simulation of sunlight throughout the full spectral range. Therefore, the CE-CERT xenon arc Teflon Chamber (CTC) was used in the experiments to study the reactivities of 2-pentanone and 2-heptanone.

The CE-CERT CTC consists of two ~3500 –liter 4' x 4' x 8' FEP Teflon reaction bags located adjacent to each other at one end of an 8' x 12' room with reflective aluminum paneling on all surfaces. Four 6.5 KW xenon arc lights were mounted on the wall opposite the reaction bags, all in a room with

walls and ceiling covered with reflective aluminum paneling to maximize light intensity and homogeneity. As discussed elsewhere (Carter et al. 1995d), this light source gives the closest approximation available of the ground-level solar spectrum for an indoor chamber. The room with the chamber has a sufficiently powerful air conditioning system to remove the heat input caused by the lights to maintain an approximately constant ambient temperature of $\sim 25^{\circ}\text{C}$. A movable panel is used to block the lights when they are first turned on and warming up, which is raised to begin the irradiation. The chamber was very similar to the Statewide Air Pollution Research Center's Xenon arc Teflon Chamber (SAPRC XTC) which is described in detail elsewhere (Carter et al. 1995c,d).

Both the DTC and CTC are designed to allow simultaneous irradiations of experiments with and without added test reactants under the same reaction conditions. Since the chambers are actually two adjacent FEP Teflon reaction bags, two mixtures can be simultaneously irradiated using the same light source and with the same temperature control system. These two reaction bags are referred to as the two "sides" of the chambers (Side A and Side B) in the subsequent discussion. The sides are interconnected with two ports, each with a box fan, which rapidly exchange their contents to assure that base case reactants have equal concentrations in both sides. In addition, a fan is located in each of the reaction bags to rapidly mix the reactants within each chamber. The ports connecting the two reactors can then be closed to allow separate injections on each side, and separate monitoring of each side.

Experimental Procedures

The reaction bags were flushed with dry air produced by an AADCO air purification system for 14 hours (6pm-8am) on the nights before experiments. The continuous monitors were connected prior to reactant injection and the data system began logging data from the continuous monitoring systems. The reactants were injected as described below (see also Carter et al, 1993, 1995c). The common reactants were injected in both sides simultaneously using a three-way (one inlet and two outlets connected to side A and B respectively) bulb of 2 liters in the injection line and were well mixed before the chamber was divided. The contents of each side were blown into the other using two box fans located between them. Mixing fans were used to mix the reactants in the chamber during the injection period, but these were turned off prior to the irradiation. The sides were then separated by closing the ports that connected them, after turning all the fans off to allow their pressures to equalize. After that, reactants for specific sides (the test compound in the case of reactivity experiments) were injected and mixed. In case of CTC chamber the lights are turned on after lowering a metal baffle between the lights and the reactors, and the lights are allowed to warm up for at least 30 minutes. Irradiation in the chamber is begun by raising the baffle between the lights and the reactors, and the irradiation proceeds for 6 hours. After the run, the contents of the chamber were emptied by allowing the bags to collapse, and then the chamber was flushed with purified air. The contents of the reactors were vented into a fume hood.

The procedures for injecting the various types of reactants were as follows. The NO and NO₂ were prepared for injection using a high vacuum rack. Known pressures of NO, measured with MKS Baratron capacitance manometers, were expanded into Pyrex bulbs with known volumes, which were

then filled with nitrogen (for NO) or oxygen (for NO₂). The contents of the bulbs were then flushed into the chamber with nitrogen. The gaseous reactants were prepared for injection either using a high vacuum rack or a gas-tight syringes whose amounts were calculated to achieve the desired concentrations in the chamber. Sufficiently volatile liquid reactants (which included all the test compounds and liquid surrogate components used in this study) were injected using a micro syringe into a 1-liter Pyrex bulb equipped with stopcocks on each end and a port for the injection of the liquid. Then one end of the bulb was attached to the injection port of the chamber and the other to a nitrogen source. The stopcocks were then opened, and the contents of the bulb were flushed into the chamber with a combination of nitrogen and heat gun for approximately 5 minutes. Formaldehyde was prepared in a vacuum rack system by heating paraformaldehyde in an evacuated bulb until the pressure corresponded to the desired amount of formaldehyde. The bulb was then closed and detached from the vacuum system and its contents were flushed into the chamber with dry air through the injection port.

Analytical Methods

Ozone and nitrogen oxides (NO_x) were continuously monitored using commercially available continuous analyzers with Teflon sample lines inserted directly into the chambers. The sampling lines from each side of the chamber were connected to solenoids that switched from side to side every 10 minutes, so the instruments alternately collected data from each side. Ozone was monitored using a Dasibi 1003-AH UV photometric ozone analyzer and NO and total oxides of nitrogen (including organic nitrates and perhaps HNO₃) were monitored using a Teco Model 42 chemiluminescent NO/NO_x monitor. The output of these instruments, along with that from the temperature sensors and the formaldehyde instrument, were attached to a computer data acquisition system, which recorded the data at 10 minutes intervals for ozone, NO_x and temperature (and at 15 minutes for formaldehyde), using 30 second averaging times. This yielded a sampling interval of 20 minutes for taking data from each side.

The Teco instrument and Dasibi CO analyzer were calibrated prior to each experiment using a certified NO and CO source and CSI gas-phase dilution system. The Dasibi ozone analyzer was calibrated against transfer standard ozone analyzer using transfer standard method in a interval of three months and was check with CSI ozone generator for each experiment to assure that the instrument worked properly. The details were discussed elsewhere (Carter et al, 1995c)

Organic reactants other than formaldehyde were measured by gas chromatography with FID detection as described elsewhere (Carter et al. 1993; 1995c). GC samples were taken for analysis at intervals from 20 minutes to 30 minutes either using 100 ml gas-tight glass syringes or by collecting the 100 ml sample from the chamber onto Tenax-GC solid adsorbent cartridge. These samples were taken from ports directly connected to the chamber after injection and before irradiation and at regular intervals after irradiation was started. The sampling method employed for injecting the sample onto the GC column depended on the volatility or “stickiness” of the compound. For analysis of the more volatile species, which includes all the organic compounds monitored in this study, the contents of the syringe were

flushed through a 10 ml and 5 ml stainless steel or 1/8' Teflon tube loop and subsequently injected onto the column by turning a gas sample valve.

The calibrations for the GC analyses for most compounds were carried out by sampling from chambers or vessels of known volume into which known amounts of the reactants were injected, as described previously (Carter et al, 1995c).

Formaldehyde was monitored using an adaptation of the diffusion scrubber method developed by Dasgupta et al (1988, 1990), as described by Carter et al (1995c). It was calibrated using a formaldehyde diffusion tube whose weight loss was monitored over time. The system cycled between zero, calibrate, and sample modes to correct for zero and span drifts.

Characterization Methods

Temperature

Three temperature thermocouples were used to monitor the chamber temperature, two of which were located in the sampling line of continuous analyzers to monitor the temperature in each side. The third one was located in the outlet of the air conditioning system used to control the chamber temperature. The temperature range in these experiments was typically 25-30 C.

Xenon Arc Light Source

The spectrum of the xenon arc light source was measured several (usually five) times during each CTC experiment using a LiCor LI-1800 spectroradiometer. The absolute light intensity in this chamber was measured by “photostationary state” NO₂ actinometry experiments and by Cl₂ actinometry, which in both cases were carried out prior to the period of the experiments discussed in this report. The photostationary state experiments consisted of simultaneous measurements of photostationary state concentrations of NO, NO₂, and O₃ in otherwise pure air, with the NO₂ photolysis rate being calculated from the [NO][O₃]/[NO₂] ratio (Carter et al. 1997). The Cl₂ actinometry experiments consisted of photolyzing ~0.1 ppm of Cl₂ in ~1 ppm of n-butane, calculating the Cl₂ photolysis rate from the rate of consumption of n-butane, and then calculating the corresponding NO₂ photolysis rate from the absorption cross sections and quantum yields for NO₂ and Cl₂ (assuming unit quantum yields for Cl₂) and the spectral distribution of the light source (Carter et al, 1997).

Relative trends in light intensity with time are obtained using the quartz tube method of Zafonte et al. (1977), modified as discussed by Carter et al. (1995c; 1997). The results of these experiments were analyzed to determine the NO₂ photolysis rates for modeling as discussed by Carter et al (2000). The NO₂ photolysis rate used for modeling these experiments was 0.136 min⁻¹ for the first run in the series (CTC255), and declined to 0.133 min⁻¹ for the last run in the series (CTC263).

Blacklight Light Source

The light intensity in the DTC chamber was monitored by periodic NO₂ actinometry experiments utilizing the quartz tube method of Zafonte et al (1977), with the data analysis method modified as discussed by Carter et al. (1995c). The results of these experiments were tracked over time, and there was a gradual decrease in light intensity over time during most of the operational lifetime of this chamber. The actinometry results around the time of these experiments were fit reasonably well by a straight line, which was used to determine the NO₂ photolysis rates used for modeling. These were 0.165 min⁻¹ for the first DTC run for this project (DTC688) and 0.162 min⁻¹ for the last such run.

The spectrum of the blacklight light source is periodically measured using a LiCor LI-1200 spectroradiometer, and found to be essentially the same as the general blacklight spectrum recommended by Carter et al (1995c) for use in modeling blacklight chamber experiments

Dilution

The dilution of the chambers due to sampling is expected to be small because the flexible reaction bags can collapse as samples are withdrawn for analysis. Also, the chambers were designed to operate under slightly positive pressure, so any small leaks would result in reducing the bag volume rather than diluting the contents of the chamber. Information concerning dilution in an experiment can be obtained from relative rates of decay of added VOCs which react with OH radicals with differing rate constants (Carter et al. 1993; 1995c). Most experiments had a more reactive compounds such as m-xylene and n-octane present either as a reactant or added in trace amounts to monitor OH radical levels. Trace amounts (~0.1 ppm) of n-butane were also added to experiments if needed to provide a less reactive compound for monitoring dilution. In addition, specific dilution check experiments such as CO irradiations were carried out. Based on these results, the dilution rate was found to be negligible in this chamber during this period, being less than 0.3% per hour in all runs, and usually less than 0.1% per hour.

Reactivity Data Analysis Methods

As indicated above, most of the experiments for this program consisted of simultaneous irradiation of a “base case” reactive organic gas (ROG) surrogate - NO_x mixture in one of the dual reaction chambers, together with an irradiation, in the other reactor, of the same mixture with added. The results are analyzed to yield two measures of VOC reactivity: the effect of the added VOC on the amount of NO reacted plus the amount of ozone formed, and integrated OH radical levels. These are discussed in more detail below.

The first measure of reactivity is the effect of the VOC on the change in the quantity [O₃]-[NO], or Δ([O₃]-[NO]). As discussed elsewhere (e.g., Johnson, 1983; Carter and Atkinson, 1987; Carter and Lurmann, 1990, 1991, Carter et al, 1993, 1995a), this gives a direct measure of the amount of conversion of NO to NO₂ by peroxy radicals formed in the photooxidation reactions, which is the process that is directly responsible for ozone formation in the atmosphere. (Johnson calls it “smog produced” or “SP”.)

The incremental reactivity of the VOC relative to this quantity, which is calculated for each hour of the experiment, is given by

$$\text{IR}[\Delta([\text{O}_3]-[\text{NO}])_t^{\text{VOC}}] = \frac{\Delta([\text{O}_3]-[\text{NO}])_t^{\text{Test}} - \Delta([\text{O}_3]-[\text{NO}])_t^{\text{Base}}}{[\text{VOC}]_0} \quad (\text{I})$$

where $\Delta([\text{O}_3]-[\text{NO}])_t^{\text{Test}}$ is the $\Delta([\text{O}_3]-[\text{NO}])$ measured at time t from the experiment where the test VOC was added, $\Delta([\text{O}_3]-[\text{NO}])_t^{\text{Base}}$ is the corresponding value from the corresponding base case run, and $[\text{VOC}]_0$ is the amount of test VOC added. An estimated uncertainty for $\text{IR}[\Delta([\text{O}_3]-[\text{NO}])]$ is derived based on assuming an ~3% uncertainty or imprecision in the measured $\Delta([\text{O}_3]-[\text{NO}])$ values. This is consistent with the results of the side equivalency test, where equivalent base case mixtures are irradiated on each side of the chamber.

Note that reactivity relative to $\Delta([\text{O}_3]-[\text{NO}])$ is essentially the same as reactivity relative to O_3 in experiments where O_3 levels are high, because under such conditions $[\text{NO}]_t^{\text{base}} \cdot [\text{NO}]_t^{\text{test}} \cdot 0$, so a change in $\Delta([\text{O}_3]-[\text{NO}])$ caused by the test compound is due to the change in O_3 alone. However, $\Delta([\text{O}_3]-[\text{NO}])$ reactivity has the advantage that it provides a useful measure of the effect of the VOC on processes responsible for O_3 formation even in experiments where O_3 formation is suppressed by relatively high NO levels.

The second measure of reactivity is the effect of the VOC on integrated hydroxyl (OH) radical concentrations in the experiment, which is abbreviated as “IntOH” in the subsequent discussion. This is an important factor affecting reactivity because radical levels affect how rapidly all VOCs present, including the base ROG components, react to form ozone. If a compound is present in the experiment which reacts primarily with OH radicals, then the IntOH at time t can be estimated from

$$\text{IntOH}_t = \frac{\ln([\text{tracer}]_0/[\text{tracer}]_t) - Dt}{k\text{OH}^{\text{tracer}}} \quad (\text{II})$$

where $[\text{tracer}]_0$ and $[\text{tracer}]_t$ are the initial and time= t concentrations of the tracer compound, $k\text{OH}^{\text{tracer}}$ its OH rate constant, and D is the dilution rate in the experiments. The latter was found to be small and was neglected in our analysis. The concentration of tracer at each hourly interval was determined by linear interpolation of the experimentally measured values. M-xylene was used as the OH tracer in these experiments because it is a surrogate component present in all experiments, its OH rate constant is known (the value used was $2.36 \times 10^{-11} \text{ cm}^3 \text{ molec}^{-1} \text{ s}^{-1}$ [Atkinson, 1989]), and it reacts relatively rapidly.

The effect of the VOC on OH radicals can thus be measured by its IntOH incremental reactivity, which is defined as

$$\text{IR}[\text{IntOH}]_t = \frac{\text{IntOH}_t^{\text{Test}} - \text{IntOH}_t^{\text{Base}}}{[\text{VOC}]_0} \quad (\text{III})$$

where $\text{IntOH}^{\text{Test}}$ and $\text{IntOH}^{\text{Base}}$ are the IntOH values measured at time t in the added VOC and the base case experiment, respectively. The results are reported in units of 10^6 min. The uncertainties in IntOH and $\text{IR}[\text{IntOH}]$ are estimated based on assuming an ~2% imprecision in the measurements of the m-xylene concentrations. This is consistent with the observed precision of results of replicate analyses of this compound.

CHEMICAL MECHANISMS AND MODELING METHODS

Chemical Mechanism

General Atmospheric Photooxidation Mechanism

The chemical mechanism used in the environmental chamber and atmospheric model simulations in this study is the “SAPRC-99” mechanism, which is documented in detail by Carter (2000). This mechanism represents a complete update of the SAPRC-90 mechanism of Carter (1990), and incorporates recent reactivity data from a wide variety of VOCs, including those discussed in this report. This includes assignments for ~400 types of VOCs, and can be used to estimate reactivities for ~550 VOC categories. A condensed version, developed for use in regional models, is used to represent base case emissions in the atmospheric reactivity simulations discussed in this report. A unique feature of this mechanism is the use of a computerized system to estimate and generate complete reaction schemes for most non-aromatic hydrocarbons and oxygenates in the presence of NO_x, from which condensed mechanisms for the model can be derived. This includes the mechanisms for the VOCs discussed in this report and (in the case of 2-heptanone) some of their major reactive products. The SAPRC-99 mechanism was evaluated against the results of almost 1700 environmental chamber experiments carried out at the University of California at Riverside, including experiments to test ozone reactivity predictions for over 80 types of VOCs. This also includes experiments discussed in this report.

A listing of the mechanism as used in the model simulations in this report is given in Appendix A. This consists of the “base mechanism” representing the reactions of the inorganics and common organic products, the reactions of the specific VOCs used in the environmental chamber experiments (including the three test compounds whose mechanisms are discussed in the following sections), and the reactions of the lumped model species used when representing base case VOCs in the ambient reactivity simulations. The mechanisms used for isopropyl acetate, 2-pentanone and 2-heptanone are discussed in more detail below, and the report of Carter (2000) can be consulted for a more detailed discussion of the other portions of the mechanism. Note that, as discussed by Carter (2000) and also below, the data obtained in this study was used in part as the basis for deriving general estimation methods for the photolysis rates for the higher ketones used in the SAPRC-99 mechanism.

Atmospheric Reactions of Isopropyl Acetate

Isopropyl acetate is expected to react in the atmosphere primarily with OH radicals. The two reported measured values of this rate constant are $3.08 \pm 0.84 \times 10^{-12} \text{ cm}^3 \text{ molec}^{-1} \text{ s}^{-1}$ at 303K (Kerr and Stocker, 1994) and $3.72 \pm 0.29 \times 10^{-12} \text{ cm}^3 \text{ molec}^{-1} \text{ s}^{-1}$ at 298K (Wallington et al, 1988). Based on this, Atkinson (1989) recommends

$$k(\text{OH} + \text{isopropyl acetate}) = 3.4 \times 10^{-12} \text{ cm}^3 \text{ molec}^{-1} \text{ s}^{-1} \text{ at } 298\text{K},$$

which is the value incorporated in the mechanism used in this work. This is in good agreement with the rate constant estimated using the structure-reactivity methods of Kwok and Atkinson (1995) as incorporated in the SAPRC-99 mechanism, which is $3.48 \times 10^{-12} \text{ cm}^3 \text{ molec}^{-1} \text{ s}^{-1}$. The temperature dependence of this reaction is unknown and is neglected in the present mechanism.

The products in the reaction of OH radicals with isopropyl acetate were measured by Tuazon et al (1998), who reported $76 \pm 7\%$ yields for acetic anhydride, $24 \pm 2\%$ yields for acetone, and $9 \pm 3\%$ yields for acetic acid. These products can be accounted for by the expected mechanism for the reactions of OH with isopropyl acetate, which are shown on Table 1, which gives the mechanism as predicted by the SAPRC-99 mechanism generation system. (Reactions that are estimated to occur 1% or of the time or less are not shown.) The estimated branching ratios for the various reactions are also shown, and footnotes to the table indicate the estimation methods used, and those that were derived in part based on product data for this compound. The estimated mechanism predicts that acetic anhydride, acetone, and acetic acid would be formed in yields of 56%, 17% and 5%, respectively. These are uniformly lower than the yields measured by Tuazon et al (1998), but are well within the uncertainty of the estimation methods. In addition, at least some of the yields reported by Tuazon et al (1998) must be high, since together they account for 109% of the total reaction, and some alkyl nitrate formation from reactions of the peroxy radicals with NO must also be occurring. Note, however, that as indicated in the footnotes some of the parameters used in the estimates for these alkoxy radicals are based in part on considerations of these product data, as well as data for other compounds.

Table 1 also shows the branching ratios for the reactions and the overall process if they are adjusted to give better agreements to the product data of Tuazon et al (1998). These adjustments were based on the assumption that the products observed by Tuazon et al (1998) account for all of the reaction routes other than nitrate formation, and that competing reaction routes forming other products are less important than estimated. In particular, the reaction of the $\text{CH}_3\text{CH}(\text{CH}_2\text{O}\cdot)\text{OC}(\text{O})\text{CH}_3$ radical with O_2 forming $\text{CH}_3\text{-CH}(\text{CHO})\text{OC}(\text{O})\text{CH}_3$, which competes with formation of acetic acid, and the isomerization of the $\text{CH}_3\text{C}(\text{O}\cdot)(\text{CH}_3)\text{OC}(\text{O})\text{CH}_3$ radical, which competes with the reactions forming acetone and acetic anhydride, are assumed not to be important. Since these are already estimated not to be dominant processes, this is probably not outside the overall uncertainty of the estimation method. This adjusted mechanisms predicts acetic anhydride, acetone, and acetic acid would be formed in yields of 63%, 20% and 8%, respectively. These are only 10-20% lower than the yields reported by Tuazon et al (1998), which is considered to be good agreement as indicated above these yields must be high by at least 10%.

As indicated on Table 1, the peroxy radicals in the mechanism can react either with NO to form NO_2 and the alkoxy radicals that react to form the observed oxygenated products, or they can add NO to form an organic nitrate. The relative importances of the nitrate formation reactions (the “nitrate yields”) are unknown, and have to be estimated or adjusted to optimize fits of model simulations to environmental chamber data. Model simulations environmental chamber experiments for many compounds are sensitive to these nitrate yields (Carter, 1995, 2000), so optimizations to fit chamber data is often a sensitive method to derive these parameters, though possible compensating errors due to other uncertainties in the

Table 1. Detailed mechanism for the atmospheric reactions of isopropyl acetate in the presence of NO_x, showing the estimated and adjusted branching ratios. Products observed by Tuazon et al (1998) are shown in bold font.

Reactions [a]	Note [b]	Branching [c]			
		Reaction		Total	
		Est.	Adj.	Est.	Adj.
CH ₃ CH(CH ₃)OC(O)CH ₃	1				
1 + OH → H ₂ O + CH ₃ CH(CH ₂ ·)OC(O)CH ₃	2	10%		10%	
2 + OH → H ₂ O + CH ₃ C(·)(CH ₃)OC(O)CH ₃	2	89%		89%	
3 + OH → H ₂ O + CH ₃ CH(CH ₃)OC(O)CH ₂ ·	2	1%		1%	
<u>Reactions of radical formed in Reaction (1).</u>					
4 CH ₃ CH(CH ₂ ·)OC(O)CH ₃ + O ₂ → CH ₃ CH(CH ₂ OO·)OC(O)CH ₃				10%	
6 CH ₃ CH(CH ₂ OO·)OC(O)CH ₃					
+ NO → NO ₂ + CH ₃ CH(CH ₂ O·)OC(O)CH ₃	3	6%	5%	9%	9%
+ NO → CH ₃ CH(CH ₂ ONO ₂)OC(O)CH ₃		94%	95%	<1%	<1%
7 CH ₃ CH(CH ₂ O·)OC(O)CH ₃					
+ O ₂ → CH ₃ CH(CHO)OC(O)CH ₃ + HO ₂ ·	4	37%	0%	3%	0%
8 → HCHO + CH ₃ C(O)OCH(·)CH ₃	5	63%	100%	6%	9%
9 CH ₃ C(O)OCH(·)CH ₃ + O ₂ → CH ₃ C(O)OCH(OO·)CH ₃				6%	9%
10 CH ₃ C(O)OCH(OO·)CH ₃					
+ NO → CH ₃ C(O)OCH(ONO ₂)CH ₃	6	4%		<1%	<1%
11 + NO → NO ₂ + CH ₃ C(O)OCH(O·)CH ₃		96%		6%	9%
12 CH ₃ C(O)OCH(O·)CH ₃ → CH₃C(O)OH + CH ₃ C(O)·	7			5%	8%
13 CH ₃ C(O)· + O ₂ → CH ₃ C(O)OO·				5%	8%
<u>Reactions of radical formed in Reaction (2).</u>					
14 CH ₃ C(·)(CH ₃)OC(O)CH ₃ + O ₂ → CH ₃ C(OO·)(CH ₃)OC(O)CH ₃				89%	
15 CH ₃ C(OO·)(CH ₃)OC(O)CH ₃					
+ NO → CH ₃ C(CH ₃)(ONO ₂)OC(O)CH ₃	3	6%	5%	6%	4%
16 + NO → NO ₂ + CH ₃ C(O·)(CH ₃)OC(O)CH ₃		94%	95%	83%	84%
17 CH ₃ C(O·)(CH ₃)OC(O)CH ₃					
→ CH₃C(O)OC(O)CH₃ + CH ₃ ·	8	67%	76%	56%	64%
18 → CH₃C(O)CH₃ + CH ₃ C(O)O·	9	21%	24%	17%	20%
19 → CH ₃ C(CH ₃)(OH)OC(O)CH ₂ ·	10	12%	0%	10%	
29 CH ₃ · + O ₂ → CH ₃ OO·				73%	85%
21 CH ₃ C(O)O· → CO ₂ + CH ₃ ·	11			17%	20%
22 CH ₃ C(CH ₃)(OH)OC(O)CH ₂ · + O ₂ →				10%	0%
CH ₃ C(CH ₃)(OH)OC(O)CH ₂ OO·					
23 CH ₃ C(CH ₃)(OH)OC(O)CH ₂ OO·					
+ NO → NO ₂ + CH ₃ C(CH ₃)(OH)OC(O)CH ₂ O·	6	6%		10%	0%
24 + NO → CH ₃ C(CH ₃)(OH)OC(O)CH ₂ ONO ₂		94%		<1%	0%
25 CH ₃ C(CH ₃)(OH)OC(O)CH ₂ O· + O ₂ →	11			10%	0%
CH ₃ C(CH ₃)(OH)OC(O)CHO + HO ₂ ·					

[a] Reactions that contribute 1% or less of the total process are not shown.

Table 1 (continued)

[b] Documentation notes for branching ratios are as follows. See Carter (2000) for details concerning the estimates of the alkoxy radical reactions.

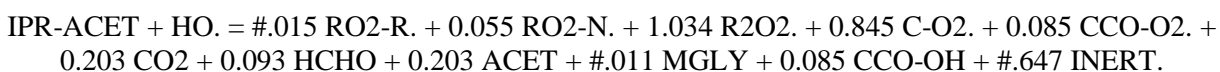
- 1 Total rate constant estimated using methods of Kwok and Atkinson is $3.48 \times 10^{-12} \text{ cm}^3 \text{ molec}^{-1} \text{ s}^{-1}$. Rate constant used is $3.40 \times 10^{-12} \text{ cm}^3 \text{ molec}^{-1} \text{ s}^{-1}$ Atkinson (1989).
- 2 Relative rate of reaction at this position estimated using group-additivity method of Kwok and Atkinson (1995) as updated by Kwok et al (1996).
- 3 The nitrate yield estimates are derived based on nitrate yields for other compounds as discussed by Carter (2000). Nitrate yields from the initially formed peroxy radicals are adjusted downwards slightly to improve the fits of model simulations to the mini-surrogate reactivity experiment carried out for this project.
- 4 Estimated rate constant derived using the estimation methods derived for alkoxy radical reactions by Carter (2000). No adjustments were made to fit the data for this compound. The adjusted branching ratio are derived based on the assumption that the products observed by Tuazon et al (1998) are the only non-nitrate products formed in significant yields, as discussed in the text.
- 5 Estimated rate constant derived using the estimation methods derived for alkoxy radical reactions by Carter (2000). The activation energy estimate for this type of reaction is based in part on the need to approximately predict the yields of acetic acid from the reaction of OH with isopropyl acetate (Tuazon et al, 1998), however other data are also used to derive this estimate (Carter, 2000). The adjusted branching ratio is derived as indicated by Note 4.
6. The nitrate yield for the reaction of NO with this radical was adjusted based on model simulations of reactivity data for ethyl acetate (Carter, 2000; Carter et al, 2000).
- 7 The ester rearrangement is estimated to be the major reaction route for this radical. The competing decompositions and reaction with O_2 are estimated to be relatively unimportant compared to this reaction.
- 8 The estimated rate constant is derived using the estimation methods derived for alkoxy radical decomposition reactions by Carter (2000). Note that estimates for decompositions forming anhydride groups are given an activation energy reduction of 2 kcal mol^{-1} to be consistent with product data from isopropyl acetate (Tuazon et al, 1998) and related compounds (Carter et al, unpublished results, 2000). The adjusted branching ratio are derived based on the assumption that the products observed by Tuazon et al (1998) are the only non-nitrate products formed in significant yields, as discussed in the text. The branching ratio for acetone relative to acetic anhydride formation is assumed to be the same as the ratio of yields of these two products.
- 9 The estimated rate constant is derived using the estimation methods for alkoxy radical decomposition reactions discussed by Carter (2000). Note that decompositions forming RCO_2 radicals are assumed to have higher activation energies than decompositions forming $\text{RO}\cdot$ radicals to be consistent with product data for isopropyl and t-butyl acetates (Tuazon et al, 1998), and for the model to fit chamber data for propylene carbonate (Carter, 2000). The adjusted branching ratio is derived as indicated in Note 8.
- 10 The estimated rate constant is derived using the estimation methods for alkoxy radical isomerization reactions discussed by Carter (2000). Note that an additional 3.5 kcal/mole ring strain is when estimating isomerization rate constants for $\text{C}(\text{O})\text{O}-$ groups in the transition state is assumed to be consistent with results of product studies from esters. The adjusted branching ratio is derived as indicated in Note 8.
- 11 This decomposition is estimated to be extremely fast (Carter, 2000).
- 12 Reaction with O_2 is estimated to be the major fate of this radical. Competing decompositions are estimated to occur less than 1% of the time (Carter, 2000).

Table 1 (continued)

[c] Branching ratios showed relative to the individual reactions (“Reaction”) or the total OH + isopropyl acetate process (“Total”). The “Est.” columns are the ratios estimated using the methods of Carter (2000), and the “Adj” column shows the ratios adjusted based on the product data of Tuazon et al (1998) if they are different.

mechanism is clearly a concern. The estimates used in the SAPRC-99 mechanism for compounds where no data are available are derived based primarily on adjusted nitrate yields to optimize fits of model simulations to chamber data for compounds where such data are available. This approach gives an estimated 6.5% nitrate yield for the reactions of the initially formed peroxy radicals in the OH + isopropyl acetate system, as shown in the estimated mechanism column in Table 1. However, as discussed in the Results section, the mini-surrogate reactivity experiment carried out with isopropyl acetate for this program is somewhat better fit if the nitrate yield from the reactions of the initially peroxy radicals is reduced from the estimated 6.5% to 5%. (Note that the overall nitrate yield is higher because of nitrate formation from peroxy radicals formed in secondary reactions.) This adjustment is well within the uncertainty of the estimates of these yields, and is therefore incorporated in the adjusted mechanism, as shown on Table 1.

In terms of SAPRC-99 model species, the overall process for the reactions of OH with isopropyl acetate is represented as follows:



Here RO2-R. represents formation of peroxy radicals that form HO₂ after an NO to NO₂ conversion, RO2-N. represents formation of peroxy radicals that react with NO to form organic nitrates, R2O2. represents extra NO to NO₂ conversions caused by peroxy radicals in multi-step mechanisms, CCO-O2. represents acyl peroxy radicals, ACET represents acetone, MGLY is the methyl glyoxal model species that is used to represent the CH₃C(CH₃)(OH)OC(O)CHO that is predicted to be the major product formed from the reactions of the CH₃CH(CH₃)OC(O)CH₂· radical (not shown on Table 1), CCO-OH is acetic acid, and INERT is the unreactive product model species that is used to represent acetic anhydride, whose subsequent reactions are ignored..

Atmospheric Reactions of 2-Pentanone

The major gas-phase loss for ketones in the atmosphere is expected to be reaction with OH radicals and perhaps photolysis. Based on available information for various ketones, reaction with NO₃ radicals (Atkinson, 1991) and O₃ (Atkinson and Carter, 1984; Atkinson, 1994) are expected to be unimportant, and these are not considered further. The expected mechanisms for the reactions of 2-pentanone with OH radicals and by photolysis are discussed below.

Reaction with OH Radicals

The rate constant for the reaction of 2-pentanone with OH radicals has been measured in several studies (Atkinson et al, 1982; Wallington and Kurylo, 1987, Atkinson and Aschmann, 1988, Atkinson et al, 2000), and the these data are summarized by Atkinson et al (2000), with the earlier relative rate data updated based on currently recommended rate constants for the reference compound (Atkinson, 1997). All these measurements are in good agreement, with the most recently determined value of Atkinson et al (2000) being less than 2% different from the average of all the determinations. Based on these data, the rate constant used in this work is

$$k(\text{OH} + \text{2-Pentanone}) = 4.56 \times 10^{-12} \text{ cm}^3 \text{ molec}^{-1} \text{ s}^{-1}$$

which is the value of Atkinson et al (2000). This is in reasonably good agreement with the value predicted using the structure-reactivity methods of Kwok and Atkinson (1995) as implemented in the SAPRC-99 mechanism, which predicts an overall rate constant of $4.78 \times 10^{-12} \text{ cm}^3 \text{ molec}^{-1} \text{ s}^{-1}$.

The products of this reaction under atmospheric conditions have been studied by Atkinson et al (2000), and their results are summarized on Table 2. These products are consistent with the estimated mechanism for this reaction that is derived by the SAPRC-99 mechanism generation system, which is shown on Table 3. Estimated branching ratios and total yields for the various process are also shown on that table. The yields of these products as predicted with this mechanism are shown on Table 2 in the “unadjusted mechanism” column, where they can be compared with the experimental values. Other products predicted to be formed in yields greater than 3% are also shown.

The predicted yields of these products are in generally good agreement with the observed products given the uncertainties of the estimation methods involved. The prediction of the acetaldehyde to 2,3-pentadione yield ratio is based on rate constant estimates for competing reactions of the $\text{CH}_3\text{C}(\text{O})\text{CH}_2\text{CH}(\text{O}\cdot)\text{CH}_3$ radical, which are quite uncertain, particularly in the case of the decomposition.

Table 2. Measured and predicted product yields for the reactions of OH radicals with 2-pentanone.

Product	Product Yields (%)		
	Experimental [a]	Unadjusted Mechanism	Adjusted Mechanism
Formaldehyde	103 ± 10 [b]	48	61
Acetaldehyde	51 ± 11	46	59
Propionaldehyde	19 ± 3	17	17
$\text{CH}_3\text{C}(\text{O})\text{CH}_2\text{C}(\text{O})\text{CH}_3$	12 ± 3	25	12
$\text{CH}_3\text{C}(\text{O})\text{CH}_2\text{CH}_2\text{CHO}$	-	3	3
Organic Nitrates	25 ± 4 [c]	6.5	6.5

[a] From Atkinson et al (2000).

[b] Probably high because of possible formaldehyde formation from secondary reactions of products.

[c] Estimated from nitrate IR bands.

Table 3. Detailed mechanism for the atmospheric reactions of 2-pentanone with OH radicals in the presence of NO_x, as produced by the SAPRC-99 mechanism generation system. Products observed by Atkinson et al (2000) are shown in bold font.

Reactions [a]	Note [b]	Branching [c]			
		Reaction		Total	
		Est.	Adj.	Est.	Adj.
CH₃CH₂CH₂C(O)CH₃					
1	+ OH → H ₂ O + CH ₃ C(O)CH ₂ CH ₂ CH ₂ ·	1	4%	4%	
2	+ OH → H ₂ O + CH ₃ C(O)CH ₂ CH(·)CH ₃	1	76%	76%	
3	+ OH → H ₂ O + CH ₃ CH ₂ CH(·)C(O)CH ₃	1	18%	18%	
4	+ OH → H ₂ O + CH ₃ CH ₂ CH ₂ C(O)CH ₂ ·	1	2%	2%	
<u>Reactions of radical formed in Reaction (1).</u>					
5	CH ₃ C(O)CH ₂ CH ₂ CH ₂ · + O ₂ → CH ₃ C(O)CH ₂ CH ₂ CH ₂ OO·			4%	
6	CH ₃ C(O)CH ₂ CH ₂ CH ₂ OO· + NO → NO ₂ + CH ₃ C(O)CH ₂ CH ₂ CH ₂ O·	2		3%	
7	CH ₃ C(O)CH ₂ CH ₂ CH ₂ O· + O ₂ → CH ₃ C(O)CH ₂ CH ₂ CHO + HO ₂ ·	3		3%	
<u>Reactions of radical formed in Reaction (2).</u>					
8	CH ₃ C(O)CH ₂ CH(·)CH ₃ + O ₂ → CH ₃ C(O)CH ₂ CH(OO·)CH ₃ CH ₃ C(O)CH ₂ CH(OO·)CH ₃			76%	
9	+ NO → CH ₃ CH(ONO ₂)CH ₂ C(O)CH ₃	2	6%	5%	
10	+ NO → NO ₂ + CH ₃ C(O)CH ₂ CH(O·)CH ₃ CH ₃ C(O)CH ₂ CH(O·)CH ₃		94%	71%	
11	+ O ₂ → CH₃C(O)CH₂C(O)CH₃ + HO ₂ ·	3	35%	17%	25% 12%
12	→ CH₃CHO + CH ₃ C(O)CH ₂ ·	4	65%	83%	46% 59%
13	CH ₃ C(O)CH ₂ · + O ₂ → CH ₃ C(O)CH ₂ OO·			46%	59%
14	CH ₃ C(O)CH ₂ OO· + NO → NO ₂ + CH ₃ C(O)CH ₂ O·			46%	59%
15	CH ₃ C(O)CH ₂ O· → HCHO + CH ₃ C(O)·	3		46%	59%
16	CH ₃ C(O)· + O ₂ → CH ₃ C(O)OO·			63%	76%
<u>Reactions of radical formed in Reaction (3).</u>					
17	CH ₃ CH ₂ CH(·)C(O)CH ₃ + O ₂ → CH ₃ CH ₂ CH(OO·)C(O)CH ₃ CH ₃ CH ₂ CH(OO·)C(O)CH ₃			18%	
18	+ NO → CH ₃ CH ₂ CH(ONO ₂)C(O)CH ₃	2	6%	1%	
19	+ NO → NO ₂ + CH ₃ CH ₂ CH(O·)C(O)CH ₃		94%	17%	
20	CH ₃ CH ₂ CH(O·)C(O)CH ₃ → CH₃CH₂CHO + CH ₃ C(O)·	3		17%	
<u>Reactions of radical formed in Reaction (4).</u>					
21	CH ₃ CH ₂ CH ₂ C(O)CH ₂ · + O ₂ → CH ₃ CH ₂ CH ₂ C(O)CH ₂ OO·			2%	
22	CH ₃ CH ₂ CH ₂ C(O)CH ₂ OO· + NO → NO ₂ + CH ₃ CH ₂ CH ₂ C(O)CH ₂ O·	2		2%	
23	CH ₃ CH ₂ CH ₂ C(O)CH ₂ O· → HCHO + CH ₃ CH ₂ CH ₂ C(O)·	3		2%	
24	CH ₃ CH ₂ CH ₂ C(O)· + O ₂ → CH ₃ CH ₂ CH ₂ C(O)OO·			2%	

[a] Reactions that contribute 1% or less of the total process are not shown.

[b] Documentation notes for branching ratios are as follows. See Carter (2000) for details concerning the estimates of the alkoxy radical reactions.

- 1 Relative rate of reaction at this position estimated using group-additivity method of Kwok and Atkinson (1995) as updated by Kwok et al (1996).

Table 3 (continued)

- 2 Nitrate yields estimated based on nitrate yields for other compounds as discussed by Carter (2000). The nitrate yields in the isopropyl acetate reactions were not adjusted. The nitrate yield reaction competing with Reaction 6 is estimated to be less than 1%, so is not shown.
 3. The rate constant for this reaction and the competing processes are estimated using the alkoxy radical rate constant estimation methods derived by Carter (2000). If not all the competing reactions are shown, then those reactions are estimated to occur less than 1% of the time relative to the total reaction of 2-pentanone.
 - 4 Estimated rate constant derived using the estimation methods derived for alkoxy radical reactions by Carter (2000). In the adjusted mechanism the rate constant is derived to better fit the acetaldehyde and 2,4-pentadione yield data of Atkinson et al (2000).
- [c] Branching ratios showed relative to the individual reactions (“Reaction”) or the total OH + 2-pentanone process (“Total”). The “Est.” columns are the ratios estimated using the methods of Carter (2000), and the “Adj” column shows the ratios adjusted based on the product data of Atkinson et al (2000) if they are different.

Therefore, the SAPRC-99 mechanism for 2-pentanone incorporates an upward adjustment of the decomposition reaction of the $\text{CH}_3\text{C}(\text{O})\text{CH}_2\text{CH}(\text{O}\cdot)\text{CH}_3$ radical to more closely predict the observed relative yields of these two products. The branching ratios using this adjusted mechanism are also shown on Table 3, and the products predicted after this adjustment is made are shown on Table 2. It can be seen that the adjusted mechanism not only gives somewhat better predictions of the yields of these two products, the prediction of the formaldehyde yield is also improved. This is because formaldehyde is a co-product formed in the decomposition of $\text{CH}_3\text{C}(\text{O})\text{CH}_2\text{CH}(\text{O}\cdot)\text{CH}_3$ whose rate constant was adjusted.

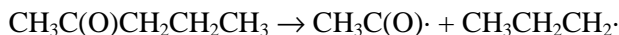
The experimentally derived nitrate yields are based on estimates of absorption cross sections of nitrate bands that have not been calibrated using authentic samples, and are considered to be quite uncertain. Our experience with most of the compounds for which such yield estimates have been made with IR bands is that using such yields as a basis deriving mechanisms results in models whose predictions are not consistent with environmental chamber reactivity data. Therefore, the nitrate yields used in when deriving an estimated mechanism for 2-pentanone are those derived using the SAPRC-99 estimation procedures, which are based on overall nitrate yields that give best fits of model simulations to available environmental chamber reactivity data (Carter, 2000). As discussed below, these SAPRC-99 nitrate yield estimates give satisfactory fits to the environmental chamber reactivity data for 2-pentanone, and thus are not adjusted. Although the estimated 6.5% overall nitrate yields are lower than the experimentally estimated values of 12%, they are probably not outside the uncertainty range of the experimental determination.

Photolysis

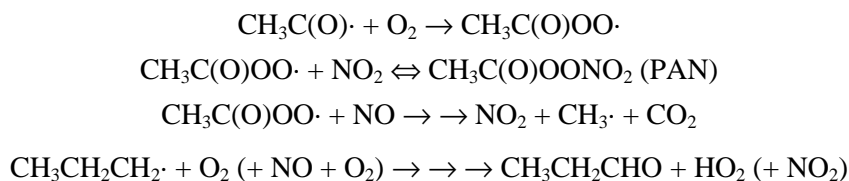
Acetone and methyl ethyl ketone undergo non-negligible reaction by photolysis in the atmosphere (Atkinson, 1990; Carter, 2000, and references therein), so this is expected to be the case for the higher ketones studied in this program. Information concerning the absorption cross sections for these

compounds could not be found, and we assume that they are approximately the same as those used for methyl ethyl ketone in the SAPRC-99 mechanism. If the quantum yield for reaction were sufficiently high, this would result in a non-negligible loss process for these ketones in the atmosphere, which would have to be represented in the mechanism.

Although the actual atmospheric photolysis reactions for the higher ketones are probably more complex (e.g., see Calvert and Pitts, 1966 and Wirtz, 1999), because of lack of available information the approach used in the estimated SAPRC-99 mechanisms is to assume that the major radical forming process is scission of the weakest C..C(O) bond (Carter, 2000), which in the case of 2-pentanone is:



The major subsequent reactions are then



In the SAPRC-99 mechanism, the formation of $\text{CH}_3\text{C(O)OO}\cdot$ is represented by the model species CCO-O2., and the formation of $\text{CH}_2\text{CH}_2\text{CH}_2\cdot$ and its subsequent reactions are represented by RO2-R. + RCHO + HO2 (Carter, 2000). RO2-R. is the model species representing formation of peroxy radicals whose overall reactions in the presence of NO_x involve conversion of NO to NO_2 and formation of HO_2 , and RCHO is the model species representing propionaldehyde and the lumped higher aldehydes.

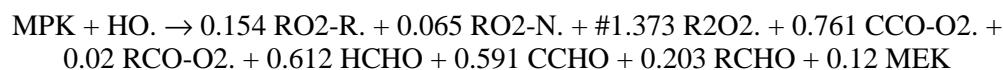
It should be noted, however, that the data of Wirtz (1999), indicates that the actual mechanism is more complicated. He observed formation of ethene, propionaldehyde, and methyl and propyl hydroperoxides when 2-pentanone was photolyzed in air in an outdoor environmental chamber in the absence of NO_x . (The yields were not given, but ethene was indicated as the “major product”). Although the formation of propyl hydroperoxide would be expected from the assumed mechanism, ethene and propionaldehyde suggest molecular mechanisms, which do not involve radical formation, may also be occurring. However, results of model simulations of O_3 formation are not sensitive to photodecomposition processes that do not form radicals, so these routes are ignored in the current study.

The quantum yields for the photodecomposition of 2-pentanone to form radicals have not been determined directly. Based on overall photolysis rates measured in an outdoor chamber compared to theoretically photolysis rates assuming unit quantum yield, Wirtz (1999) estimates an overall effective quantum yield of 0.07 for 2-pentanone. Since this would include molecular as well as radical forming loss processes, this means that the quantum yield for radical formation would have to be less than this. On the other hand, the overall radical formation quantum yield that best fits the environmental chamber data for methyl ethyl ketone is 0.15 (Carter, 2000; Carter et al., 2000), and the environmental chamber data for 2-pentanone are best fit by assuming an overall radical formation quantum yield of 0.10 for this

compound (see below). The latter is used in the 2-pentanone mechanism recommended for atmospheric reactivity estimates because it gives the best performance in predicting experimentally measured ozone impacts of this compound. Although somewhat higher 0.07 upper limit quantum yield derived from the data of Wirtz (1999), the assumed 0.1 overall quantum yield for radical formation is probably not outside the experimental uncertainty of the derivation of Wirtz (1999).

Representation in the SAPRC-99 Mechanism

In terms of model species used in the SAPRC-99 mechanism, the reactions of 2-pentanone can be represented as follows:



The photolysis reaction uses the “KETONE” absorption cross sections and an overall quantum yield of 0.1. The RO₂-R. represents formation of peroxy radicals that form HO₂ after an NO to NO₂ conversion, RO₂-N. represents formation of peroxy radicals that react with NO to form organic nitrates, R₂O₂. represents extra NO to NO₂ conversions caused by peroxy radicals in multi-step mechanisms, CCO-O₂. represents acetyl peroxy radicals, RCO-O₂. represents higher acyl peroxy radicals, CCHO represents acetaldehyde, RCHO represents lumped higher aldehydes (primarily propionaldehyde and to a lesser extent CH₃C(O)CH₂CH₂CHO in this case), and MEK represents 2,4-pentanedione. This mechanism was used as the “best fit” mechanism in the chamber simulations discussed below, and was used in the atmospheric reactivity calculations discussed later in this report.

Atmospheric Reactions of 2-Heptanone

Reaction with OH Radicals

As discussed above, the major gas-phase atmospheric loss processes that need to be considered for this compound is reaction with OH radicals and photolysis. The OH rate constant has been measured to be $8.67 \pm 0.84 \times 10^{-12} \text{ cm}^3 \text{ molec}^{-1} \text{ s}^{-1}$ by Wallington and Kurylo (1987) and $1.17 \pm 1.1 \times 10^{-11} \text{ cm}^3 \text{ molec}^{-1} \text{ s}^{-1}$ by Atkinson et al (2000). Although the two determinations agree within their stated uncertainties, we use the value determined by Atkinson et al (2000) of

$$k(\text{OH} + \text{2-heptanone}) = 1.17 \times 10^{-11} \text{ cm}^3 \text{ molec}^{-1} \text{ s}^{-1}$$

because the measurement of the OH + 2-pentanone rate constant of Atkinson et al (2000) was somewhat more consistent with the results of the other studies for that compound than the 2-pentanone rate constant of Wallington and Kurylo (1987). This is somewhat higher than the rate constant estimated using the structure-reactivity method of Kwok and Atkinson (1997) as implemented in SAPRC-99 (Carter, 2000), which predicts an OH + 2-heptanone rate constant of $8.2 \times 10^{-12} \text{ cm}^3 \text{ molec}^{-1} \text{ s}^{-1}$. However, this disagreement is not outside the range of uncertainty of these estimates.

Atkinson et al (2000) also conducted a product study of the reactions of 2-heptanone with OH radicals under atmospheric conditions in the presence of NO_x, and the results are summarized on Table 4. Only a relatively small fraction of the reaction routes have been identified, so the available product data are not sufficient to derive an overall mechanism for the atmospheric reactions of this compound.

The detailed mechanism for the atmospheric reactions of 2-heptanone with OH radicals in the presence of NO_x is given on Table 5, with reactions predicted to occur less than 1% of the time omitted. The importances of each of the reactions relative to the overall OH + 2-heptanone reaction and (where applicable) relative to competing reactions of the reacting compound are also shown. Footnotes to the table indicate how the branching ratios were derived, but in all cases the SAPRC-99 estimation methods (Carter, 2000) were used without adjustment. The major stable products predicted by this mechanism are summarized on Table 4, where they can be compared with the limited product data of Atkinson et al (2000).

The agreement between the estimated OH + 2-heptanone product yields and those measured by Atkinson et al (2000) is considered to be sufficiently good that no adjustments were made to the mechanism. The predicted acetaldehyde and propionaldehyde yields are respectively lower and higher than measured, but given the relatively low yields and the uncertainty in the experimental determination, adjustment is not considered to be appropriate. The high measured formaldehyde yield compared to the estimated yield may be due to formaldehyde formation from secondary reactions of products, and thus the discrepancy may not necessarily indicate a problem with the mechanism. The predicted products that

Table 4. Measured and predicted product yields for the reactions of OH radicals with 2-heptanone.

Product	Product Yields (%)	
	Experimental [a]	Estimated Mechanism
Formaldehyde	38 ± 8 [b]	10
Acetaldehyde	~5	1
Propionaldehyde	~5	14
Butyraldehyde	7 ± 1	9
Pentanal	9 ± 1	9
CH ₃ C(O)CH ₂ C(O)CH ₂ CH ₂ CH ₂ OH		23
CH ₃ CH(OH)CH ₂ CH ₂ CHO		10
CH ₃ C(O)CH ₂ CHO		13
CH ₃ CH ₂ C(O)CH ₂ CH ₂ C(O)CH ₃		7
CH ₃ CH ₂ CH ₂ C(O)CH ₂ C(O)CH ₃		5
Organic Nitrates	18 ± 5 [c]	19

[a] From Atkinson et al (2000).

[b] Probably high because of possible formaldehyde formation from secondary reactions of products.

[c] Estimated from nitrate IR bands.

Table 5. Detailed mechanism for the atmospheric reactions of 2-heptanone with OH radicals in the presence of NO_x, as produced by the SAPRC-99 mechanism generation system.

Reactions [a]	Note [b]	Branching [c] Rxn.	Tot.
<u>CH₃CH₂CH₂CH₂CH₂C(O)CH₃</u>			
1 + OH → H ₂ O + CH ₃ C(O)CH ₂ CH ₂ CH ₂ CH ₂ CH ₂ ·	1	2%	2%
2 + OH → H ₂ O + CH ₃ C(O)CH ₂ CH ₂ CH ₂ CH(·)CH ₃	1	14%	14%
3 + OH → H ₂ O + CH ₃ CH ₂ CH(·)CH ₂ CH ₂ C(O)CH ₃	1	17%	17%
4 + OH → H ₂ O + CH ₃ CH ₂ CH ₂ CH(·)CH ₂ C(O)CH ₃	1	55%	55%
5 + OH → H ₂ O + CH ₃ CH ₂ CH ₂ CH ₂ CH(·)C(O)CH ₃	1	11%	11%
6 + OH → H ₂ O + CH ₃ CH ₂ CH ₂ CH ₂ CH ₂ C(O)CH ₂ ·	1	1%	1%
<u>Reactions of radical formed in Reaction (1).</u>			
7 CH ₃ C(O)CH ₂ CH ₂ CH ₂ CH ₂ CH ₂ · + O ₂ → CH ₃ C(O)CH ₂ CH ₂ CH ₂ CH ₂ CH ₂ OO·			2%
8 CH ₃ C(O)CH ₂ CH ₂ CH ₂ CH ₂ CH ₂ OO· + NO → NO ₂ + CH ₃ C(O)CH ₂ CH ₂ CH ₂ CH ₂ CH ₂ O·	2		2%
9 CH ₃ C(O)CH ₂ CH ₂ CH ₂ CH ₂ CH ₂ O· → CH ₃ C(O)CH ₂ CH(·)CH ₂ CH ₂ CH ₂ OH	3		2%
10 CH ₃ C(O)CH ₂ CH(·)CH ₂ CH ₂ CH ₂ OH + O ₂ → CH ₃ C(O)CH ₂ CH(OO·)CH ₂ CH ₂ CH ₂ OH			2%
11 CH ₃ C(O)CH ₂ CH(OO·)CH ₂ CH ₂ CH ₂ OH + NO → NO ₂ + CH ₃ C(O)CH ₂ CH(O·)CH ₂ CH ₂ CH ₂ OH	2		2%
12 CH ₃ C(O)CH ₂ CH(O·)CH ₂ CH ₂ CH ₂ OH → CH ₃ C(O)CH ₂ CH(OH)CH ₂ CH ₂ CH(·)OH	3		2%
13 CH ₃ C(O)CH ₂ CH(OH)CH ₂ CH ₂ CH(·)OH + O ₂ → CH ₃ C(O)CH ₂ CH(OH)CH ₂ CH ₂ CHO + HO ₂ ·			2%
<u>Reactions of radical formed in Reaction (2).</u>			
14 CH ₃ C(O)CH ₂ CH ₂ CH ₂ CH(·)CH ₃ + O ₂ → CH ₃ C(O)CH ₂ CH ₂ CH ₂ CH(OO·)CH ₃			14%
15 CH ₃ C(O)CH ₂ CH ₂ CH ₂ CH(OO·)CH ₃ + NO → CH ₃ CH(ONO ₂)CH ₂ CH ₂ CH ₂ C(O)CH ₃	2	14%	2%
16 + NO → NO ₂ + CH ₃ C(O)CH ₂ CH ₂ CH ₂ CH(O·)CH ₃		86%	12%
17 CH ₃ C(O)CH ₂ CH ₂ CH ₂ CH(O·)CH ₃ → CH ₃ CH(OH)CH ₂ CH ₂ CH(·)C(O)CH ₃	3		12%
18 CH ₃ CH(OH)CH ₂ CH ₂ CH(·)C(O)CH ₃ + O ₂ → CH ₃ CH(OH)CH ₂ CH ₂ CH(OO·)C(O)CH ₃			12%
19 CH ₃ CH(OH)CH ₂ CH ₂ CH(OO·)C(O)CH ₃ + NO → CH ₃ CH(OH)CH ₂ CH ₂ CH(ONO ₂)C(O)CH ₃	2	14%	2%
20 + NO → NO ₂ + CH ₃ CH(OH)CH ₂ CH ₂ CH(O·)C(O)CH ₃		86%	10%
21 CH ₃ CH(OH)CH ₂ CH ₂ CH(O·)C(O)CH ₃ → CH ₃ CH(OH)CH ₂ CH ₂ CHO + CH ₃ C(O)·	3		10%
22 CH ₃ C(O)· + O ₂ → CH ₃ C(O)OO·			28%
<u>Reactions of radical formed in Reaction (3).</u>			
23 CH ₃ CH ₂ CH(·)CH ₂ CH ₂ C(O)CH ₃ + O ₂ → CH ₃ CH ₂ CH(OO·)CH ₂ CH ₂ C(O)CH ₃			17%
24 CH ₃ CH ₂ CH(OO·)CH ₂ CH ₂ C(O)CH ₃ + NO → CH ₃ CH ₂ CH(ONO ₂)CH ₂ CH ₂ C(O)CH ₃	2	14%	2%
25 + NO → NO ₂ + CH ₃ CH ₂ CH(O·)CH ₂ CH ₂ C(O)CH ₃ CH ₃ CH ₂ CH(O·)CH ₂ CH ₂ C(O)CH ₃		86%	15%

Table 5 (continued)

Reactions [a]	Note [b]	Branching [c]	
		Rxn.	Tot.
26 $+ O_2 \rightarrow CH_3CH_2C(O)CH_2CH_2C(O)CH_3 + HO_2\cdot$	3	48%	7%
27 $\rightarrow CH_3C(O)CH_2CH_2CHO + CH_3CH_2\cdot$	3	9%	1%
28 $\rightarrow CH_3CH_2CHO + CH_3C(O)CH_2CH_2\cdot$	3	43%	6%
29 $CH_3CH_2\cdot + O_2 \rightarrow CH_3CH_2OO\cdot$			1%
30 $CH_3CH_2OO\cdot + NO \rightarrow NO_2 + CH_3CH_2O\cdot$			1%
31 $CH_3CH_2O\cdot + O_2 \rightarrow CH_3CHO + HO_2\cdot$	3		1%
32 $CH_3C(O)CH_2CH_2\cdot + O_2 \rightarrow CH_3C(O)CH_2CH_2OO\cdot$			6%
33 $CH_3C(O)CH_2CH_2OO\cdot + NO \rightarrow NO_2 + CH_3C(O)CH_2CH_2O\cdot$	2		6%
34 $CH_3C(O)CH_2CH_2O\cdot + O_2 \rightarrow CH_3C(O)CH_2CHO + HO_2\cdot$	3		6%
<u>Reactions of radical formed in Reaction (4).</u>			
35 $CH_3CH_2CH_2CH(\cdot)CH_2C(O)CH_3 + O_2 \rightarrow$ $CH_3CH_2CH_2CH(OO\cdot)CH_2C(O)CH_3$ $CH_3CH_2CH_2CH(OO\cdot)CH_2C(O)CH_3$			55%
36 $+ NO \rightarrow CH_3CH_2CH_2CH(ONO_2)CH_2C(O)CH_3$	2	14%	7%
37 $+ NO \rightarrow NO_2 + CH_3CH_2CH_2CH(O\cdot)CH_2C(O)CH_3$ $CH_3CH_2CH_2CH(O\cdot)CH_2C(O)CH_3$		86%	47%
38 $+ O_2 \rightarrow CH_3CH_2CH_2C(O)CH_2C(O)CH_3 + HO_2\cdot$	3	10%	5%
39 $\rightarrow CH_3C(O)CH_2CHO + CH_3CH_2CH_2\cdot$	3	16%	8%
40 $\rightarrow CH_3CH_2CH_2CHO + CH_3C(O)CH_2\cdot$	3	18%	9%
41 $\rightarrow CH_3C(O)CH_2CH(OH)CH_2CH_2CH_2\cdot$	3	55%	26%
42 $CH_3CH_2CH_2\cdot + O_2 \rightarrow CH_3CH_2CH_2OO\cdot$			8%
43 $CH_3CH_2CH_2OO\cdot + NO \rightarrow NO_2 + CH_3CH_2CH_2O\cdot$	2		8%
44 $CH_3CH_2CH_2O\cdot + O_2 \rightarrow CH_3CH_2CHO + HO_2\cdot$	3		8%
45 $CH_3C(O)CH_2\cdot + O_2 \rightarrow CH_3C(O)CH_2OO\cdot$			9%
46 $CH_3C(O)CH_2OO\cdot + NO \rightarrow NO_2 + CH_3C(O)CH_2O\cdot$	2		9%
47 $CH_3C(O)CH_2O\cdot \rightarrow HCHO + CH_3C(O)\cdot$	3		9%
48 $CH_3C(O)CH_2CH(OH)CH_2CH_2CH_2\cdot + O_2 \rightarrow$ $CH_3C(O)CH_2CH(OH)CH_2CH_2CH_2OO\cdot$ $CH_3C(O)CH_2CH(OH)CH_2CH_2CH_2OO\cdot$			26%
49 $+ NO \rightarrow CH_3C(O)CH_2CH(OH)CH_2CH_2CH_2ONO_2$	2	14%	4%
50 $+ NO \rightarrow NO_2 + CH_3C(O)CH_2CH(OH)CH_2CH_2CH_2O\cdot$		86%	23%
51 $CH_3C(O)CH_2CH(OH)CH_2CH_2CH_2O\cdot \rightarrow$ $CH_3C(O)CH_2C(\cdot)(OH)CH_2CH_2CH_2OH$	3		23%
52 $CH_3C(O)CH_2C(\cdot)(OH)CH_2CH_2CH_2OH + O_2 \rightarrow$ $CH_3C(O)CH_2C(O)CH_2CH_2CH_2OH + HO_2\cdot$			23%
<u>Reactions of radical formed in Reaction (5).</u>			
53 $CH_3CH_2CH_2CH_2CH(\cdot)C(O)CH_3 + O_2 \rightarrow$ $CH_3CH_2CH_2CH_2CH(OO\cdot)C(O)CH_3$ $CH_3CH_2CH_2CH_2CH(OO\cdot)C(O)CH_3$			11%
54 $+ NO \rightarrow CH_3CH_2CH_2CH_2CH(ONO_2)C(O)CH_3$	2	14%	1%
55 $+ NO \rightarrow NO_2 + CH_3CH_2CH_2CH_2CH(O\cdot)C(O)CH_3$		86%	9%
56 $CH_3CH_2CH_2CH_2CH(O\cdot)C(O)CH_3 \rightarrow CH_3CH_2CH_2CH_2CHO + CH_3C(O)\cdot$	3		9%

[a] Reactions that contribute 1% or less of the total process are not shown.

Table 5 (continued)

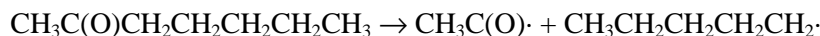
- [b] Documentation notes for branching ratios are as follows. See Carter (2000) for details concerning the estimates of the alkoxy radical reactions.
- 1 Relative rate of reaction at this position estimated using group-additivity method of Kwok and Atkinson (1995) as updated by Kwok et al (1996).
 - 2 Nitrate yields estimated based on nitrate yields for other compounds as discussed by Carter (2000). The nitrate yield reactions estimated to occur less than 1% of the time are not shown.
 3. The rate constant for this reaction and the competing processes are estimated using the alkoxy radical rate constant estimation methods derived by Carter (2000). If not all the competing reactions are shown, then those reactions are estimated to occur less than 1% of the time relative to the total reaction of 2-heptanone.
- [c] Branching ratios estimated using the methods of Carter (2000) are shown relative to the individual reactions (“Rxn.”) or the total OH + 2-heptanone process (“Tot.”).

were not reported by Atkinson et al (2000) are all multifunctional compounds that are difficult to monitor and quantify without the availability of calibration standards.

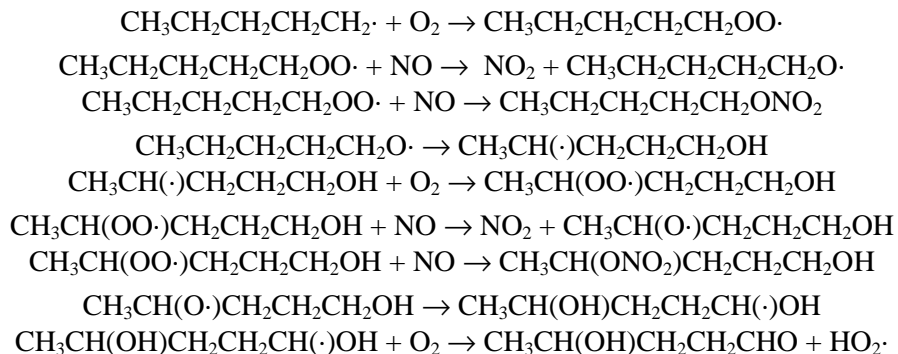
The total nitrate yield estimated using the IR bands is surprisingly close to the estimated total yield. Since use of these yields gave reasonably good simulations of the environmental chamber data obtained in this program (see Results section), the estimated yields were used without adjustment.

Photolysis

The photolysis mechanism assumed for 2-heptanone was analogous to that assumed for 2-pentanone as discussed above. The reaction is assumed to have the same absorption cross sections as that used in the SAPRC-99 mechanism for methyl ethyl ketone and all higher saturated monoketones, and the major reaction that is considered is radical formation via breaking the weakest C..C(O) bond, i.e.,



The major subsequent reactions of the $\text{CH}_3\text{CH}_2\text{CH}_2\text{CH}_2\text{CH}_2\cdot$ radical are expected to be



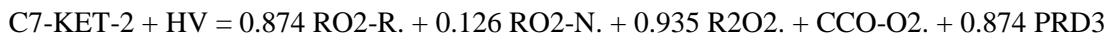
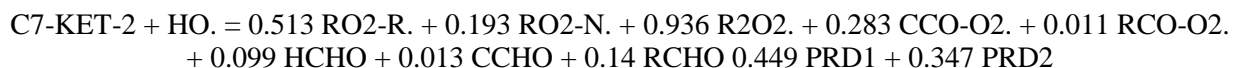
The nitrate yields in the above peroxy + NO reactions are as estimated or assigned in the SAPRC-99 mechanism (Carter, 2000). The alkoxy radical reactions shown are estimated to be the dominant process

for these radicals (Carter, 2000). Note that the major predicted products are the PAN precursor $\text{CH}_3\text{C}(\text{O})\text{OO}\cdot$ radicals and $\text{CH}_3\text{CH}(\text{OH})\text{CH}_2\text{CH}_2\text{CHO}$.

No information could be found concerning the actual products formed when 2-heptanone undergoes photolysis under atmospheric conditions, or the quantum yields of its photolysis reactions. Based on the data for 2-pentanone discussed above it is expected that the actual mechanism may be more complex than indicated above, and photolysis forming non-radical products that are ignored in this mechanism may be occurring, and the quantum yield for radical production is probably relatively low. As discussed below, best fits to the chamber data obtained in this program if it is assumed that the overall quantum yield for radical production is 0.02. Comparing this with the overall quantum yields that best fit the data for 2-pentanone (this work), MEK and methyl isobutyl ketone (Carter, 2000, Carter et al, 2000), this suggests that overall quantum yields for radical production from ketone photolysis decline as the size of the ketone decreases. This assumption is incorporated in the estimation methods for ketone photolysis that are incorporated in the SAPRC-99 mechanisms (Carter, 2000), based largely on these data.

Representation in SAPRC-99 Mechanism

In terms of model species used in the SAPRC-99 mechanism, the reactions of 2-heptanone can be represented as follows:



The photolysis reaction uses the “KETONE” absorption cross sections and an overall quantum yield of 0.02. The model species used are as discussed above except that RCHO represents propionaldehyde explicitly, and separate model species, PRD1, PRD2 and PRD3 are added to represent the major reactive products that are formed in significant yields, following the procedures used in the SAPRC-99 mechanism for other. In this case, PRD1 and PRD2 represent respectively the mixture of higher aldehyde or reactive non-aldehyde oxygenated products formed from in the OH reaction (see Table 5), and PRD3 represents the $\text{CH}_3\text{CH}(\text{OH})\text{CH}_2\text{CH}_2\text{CHO}$ that is predicted to be formed in high yield in the photolysis reactions. The mechanisms for the product species are derived using the SAPRC-99 mechanism generation system as documented by Carter (2000), and these were used to derive the representations for the PRD model species in terms of SAPRC-99 model species. These are given in the full mechanism listing in Appendix A.

Modeling Methods

Environmental Chamber Simulations

The ability of the chemical mechanisms to appropriately simulate the atmospheric impacts of the compounds studied was evaluated by conducting model simulations of the environmental chamber experiments carried out for this study. This requires including in the model appropriate representations of

chamber-dependent effects such as wall reactions and characteristics of the light source. The methods used are based on those discussed in detail by Carter and Lurmann (1990, 1991), updated as discussed by Carter et al. (1995c; 1997, 2000). The photolysis rates were derived from results of NO₂ actinometry experiments and measurements of the relative spectra of the light source. In the case of the xenon arc lights used in the CTC, the spectra were derived from those measured during the individual experiments, assuming continuous linear changes in relative intensity at the various wavelengths, as discussed by Carter et al. (1997). The thermal rate constants were calculated using the temperatures measured during the experiments, with the small variations in temperature with time during the experiment being taken into account. The computer programs and modeling methods employed are discussed in more detail elsewhere (Carter et al, 1995c). The specific values of the chamber-dependent parameters used in the model simulations of the experiments for this study are given in Table A-4 in Appendix A.

In the case of the three test compounds studied in this program, the model calculations used the best fit or adjusted mechanisms discussed above, or the estimated mechanism in the case of 2-heptanone, which was not adjusted. Model simulations of environmental chamber experiments include simulations using different values of the overall quantum yields and (for isopropyl acetate) different overall nitrate yields are also shown to illustrate the sensitivity of the model simulation results to these parameters.

Atmospheric Reactivity Simulations

To estimate their effects on ozone formation under conditions more representative of polluted urban atmospheres, incremental reactivities, defined as the change in O₃ caused by adding small amounts of a compound to the emissions, were calculated for the three test compounds studied for this program, as well as for several other representative compounds. The scenarios employed are discussed in more detail later in this report, and are the same as used in our previous studies (Carter 1994a,b, 2000), and the software and input data are described by Carter (1994b). The mechanism used for the inorganic pollutants mixture used to represent ambient VOCs is given in Appendix A. The mechanisms used for the test compounds were the mechanisms that gave the best fits to the environmental chamber data.

EXPERIMENTAL RESULTS AND MECHANISM EVALUATION

Summary of Experiments and Characterization Results

Table 6 gives a chronological listing of all the experiments carried out for this program. These consisted primarily of the experiments with the three test compounds, whose conditions and selected results are summarized in more detail on Table 7. In addition, several characterization runs were carried out to determine the chamber-dependent inputs needed for the model simulations of the experiments. Table 6 summarizes the purposes and relevant results from these runs. As indicated there, the results of these experiments were as expected based on our previous experience with these and similar chambers in our laboratories (Carter et al., 1995c and references therein; Carter et al, 2000), and indicated no special problems with when characterizing run conditions for mechanism evaluation. See Carter et al (2000) for more discussion of the characterization results for these chambers during this time period, particularly with respect to light intensity and the chamber radical source.

Isopropyl Acetate Experiments

As indicated on Table 6 and Table 7, three incremental reactivity experiments were carried out with isopropyl acetate, one using the mini-surrogate and two using the high NO_x full surrogate. The results are summarized on Table 7 and concentration-time plots of the major reactivity results are shown on Figure 1. Results of model calculations using the adjusted mechanism are also shown in the figure.

Isopropyl acetate was found to cause an increase in NO oxidation and O₃ formation rates and in the peak O₃ concentrations in all three of these experiments. However, it also caused a slight inhibition in overall radical levels, as indicated by the slightly negative IntOH reactivities. Acetone was observed to be a product in all these experiments where isopropyl acetate was added (it is not formed in any of the base case experiments), and the addition of isopropyl acetate also caused increased formaldehyde formation in the full surrogate run where formaldehyde data are available.

The inhibition of radicals caused by the addition of isopropyl acetate to the surrogate experiments can be attributed to radical removal by the formation of nitrates in the peroxy + NO reactions and also by the formation of the PAN precursor, CH₃C(O)· radicals, in the OH reaction. The radical inhibition by these processes is offset to some extent by the formation of formaldehyde as a product, whose subsequent photolysis serves as a non-negligible radical source. The net effect of these processes is a relatively minor radical inhibition that is not enough to counter the positive effects of isopropyl acetate on O₃ formation due to the NO to NO₂ conversions of its direct reactions.

Table 6. Chronological listing of the environmental chamber experiments carried out for this program.

Run ID	Date	Title	Comments
<u>DTC Experiments</u>			
DTC657	5/26/98	NO ₂ Actinometry	NO ₂ actinometry experiment using the quartz tube method. The measured NO ₂ photolysis rate was 0.173 min ⁻¹ , in good agreement with the trend indicated by the other actinometry experiments carried out around this period.
DTC659	5/28/98	N-Butane - NO _x	Characterization run to measure the chamber radical source. The NO oxidation rates were slightly lower than predicted by the standard chamber model, but the results were well within the normal range. Good side equivalency was observed.
DTC673	6/22/98	NO ₂ Actinometry	The measured NO ₂ photolysis rate was 0.156 min ⁻¹ , in reasonable agreement with the trend indicated by the other actinometry experiments carried out around this period.
DTC682	7/8/98	Ozone and CO dark decay	Control run to check for leaks and measure the O ₃ wall decay rate. Essentially no CO decay was observed, indicating negligible leakage. The O ₃ decay rates were 1.4 x 10 ⁻⁴ min ⁻¹ on Side A and 1.6 x 10 ⁻⁴ min ⁻¹ on Side B, in excellent agreement with the value of 1.5 x 10 ⁻⁴ min ⁻¹ that is used when modeling these DTC runs.
DTC683	7/9/98	Propene - NO _x	Standard propene - NO _x control run for comparison with other such runs in this and other chambers. Results in normal range.
DTC684	7/13/98	NO ₂ Actinometry	The measured NO ₂ photolysis rate was 0.160 min ⁻¹ , in reasonable agreement with the trend indicated by the other actinometry experiments carried out around this period.
DTC687	7/22/98	n-Butane - NO _x	Characterization run to measure the chamber radical source. The NO oxidation rates were slightly lower than predicted by the standard chamber model, but the results were well within the normal range. Good side equivalency was observed.
DTC688	7/23/98	Mini-Surrogate + Isopropyl Acetate (B)	Mini-surrogate reactivity experiment with 6.8 ppm isopropyl acetate added to Side B. Results shown on Table 7 and Figure 1.
DTC689	7/24/98	Full Surrogate + Isopropyl Acetate (A)	High NO _x full surrogate reactivity experiment with 4.8 ppm isopropyl acetate added to Side A. Results shown on Table 7 and Figure 1.
DTC697	8/18/98	Full Surrogate + Isopropyl Acetate (A)	High NO _x full surrogate reactivity experiment with 1.8 ppm isopropyl acetate added to Side A. Results shown on Table 7 and Figure 1.

Table 6 (continued)

Run ID	Date	Title	Comments
DTC699	8/20/98	n-Butane - NO _x	Characterization run to measure the chamber radical source. The NO oxidation rates were consistent with those predicted by the standard chamber model, but the rate on Side B was slightly higher than that on Side A.
DTC706	9/2/98	Propene + NO _x	Standard propene - NO _x control run for comparison with other such runs in this and other chambers. Results in normal range.
DTC709	9/8/98	Ozone and CO dark decay	Control run to check for leaks and measure the O ₃ wall decay rate just before replacing the reaction bat. Essentially no CO decay was observed, indicating negligible leakage. The O ₃ decay rates were $1.2 \times 10^{-4} \text{ min}^{-1}$ on Side A and $2.1 \times 10^{-4} \text{ min}^{-1}$, in acceptable agreement with the value of $1.5 \times 10^{-4} \text{ min}^{-1}$ that is used when modeling these DTC runs. The difference between the sides is not considered to be significant.
<u>CTC Experiments</u>			
CTC244	9/14/98	n-Butane + NO _x	Characterization run to measure the chamber radical source. NO oxidation rates were somewhat higher than predicted by the standard chamber model, but within the normal range. Results similar on both sides.
CTC245	9/15/98	Propene + NO _x	Standard control run for comparison with previous propene - NO _x runs and side equivalency test run. Equivalent results obtained on both sides. Model gave good simulation of O ₃ formation rate, but peak ozone yield somewhat higher than model predicted.
CTC247	9/17/98	NO ₂ Actinometry	Measured NO ₂ photolysis rate was 0.198 min^{-1} , corresponding to an estimated NO ₂ photolysis rate of 0.153 min^{-1} inside the reactors. This is consistent with the trend in light intensity indicated by the LiCor spectral measurements during the runs.
CTC252	9/25/98	n-Butane + NO _x	Characterization run to measure the chamber radical source. NO oxidation rate was slightly higher on Side A but rates on both sides very close to prediction of standard chamber model.
CTC255	10/1/98	Mini Surrogate + 2-Pentanone (A)	Mini-surrogate reactivity experiment with 1.6 ppm 2-pentanone added to Side A. Results shown on Table 7 and Figure 3.
CTC256	10/2/98	2-Pentanone (A) or 2-Heptanone (B) - NO _x	2-Pentanone - NO _x experiment on Side A and 2-heptanone - NO _x experiment on Side B. Same level of NO _x on both sides. Results shown on Table 7 and on Figure 2 for 2-pentanone and on Figure 4 for 2-heptanone.

Table 6 (continued)

Run ID	Date	Title	Comments
CTC257	10/7/98	Mini Surrogate + 2-Heptanone (A)	Mini-surrogate reactivity experiment with 2.4 ppm 2-heptanone added to Side A. Results shown on Table 7 and Figure 5.
CTC258	10/7/98	Low NO _x Full Surrogate + 2-Pentanone (B)	Low NO _x full surrogate reactivity experiment with 1.5 ppm 2-pentanone added to Side B. Problems with GC data. Initial VOC reactant concentrations had to be inferred from measurements in comparable experiments or on calculated amounts of compound injected. Results shown on Table 7 and Figure 3.
CTC259	10/8/98	Low NO _x full Surrogate + 2-Heptanone (A)	Low NO _x full surrogate reactivity experiment with 2.2 ppm 2-heptanone added to Side A. Results shown on Table 7 and Figure 5.
CTC260	10/9/98	Full Surrogate + 2-pentanone (B)	High NO _x full surrogate reactivity experiment with 3.0 ppm 2-pentanone added to Side B. Results shown on Table 7 and Figure 3.
CTC261	10/9/98	NO ₂ actinometry	Data not processed.
CTC262	10/13/98	Full Surrogate + 2-Heptanone (A)	High NO _x full surrogate reactivity experiment with 1.6 ppm 2-heptanone added to Side A. Results shown on Table 7 and Figure 5.
CTC263	10/14/98	Low NO _x Full Surrogate + 2-Pentanone (B)	Low NO _x full surrogate reactivity experiment with 3.6 ppm 2-pentanone added to Side B. One of the lamps broke prior to the experiments and had to be replaced. No measurable change in light spectrum was found. Results shown on Table 7 and Figure 3.
CTC264	10/15/98	Propene + NO _x	Standard propene - NO _x control run for comparison with other such runs in this and other chambers. NO oxidation and O ₃ formation rates somewhat slower than model predicted, but results in normal range.
CTC265	10/16/98	NO ₂ Actinometry	The measured NO ₂ photolysis rate using the quartz tube between the lights and the chamber was 0.211 min ⁻¹ , corresponding to an estimated NO ₂ photolysis rate of 0.156 min ⁻¹ inside the reactors. This is consistent with the trend in light intensity indicated by the LiCor spectral measurements during the runs.

Table 7 Summary of conditions and selected results of the environmental chamber experiments.

Run	Test VOC (ppm)	NO _x (ppm)	Surg. (ppm C)	Δ([O ₃]-[NO]) (ppm)						5 th Hour IntOH (10 ⁻⁶ min)		
				2 nd Hour			5 th Hour			Base	Test	IR [a]
				Base	Test	IR [a]	Base	Test	IR [a]			
<u>Mini-Surrogate + Isopropyl Acetate</u>												
DTC688B	6.75	0.43	5.78	0.13	0.19	0.009	0.48	0.73	0.037	12.4	6.5	-0.9
<u>High NO_x Full Surrogate + Isopropyl Acetate</u>												
DTC689A	4.83	0.32	4.33	0.27	0.70	0.089	0.52	1.09	0.117	20.2	12.8	-1.5
DTC697A	1.78	0.32	4.30	0.30	0.46	0.094	0.55	0.84	0.165	20.6	19.8	-0.4
<u>Mini-Surrogate + 2-Pentanone</u>												
CTC255A	1.58	0.22	5.10	0.07	0.11	0.028	0.37	0.31	-0.033	11.2	5.4	-3.7
<u>High NO_x Full Surrogate + 2-Pentanone</u>												
CTC260B	2.97	0.38	6.31	0.28	0.38	0.032	0.57	0.64	0.026	18.8	10.9	-2.7
<u>Low NO_x Full Surrogate + 2-Pentanone</u>												
CTC258B	1.50	0.17	5.82	0.39	0.38	-0.006	0.44	0.44	-0.003			
CTC263B	3.64	0.16	5.83	0.37	0.36	-0.003	0.42	0.40	-0.004	17.6	5.5	-3.3
<u>2-Pentanone - NO_x</u>												
CTC256A	5.33	0.20			0.11			0.22				
<u>Mini-Surrogate + 2-Heptanone</u>												
CTC257A	2.37	0.24	5.27	0.07	0.04	-0.011	0.36	0.16	-0.086	11.7	1.6	-4.2
<u>High NO_x Full Surrogate + 2-Heptanone</u>												
CTC262A	1.56	0.38	5.87	0.29	0.29	0.001	0.58	0.67	0.058	19.6	8.4	-7.1
<u>Low NO_x Full Surrogate + 2-Heptanone</u>												
CTC259A	2.22	0.17	6.18	0.37	0.38	0.004	0.43	0.45	0.010	20.2	6.7	-6.1
<u>2-Heptanone - NO_x</u>												
CTC256B	5.92	0.20			0.04			0.10				

[a] IR = Incremental Reactivity = ([Test] - [Base]) / [Test Compound Added]

The results of model simulations using the isopropyl acetate mechanism discussed in the previous section are also shown on Figure 1. Two sets of calculations are shown, one (dotted lines) using the alkyl nitrate yields derived using the SAPRC-99 estimation methods, and the other (solid lines) using the reduced nitrate yields adjusted to improve fits of the calculations to the data. This relatively minor adjustment (from 6.5% yields from the initially formed peroxy radicals down to ~5%) has a non-negligible effect on the simulation of the mini-surrogate experiment, but negligible effects on the simulations of the other runs. The adjustment may in fact not be appropriate because it is based on only a single experiment, and the discrepancy observed with the unadjusted model is within the run-to-run variability (see for example Carter, 2000; Carter et al, 2000). It would have been better had there been more replicate mini-surrogate experiments to provide a better test for whether the apparent bias using the initially estimated nitrate yield is real. Nevertheless, the adjustment is well within the uncertainty of the

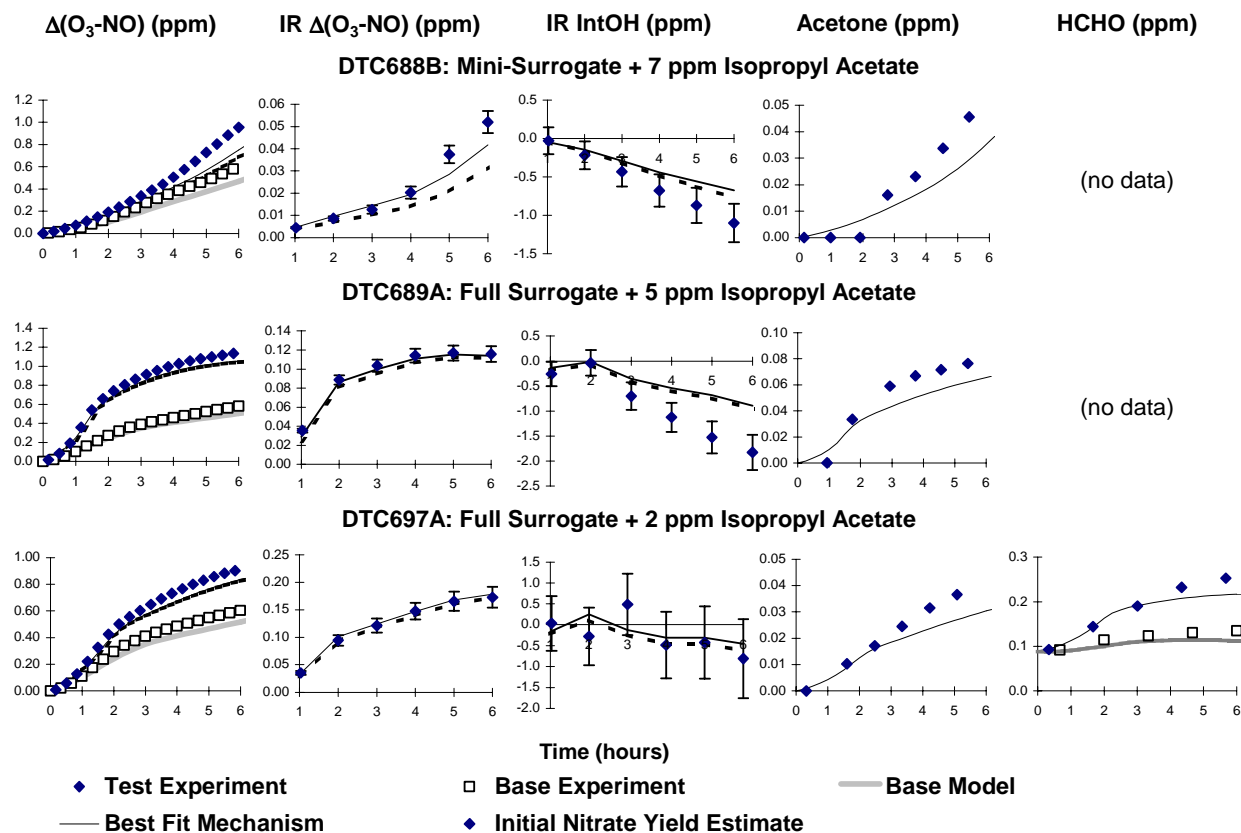


Figure 1. Selected experimental and calculated results of the incremental reactivity experiments with isopropyl acetate.

estimation method, and consequently the adjusted mechanism is used as the basis for the atmospheric reactivity model simulations discussed in this report.

2-Pentanone Experiments

As indicated on Table 6 and Table 7, four incremental reactivity experiments were carried out with 2-pentanone, one using the mini-surrogate, one using the high NO_x full surrogate, and two using the low NO_x full surrogate. In addition, a 2-pentanone - NO_x experiment was also carried out. The results are summarized on Table 7 and concentration-time plots of the selected species in the 2-pentanone - NO_x experiment are shown on Figure 2, and the major results of the reactivity experiments are shown on Figure 3. Results of model calculations using various overall quantum yields for the photolysis reaction are also shown in the figures.

The experiments showed that the effects of 2-pentanone on O_3 formation depend significantly on reaction conditions. 2-Pentanone causes O_3 formation when irradiated by itself in the presence of NO_x and has a positive effect on NO oxidation and O_3 formation rates in the high NO_x full surrogate experiments

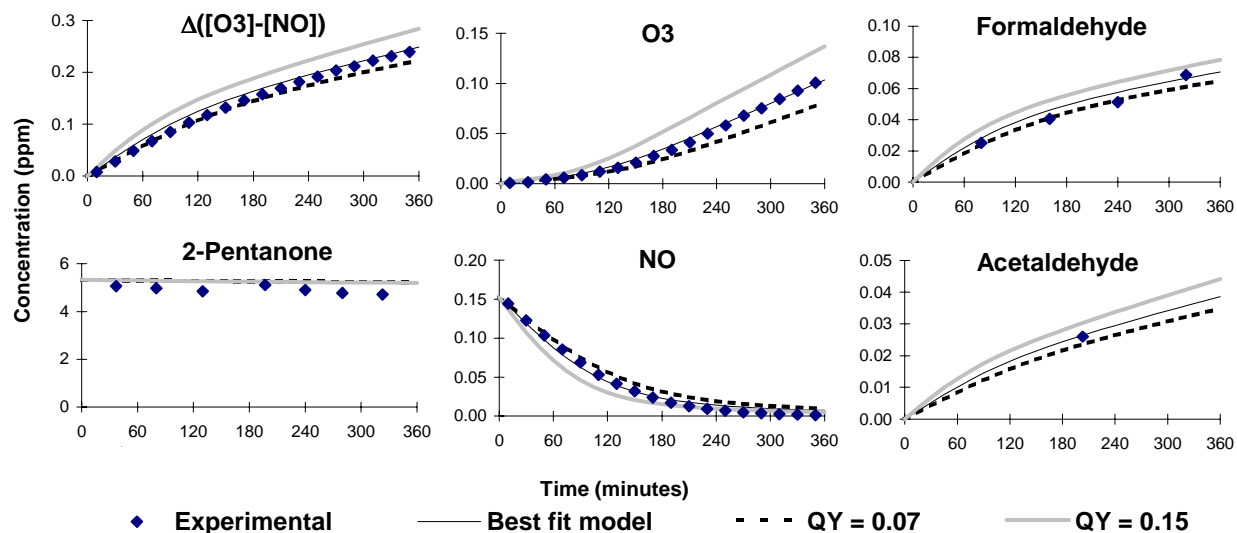


Figure 2. Experimental and calculated results of selected species in the 2-pentanone - NO_x experiment.

and in the initial stages of the mini-surrogate run. On the other hand, it had negative effects on radical levels in all the reactivity experiments, and negative effects on final O_3 yields in the mini-surrogate and the two low NO_x full surrogate runs. The negative effects on radical levels can be attributed in part to nitrate formation in the peroxy + NO reactions, but the radical and NO_x removal caused by the formation of PAN compounds from the acetyl and higher acyl radicals formed in the OH reactions may be playing a larger role. The NO_x removal effects caused by PAN formation is probably the major reason for the negative O_3 reactivities in the low NO_x full surrogate experiments, where O_3 formation is sensitive to such effects. The positive effects of direct NO to NO_2 conversions is relatively more important in the high NO_x full surrogate experiments, apparently sufficiently so that 2-pentanone has positive effects on O_3 in those experiments.

The results of various model calculations are also shown on Figure 2 and Figure 3. The calculations are shown with three different quantum yields for the overall photolysis of 2-pentanone to show the sensitivity of the results to this parameter. These include (1) the overall quantum yield of 0.15 that gives the best fits to the data for 2-butanone (Carter 2000, Carter et al, 2000); (2) the overall quantum yield of 0.10 that gives the best fit to these data; and (3) the overall quantum yield of 0.07 that was derived from the outdoor chamber data of Wirtz (1999). Figure 3 shows that the results of the reactivity experiments are not very sensitive to this parameter, but that the data are actually slightly better fit using the higher quantum yield that fit the 2-butanone data. However, Figure 2 shows that the single ketone - NO_x experiment is much more sensitive to this parameter, and that the higher quantum yield causes a non-negligible overprediction of NO oxidation and O_3 formation rates, while the lower quantum yield of Wirtz (1999) causes a slight underprediction.

It would have been better, however, had more single ketone - NO_x experiments been carried out, to minimize possible biases being introduced into the adjustment by run-to-run variability. However, as discussed by Carter (2000), the adjusted quantum yield determined from this experiment is consistent with the quantum yields adjusted to fit the data for other ketones (including 2-heptanone, discussed below), which indicate a monotonic decline in overall quantum yield with the size of the molecule.

The best fit mechanism gives good simulations of the results of the reactivity experiments, and correctly predicts how the impacts of 2-pentanone affect NO oxidation and O₃ formation rates and peak O₃ yields under various conditions, and how it affects overall radical levels. It also gives reasonably good predictions of the formaldehyde and acetaldehyde yields in the 2-pentanone - NO_x and the reactivity experiments, as shown on the figures. This mechanism was used in the atmospheric reactivity calculations discussed later in this report.

2-Heptanone Experiments

As shown on Table 6 and Table 7, three incremental reactivity experiments were carried out with 2-heptanone, one using each of the three types of base case experiments, and a single 2-heptanone - NO_x experiment was also carried out. The result are summarized on Table 7 and concentration-time plots of the selected species in the 2-pentanone - NO_x experiment are shown on Figure 4, and major results of the reactivity experiments are shown on Figure 5. Results of model calculations using various overall quantum yields for the photolysis reaction are also shown in the figures.

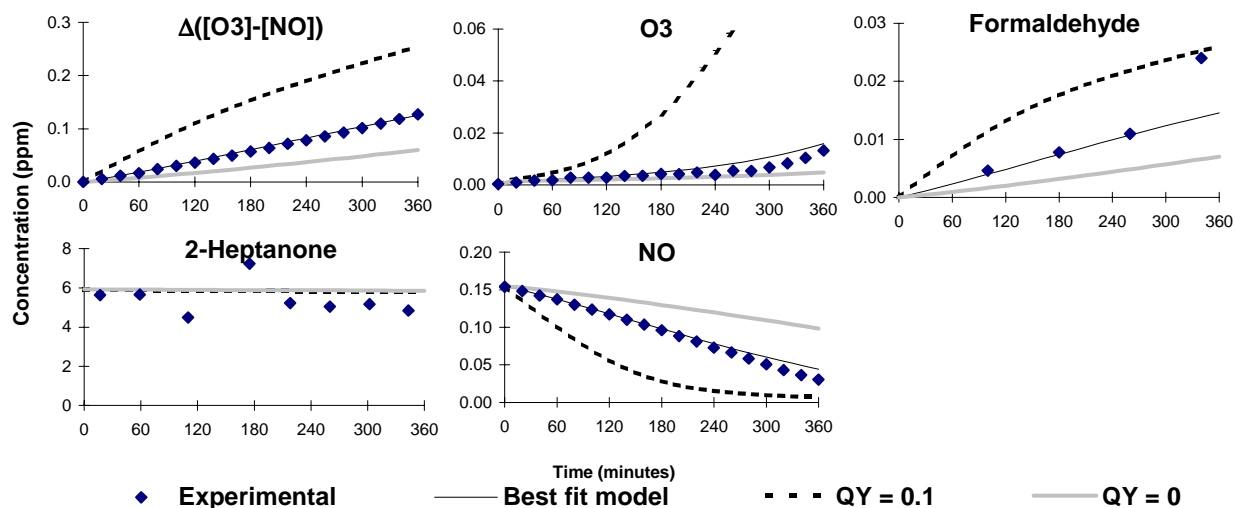


Figure 4. Experimental and calculated results of selected species in the 2-heptanone - NO_x experiment.

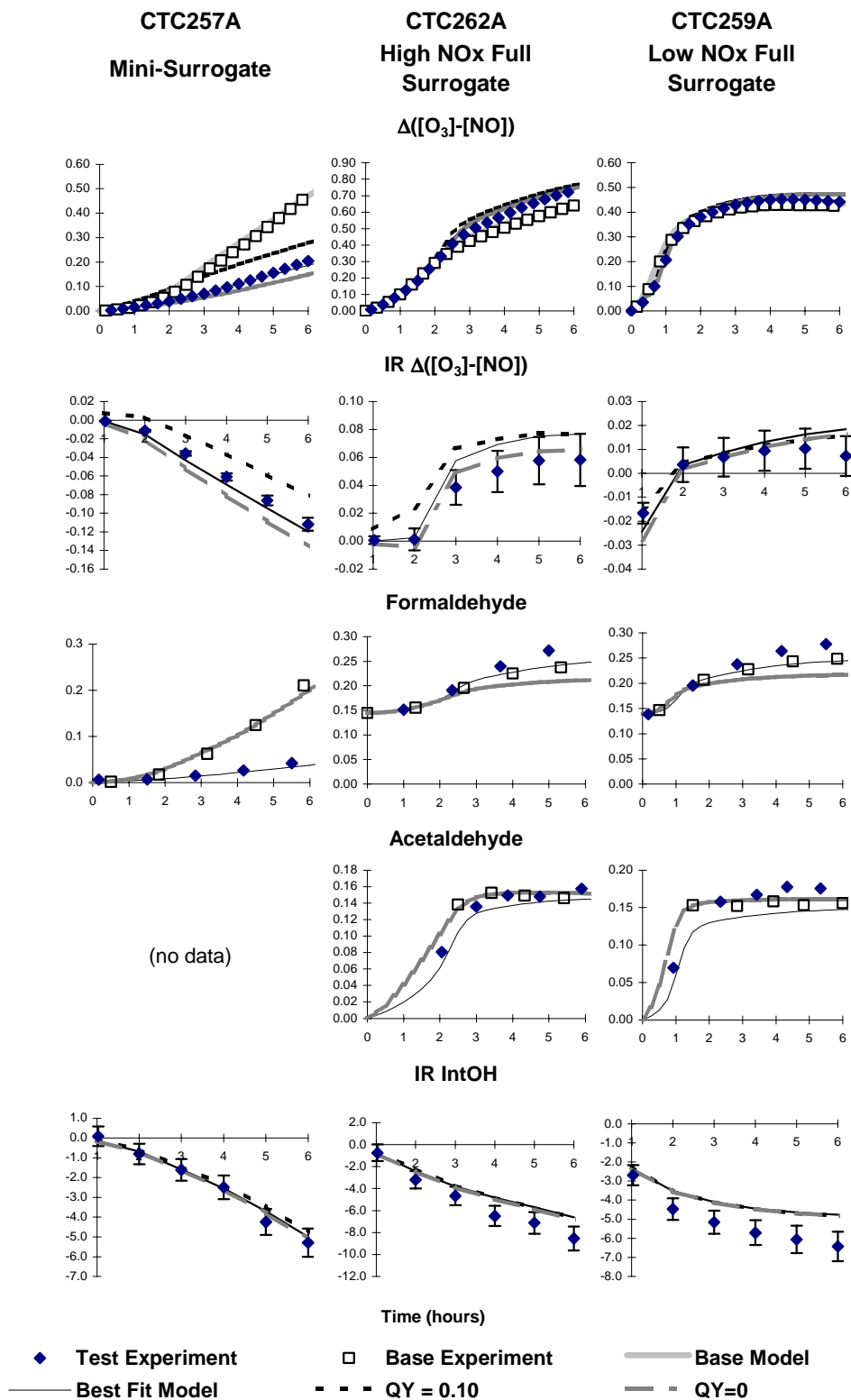


Figure 5. Selected experimental and calculated results of the incremental reactivity experiments with 2-heptanone. (Only the best fit model is shown for formaldehyde and acetaldehyde.)

2-Heptanone was less reactive than 2-pentanone in some respects and more reactive in others. Despite having similar initial ketone present, the 2-heptanone - NO_x run had significantly lower NO oxidation and O₃ formation rates than the 2-pentanone - NO_x experiment, and 2-heptanone had a much greater inhibiting effect on NO oxidation and O₃ formation in the mini-surrogate run. It also more negative IntOH reactivities than 2-pentanone in all the reactivity experiments. On the other hand, the $\Delta([\text{O}_3]-[\text{NO}])$ incremental reactivity of 2-heptanone was somewhat greater than that of 2-pentanone at the end of the high NO_x full surrogate experiments. In addition, unlike 2-pentanone, 2-heptanone had a positive effect on the final O₃ in the low NO_x full surrogate runs.

The lower reactivity of 2-heptanone in the ketone - NO_x and the mini-surrogate experiment, and its more negative IntOH reactivities, can be attributed to the much higher nitrate formation in the overall 2-heptanone mechanism than is the case for 2-pentanone. (The overall nitrate yield in the OH + 2-heptanone mechanism is almost 20%, while that in the best fit 2-pentanone mechanism is only 6.5%.) In addition, the best fit mechanism has a lower quantum yield for 2-heptanone photolysis. On the other hand, 2-heptanone has much lower yield of PAN precursor radicals in the OH reaction than does 2-pentanone (only ~30% for 2-heptanone compared to almost 80% for 2-pentanone). This lower overall PAN precursor yield means that there are less NO_x removal processes in the 2-heptanone mechanism, which means it has less O₃ inhibition under low NO_x conditions. In the case of 2-heptanone, the NO to NO₂ conversions caused by the direct reactions are sufficient to cause positive effects on O₃ in the low NO_x as well as the high NO_x full surrogate experiments.

2-Heptanone formed a measurable amount of formaldehyde in the 2-heptanone - NO_x experiment and increased the formaldehyde levels in the full surrogate runs, consistent with the data indicating it is formed as a product. The inhibition of formaldehyde in the mini-surrogate run is due to the radical inhibition characteristics of 2-heptanone decreasing formaldehyde formation from the ethene in the base surrogate mixture, which apparently is more important than the formaldehyde formed in the direct reactions of 2-heptanone. A slight increase in acetaldehyde levels was observed in the full surrogate experiments, but it was not observed in the mini-surrogate or the ketone - NO_x runs.

The results of model calculations with varying overall quantum yields are also shown on the figures. In addition to calculations with the best fit quantum yield of 0.02, calculations using the overall quantum yield that best fit the 2-pentanone data (0.1) and assuming an overall quantum yield of zero are also shown. Figure 4 shows that this variation has a significant effect on the results of the simulations of the 2-heptanone - NO_x experiment, and that the overall quantum yield for 2-heptanone is clearly much less than that for 2-pentanone but also clearly not zero. Although the model simulations of the reactivity experiments are less sensitive to the overall quantum yield than those for the single ketone run, the mini-surrogate reactivity experiments is also better fit using a quantum yield less than that for 2-pentanone and more than zero.

The model with the best fit overall quantum yields gives very good fits to the results of the ketone - NO_x and the reactivity experiments, as is shown on the figures. The model gives good predictions on

how 2-heptanone affects NO oxidation and O₃ formation rates peak O₃ yields, and formation of formaldehyde and acetaldehyde, and how these effects vary with experimental conditions. This mechanism was used in the atmospheric reactivity simulations discussed in the following section.

ATMOSPHERIC REACTIVITY CALCULATIONS

Incremental reactivities of VOCs have been shown to be highly dependent on environmental conditions, so reactivities measured in environmental chamber experiments cannot necessarily be assumed to be the same as those under atmospheric conditions (Carter and Atkinson, 1989; Carter et al, 1995b). Because of this, the only method available to obtain quantitative estimates of incremental reactivities of VOCs in ambient air pollution episodes is to conduct airshed model simulations of the episodes. Since these simulations cannot be any more reliable than the chemical mechanisms used, the major objective of this program was to assess the reliability of the mechanisms for the compounds of interest for use in such calculations. As discussed above, the results of this study suggest that the mechanisms developed for this study serve as an appropriate basis for estimating the effects of these compounds on ozone under atmospheric conditions. The atmospheric reactivity estimates based on these mechanisms are discussed in this section.

Note that Carter (2000) already gives reactivity estimates for the three compounds studied in this program, calculated using the same (SAPRC-99) mechanism. In addition, the mechanisms used for 2-pentanone and 2-heptanone are the same as used by Carter (2000), and consequently the atmospheric reactivities will be the same. However, some adjustments were made to the isopropyl acetate mechanism in the process of preparing this report that were not incorporated in the mechanism used by Carter (2000), so the reactivities calculated for this compound will be slightly different. The effect of this change is relatively minor, as can be seen in the results presented below.

Scenarios Used for Reactivity Assessment

The set of airshed scenarios employed to assess the reactivities for this study is the same as those used for calculating the MIR and other reactivity scales in our previous work (Carter, 1994a), and also in the update using the SAPRC-99 mechanism (Carter, 2000). These scenarios, and the reasons for using them, are briefly described below.

The objective is to use a set of scenarios which represents, as much as possible, a comprehensive distribution of the environmental conditions where unacceptable levels of ozone are formed. Although a set of scenarios has not been developed for the specific purpose of VOC reactivity assessment, the EPA developed an extensive set of scenarios for conducting analyses of effects of ROG and NO_x controls on ozone formation using the EKMA modeling approach (Gipson et al. 1981; Gipson and Freas, 1983; EPA, 1984; Gery et al. 1987; Baugues, 1990). The EKMA approach involves the use of single-cell box models to simulate how the ozone formation in one day episodes is affected by changes in ROG and NO_x inputs. Although single-cell models cannot represent realistic pollution episodes in great detail, they can represent dynamic injection of pollutants, time-varying changes of inversion heights, entrainment of pollutants from aloft as the inversion height raises, and time-varying photolysis rates, temperatures, and humidities (Gipson and Freas, 1981; EPA, 1984; Gipson, 1984; Hogo and Gery, 1988). Thus, they can be

used to simulate a wide range of the chemical conditions which affect ozone formation from ROG and NO_x, and which affect VOC reactivity. Therefore, at least to the extent they are suitable for their intended purpose, an appropriate set of EKMA scenarios should also be suitable for assessing reactivities over a wide range of conditions.

Base Case Scenarios

The set of EKMA scenarios used in this study were developed by the United States EPA for assessing how various ROG and NO_x control strategies would affect ozone nonattainment in various areas of the country (Baugues, 1990). The characteristics of these scenarios and the methods used to derive their input data are described in more detail elsewhere (Baugues, 1990; Carter, 1994b). Briefly, 39 urban areas in the United States were selected based on geographical representativeness of ozone nonattainment areas and data availability, and a representative high ozone episode was selected for each. The initial non-methane organic carbon (NMOC) and NO_x concentrations, the aloft O₃ concentrations, and the mixing height inputs were based on measurement data for the various areas, the hourly emissions in the scenarios were obtained from the National Acid Precipitation Assessment Program emissions inventory (Baugues, 1990), and biogenic emissions were also included. Table 8 gives a summary of the urban areas represented and other selected characteristics of the scenarios.

Several changes to the scenario inputs were made based on discussions with the California ARB staff and others (Carter, 1994a,b). Two percent of the initial NO_x and 0.1% of the emitted NO_x in all the scenarios was assumed to be in the form of HONO. The photolysis rates were calculated using solar light intensities and spectra calculated by Jeffries (1991) for 640 meters, the approximate mid-point of the mixed layer during daylight hours. The composition of the non methane organic pollutants entrained from aloft was based on the analysis of Jeffries et al. (1989). The composition of the initial and emitted reactive organics was derived as discussed below. Complete listings of the input data for the scenarios are given elsewhere (Carter, 1994b).

This set of 39 EKMA scenarios are referred to as “base case” to distinguish them from the scenarios derived from them by adjusting NO_x inputs to yield standard conditions of NO_x availability as discussed below. No claim is made as to the accuracy of these scenarios in representing any real episode, but they are a result of an effort to represent, as accurately as possible given the available data and the limitations of the formulation of the EKMA model, the range of conditions occurring in urban areas throughout the United States. When developing general reactivity scales it is more important that the scenarios employed represent a realistic distribution of chemical conditions than accurately representing the details of any one particular episode.

The Base ROG mixture is the mixture of reactive organic gases used to represent the chemical composition of the initial and emitted anthropogenic reactive organic gases from all sources in the scenarios. Consistent with the approach used in the original EPA scenarios, the same mixture was used for all scenarios. The speciation for this mixture was derived by Croes (1991) based on an analysis of the EPA database (Jeffries et al. 1989) for the hydrocarbons and the 1987 Southern California Air Quality

Table 8. Summary of the conditions of the scenarios used for atmospheric reactivity assessment.

Scenario		Max O ₃ (ppb)	Max 8- Hr Avg O ₃ (ppb)	ROG / NO _x	NO _x / MOIR NO _x	Height (kM)	Init., Emit ROG (m. mol m ⁻²)	O ₃ aloft (ppb)	Integrated OH (ppt-min)
Avg.	MIR	187	119	3.1	1.5	1.8	15	70	128
Cond.	MOIR	239	165	4.5	1.0	1.8	15	70	209
	EBIR	227	172	6.4	0.7	1.8	15	70	210
Base	Atlanta, GA	179	132	7.3	0.7	2.1	12	63	200
Case	Austin, TX	175	144	9.3	0.5	2.1	11	85	179
	Baltimore, MD	334	215	5.2	1.1	1.2	17	84	186
	Baton Rouge, LA	241	173	6.8	0.9	1.0	11	62	186
	Birmingham, AL	244	202	6.9	0.5	1.8	13	81	208
	Boston, MA	197	167	6.5	0.6	2.6	14	105	262
	Charlotte, NC	143	126	7.8	0.3	3.0	7	92	212
	Chicago, IL	278	226	11.6	0.5	1.4	25	40	164
	Cincinnati, OH	205	153	6.4	0.7	2.8	17	70	220
	Cleveland, OH	252	179	6.6	0.9	1.7	16	89	187
	Dallas, TX	208	141	4.7	1.2	2.3	18	75	176
	Denver, CO	204	139	6.3	1.1	3.4	29	57	143
	Detroit, MI	246	177	6.8	0.7	1.8	17	68	235
	El Paso, TX	182	135	6.6	1.0	2.0	12	65	138
	Hartford, CT	172	144	8.4	0.5	2.3	11	78	220
	Houston, TX	312	217	6.1	0.9	1.7	25	65	225
	Indianapolis, IN	212	148	6.6	0.9	1.7	12	52	211
	Jacksonville, FL	155	115	7.6	0.6	1.5	8	40	206
	Kansas City, MO	159	126	7.1	0.6	2.2	9	65	233
	Lake Charles, LA	286	209	7.4	0.6	0.5	7	40	233
	Los Angeles, CA	568	406	7.6	1.0	0.5	23	100	134
	Louisville, KY	212	155	5.5	0.8	2.5	14	75	260
	Memphis, TN	229	180	6.8	0.6	1.8	15	58	249
	Miami, FL	132	111	9.6	0.4	2.7	9	57	181
	Nashville, TN	167	138	8.0	0.4	1.6	7	50	225
	New York, NY	365	294	8.1	0.7	1.5	39	103	159
	Philadelphia, PA	247	169	6.2	0.9	1.8	19	53	227
	Phoenix, AZ	277	193	7.6	1.0	3.3	40	60	153
	Portland, OR	166	126	6.5	0.7	1.6	6	66	233
	Richmond, VA	242	172	6.2	0.8	1.9	16	64	217
	Sacramento, CA	204	142	6.6	0.8	1.1	7	60	209
	St Louis, MO	324	209	6.1	1.1	1.6	26	82	176
	Salt Lake City, UT	186	150	8.5	0.6	2.2	11	85	182
	San Antonio, TX	133	98	3.9	1.0	2.3	6	60	192
San Diego, CA	193	150	7.1	0.9	0.9	8	90	146	
San Francisco, CA	229	126	4.8	1.8	0.7	25	70	61	
Tampa, FL	230	153	4.4	1.0	1.0	8	68	211	
Tulsa, OK	231	160	5.3	0.9	1.8	15	70	264	
Washington, DC	283	209	5.3	0.8	1.4	13	99	239	

Study (SCAQS) database for the oxygenates (Croes et al. 1994; Lurmann and Main. 1992). This mixture consists of 52% (by carbon) alkanes, 15% alkenes, 27% aromatics, 1% formaldehyde, 2% higher aldehydes, 1% ketones, and 2% acetylene. The detailed composition of this mixture is given elsewhere (Carter, 1994b; Carter, 2000).

Adjusted NO_x scenarios

Incremental reactivities in the base case scenarios would be expected to vary widely, since incremental reactivities depend on the ROG/NO_x ratio, and that ratio varies widely among the base case scenarios. To obtain reactivity scales for specified NO_x conditions, separate scenarios, designated MIR (for maximum incremental reactivity), MOIR (for maximum ozone incremental reactivity), and Equal Benefit Incremental Reactivity (EBIR) were developed (Carter, 1994a). In the MIR scenarios, the NO_x inputs were adjusted so the base ROG mixture (and most other VOCs) have their highest incremental reactivity. This is representative of the highest NO_x conditions of relevance to VOC reactivity assessment because at higher NO_x levels O₃ yields become significantly suppressed, but is also the condition where O₃ is most sensitive to VOC emissions. In the MOIR scenarios, the NO_x inputs were adjusted to yield the highest ozone concentration. In the EBIR scenarios, the NO_x inputs were adjusted so that the relative effects of NO_x reductions and total ROG reductions on peak ozone levels were equal. This represents the lowest NO_x condition of relevance for VOC reactivity assessment, because O₃ formation becomes more sensitive to NO_x emissions than VOC emissions at lower NO_x levels. As discussed by Carter (1994a) the MIR and EBIR ROG/NO_x ratios are respectively ~1.5 and ~0.7 times those for the MOIR scenarios in all cases.

NO_x Conditions in the Base Case Scenarios

The variability of ROG/NO_x ratios in the base case scenarios suggests a variability of reactivity characteristics in those scenarios. However, as discussed previously (Carter, 1994a), the ROG/NO_x ratio is also variable in the MIR or MOIR scenarios, despite the fact that the NO_x inputs in these scenarios are adjusted to yield a specified reactivity characteristic. Thus, the ROG/NO_x ratio, by itself, is not necessarily a good predictor of reactivity characteristics of a particular scenario. The NO_x/NO_x^{MOIR} ratio is a much better predictor of this, with values greater than 1 indicating relatively high NO_x conditions where ozone formation is more sensitive to VOCs, and values less than 1 indicating NO_x-limited conditions. NO_x/NO_x^{MOIR} ratios less than 0.7 represent conditions where NO_x control is a more effective ozone control strategy than ROG control (Carter, 1994a). Note that more than half of the base case scenarios represent NO_x-limited conditions, and ~25% of them represent conditions where NO_x control is more beneficial than VOC control. A relatively small number of scenarios represent MIR or near MIR conditions. However, as discussed elsewhere (Carter, 1994a), this set of scenarios is based on near-worst-case conditions for ozone formation in each of the airsheds. Had scenarios representing less-than-worst-case conditions been included, one might expect a larger number of MIR or near MIR scenarios. This is because NO_x is consumed more slowly on days with lower light intensity or temperature, and thus the scenario is less likely to become NO_x-limited.

Quantification of Atmospheric Reactivity

The reactivity of a VOC in an airshed scenario is measured by its incremental reactivity. For ambient scenarios, this is defined as the change in ozone caused by adding the VOC to the emissions, divided by the amount of VOC added, calculated for sufficiently small amounts of added VOC that the incremental reactivity is independent of the amount added¹.

$$\text{IR}(\text{VOC}, \text{Scenario}) = \lim_{\text{VOC} \rightarrow 0} \left[\frac{\text{O}_3(\text{Scenario with VOC}) - \text{O}_3(\text{Base Scenario})}{\text{Amount of VOC Added}} \right] \quad (\text{IV})$$

The specific calculation procedure is discussed in detail elsewhere (Carter, 1994a,b).

Incremental reactivities derived as given above tend to vary from scenario to scenario because they differ in their overall sensitivity of O₃ formation to VOCs. These differences can be factored out to some extent by using “relative reactivities”, which are defined as ratios of incremental reactivities to the incremental reactivity of the base ROG mixture, which is used to represent emissions of reactive VOCs from all sources.

$$\text{RR}(\text{VOC}, \text{Scenario}) = \frac{\text{IR}(\text{VOC}, \text{Scenario})}{\text{IR}(\text{Base ROG}, \text{Scenario})} \quad (\text{V})$$

These relative reactivities can also be thought of as the relative effect on O₃ of controlling emissions of the particular VOC by itself, compared to controlling emissions from all VOC sources equally. Thus, they are more meaningful in terms of control strategy assessment than absolute reactivities, which can vary greatly depending on the episode and local meteorology.

In addition to depending on the VOC and the scenario, the incremental and relative reactivities depend on how the amounts of VOC added are quantified. In this work, this is quantified on a mass basis, since this is how VOCs are regulated, and generally approximates how VOC substitutions are made in practice. Note that relative reactivities will be different if they are quantified on a molar basis, with VOCs with higher molecular weight having higher reactivities on a mole basis than a gram basis.

Relative reactivities can also depend significantly on how ozone impacts are quantified (Carter, 1994a). Two different ozone quantification methods are used in this work, as follows:

“Ozone Yield” reactivities measure the effect of the VOC on the total amount of ozone formed in the scenario at the time of its maximum concentration. Incremental reactivities are quantified as grams O₃ formed per gram VOC added. Most previous recent studies of ozone reactivity (Dodge, 1984; Carter and

¹ Note that this differs from how the term “incremental reactivity” is used in the context of chamber experiments. In that case, the incremental reactivity refers to the relative change observed in the individual experiments, which in general depends on the amount added.

Atkinson, 1987, 1989, Chang and Rudy, 1990; Jeffries and Crouse, 1991) have been based on this quantification method. The MIR, MOIR, and EBIR scales of Carter (1994a) also use this quantification.

“Maximum 8 Hour Average” reactivities measure the effect of the VOC on the average ozone concentration during the 8-hour period when the average ozone concentration was the greatest, which in these one-day scenarios was the last 8 hours of the simulation. This provides a measure of ozone impact that is more closely related to the new Federal ozone standard that is given in terms of an 8 hour average. This quantification is used for relative reactivities in this work.

In previous reports, we have reported reactivities in terms of integrated O₃ over a standard concentration of 0.09 or 0.12 ppm. This provides a measure of the effect of the VOC on exposure to unacceptable levels of ozone. This is replaced by the maximum 8 hour average reactivities because it is more representative of the proposed new Federal ozone standard and because reactivities relative to integrated O₃ over a standard tend to be between those relative to ozone yield and those relative to 8-hour averages. Therefore, presenting both ozone yield and maximum 8-hour average relative reactivities should be sufficient to provide information on how relative reactivities vary with ozone quantification method. Incremental reactivities are quantified as ppm O₃ per milligram VOC emitted per square meter, but maximum 8 hour average reactivities are usually quantified as relative reactivities quantified on a mass basis.

Note that incremental reactivities are calculated for a total of 156 scenarios, consisting of the 39 base case scenarios and the three adjusted NO_x scenarios for each of the 39 base case scenarios. However, the incremental reactivities in the MIR, MOIR, or EBIR) scales are reported as averages of the incremental reactivities in the corresponding adjusted NO_x scenarios, because adjusting the NO_x conditions reduces the scenario variability, and this allows for a derivation single reactivity scales representing each type of NO_x condition. On the other hand, the individual scenario results will be shown for the base case scenarios, to give an indication of the scenario-to-scenario variability of the calculated reactivity results.

Results

Table 9 lists the ozone yield incremental reactivities calculated the three compounds studied for this program, ethane, and the mixture of emitted reactive organic compounds (the base ROG). The isopropyl acetate results on Table 9 are shown for both the adjusted mechanism developed in this work (“New”) and for the version of the mechanism used by Carter (2000) (“SAPRC-99”). Table 10 gives the ozone yield and maximum 8-hour average reactivities relative to the base ROG for these compounds. Ethane is chosen for comparison because it has been used by the EPA as the informal standard to determine “negligible” reactivity for VOC exemption purposes (Dimitriades, 1999). If a compound has less of an ozone impact than ethane in most or all the scenarios, it might be considered for exemption from regulation as an ozone precursor.

Table 9. Atmospheric incremental calculated for the base ROG mixture, ethane, isopropyl acetate, 2-pentanone and 2-heptanone.

Scenario		Incremental Reactivities (gm O3 / gm VOC)					
		Base ROG	Ethane	Isopropyl Acetate		2-C ₅ -Ket	2-C ₇ -Ket
				New	SAPRC-99		
Adj'd	Max React	3.71	0.31	1.12	1.24	3.07	2.80
NOx	Max Ozone	1.46	0.20	0.62	0.65	1.50	1.40
	Equal Benefit	0.85	0.15	0.44	0.44	1.02	0.93
Base	Average	1.03	0.15	0.48	0.49	1.13	1.02
Case	St.Dev	0.42	0.04	0.11	0.13	0.34	0.34
	ATL GA	0.82	0.13	0.43	0.43	0.94	0.81
	AUS TX	0.63	0.12	0.37	0.36	0.85	0.72
	BAL MD	1.59	0.20	0.64	0.67	1.61	1.53
	BAT LA	0.85	0.11	0.44	0.44	0.83	0.68
	BIR AL	0.72	0.16	0.40	0.42	1.09	1.02
	BOS MA	0.72	0.14	0.40	0.40	0.93	0.88
	CHA NC	0.53	0.11	0.32	0.31	0.78	0.67
	CHI IL	0.26	0.07	0.25	0.23	0.49	0.35
	CIN OH	1.12	0.20	0.52	0.54	1.39	1.37
	CLE OH	1.17	0.15	0.54	0.55	1.22	1.11
	DAL TX	2.14	0.23	0.77	0.84	1.95	1.71
	DEN CO	1.66	0.15	0.64	0.67	1.41	1.20
	DET MI	0.98	0.18	0.47	0.48	1.22	1.20
	ELP TX	1.45	0.14	0.57	0.60	1.33	1.09
	HAR CT	0.77	0.16	0.40	0.40	1.06	0.97
	HOU TX	1.10	0.17	0.51	0.53	1.22	1.13
	IND IN	1.24	0.18	0.56	0.57	1.32	1.20
	JAC FL	0.67	0.11	0.39	0.38	0.75	0.59
	KAN MO	1.07	0.20	0.49	0.51	1.36	1.35
	LAK LA	0.42	0.09	0.33	0.32	0.54	0.39
	LOS CA	0.76	0.08	0.35	0.35	0.69	0.59
	LOU KY	1.24	0.22	0.59	0.61	1.42	1.30
	MEM TN	0.76	0.15	0.43	0.43	0.98	0.88
	MIA FL	0.49	0.10	0.32	0.30	0.68	0.49
	NAS TN	0.67	0.15	0.38	0.39	0.99	0.82
	NEW NY	0.39	0.07	0.32	0.29	0.43	0.40
	PHI PA	1.08	0.17	0.51	0.52	1.19	1.12
	PHO AZ	1.46	0.18	0.57	0.61	1.56	1.44
	POR OR	0.96	0.17	0.47	0.48	1.15	1.01
	RIC VA	1.06	0.18	0.50	0.52	1.30	1.28
	SAC CA	1.22	0.19	0.52	0.55	1.40	1.26
	SAI MO	1.38	0.16	0.57	0.59	1.34	1.23
	SAL UT	0.90	0.15	0.44	0.45	1.17	1.06
	SAN TX	1.62	0.21	0.64	0.70	1.67	1.52
	SDO CA	0.85	0.09	0.40	0.41	0.76	0.66
	SFO CA	1.87	0.09	0.45	0.50	1.32	1.08
	TAM FL	1.52	0.19	0.67	0.70	1.44	1.25
	TUL OK	1.17	0.20	0.57	0.58	1.32	1.28
	WAS DC	0.99	0.18	0.49	0.50	1.19	1.14

Table 10. Atmospheric relative reactivities calculated for ethane, isopropyl acetate, 2-pentanone and 2-heptanone.

Scenario		Reactivities relative to the base ROG (mass basis)							
		Ozone Yield				Max 8 Hour Avg			
		Ethane	Ipr-Acet	2-C ₅ -Ket	2-C ₇ -Ket	Ethane	Ipr-Acet	2-C ₅ -Ket	2-C ₇ -Ket
Adj'd	MIR	0.08	0.30	0.82	0.75	0.07	0.28	0.74	0.67
NOx	MOIR	0.13	0.43	1.02	0.94	0.08	0.34	0.76	0.67
	EBIR	0.17	0.53	1.19	1.07	0.10	0.40	0.79	0.67
Base	Average	0.16	0.51	1.16	1.03	0.10	0.40	0.80	0.66
Case	St.Dev	0.04	0.13	0.22	0.19	0.02	0.08	0.10	0.10
	ATL GA	0.16	0.52	1.15	0.99	0.09	0.42	0.76	0.62
	AUS TX	0.19	0.59	1.35	1.14	0.11	0.50	0.82	0.67
	BAL MD	0.12	0.40	1.02	0.96	0.08	0.31	0.77	0.68
	BAT LA	0.13	0.52	0.98	0.81	0.08	0.41	0.69	0.53
	BIR AL	0.22	0.56	1.52	1.41	0.12	0.44	0.97	0.82
	BOS MA	0.20	0.56	1.28	1.22	0.13	0.48	0.93	0.85
	CHA NC	0.21	0.60	1.46	1.25	0.14	0.55	1.03	0.83
	CHI IL	0.28	0.97	1.87	1.32	0.13	0.60	0.89	0.59
	CIN OH	0.18	0.46	1.24	1.23	0.10	0.36	0.84	0.79
	CLE OH	0.13	0.46	1.04	0.95	0.08	0.35	0.75	0.65
	DAL TX	0.11	0.36	0.91	0.80	0.08	0.32	0.74	0.64
	DEN CO	0.09	0.39	0.85	0.72	0.06	0.31	0.67	0.55
	DET MI	0.18	0.48	1.24	1.22	0.10	0.37	0.84	0.77
	ELP TX	0.10	0.39	0.91	0.75	0.07	0.32	0.67	0.53
	HAR CT	0.20	0.52	1.37	1.25	0.12	0.45	0.93	0.78
	HOU TX	0.16	0.47	1.11	1.03	0.09	0.36	0.78	0.69
	IND IN	0.14	0.45	1.07	0.97	0.09	0.35	0.75	0.62
	JAC FL	0.16	0.58	1.11	0.88	0.09	0.44	0.73	0.52
	KAN MO	0.19	0.46	1.27	1.25	0.11	0.39	0.88	0.80
	LAK LA	0.22	0.79	1.28	0.91	0.11	0.55	0.75	0.47
	LOS CA	0.11	0.47	0.92	0.78	0.07	0.34	0.70	0.57
	LOU KY	0.17	0.48	1.15	1.05	0.11	0.41	0.80	0.69
	MEM TN	0.20	0.56	1.28	1.16	0.11	0.43	0.85	0.71
	MIA FL	0.20	0.65	1.40	1.01	0.11	0.52	0.84	0.54
	NAS TN	0.23	0.57	1.47	1.23	0.15	0.52	1.06	0.77
	NEW NY	0.17	0.82	1.10	1.03	0.08	0.44	0.64	0.57
	PHI PA	0.16	0.47	1.11	1.04	0.09	0.37	0.79	0.70
	PHO AZ	0.12	0.39	1.07	0.99	0.08	0.30	0.77	0.66
	POR OR	0.17	0.50	1.21	1.06	0.11	0.44	0.83	0.67
	RIC VA	0.17	0.47	1.22	1.20	0.09	0.36	0.81	0.73
	SAC CA	0.15	0.43	1.15	1.03	0.09	0.35	0.83	0.67
	SAI MO	0.11	0.41	0.97	0.89	0.07	0.32	0.73	0.63
	SAL UT	0.17	0.49	1.30	1.18	0.10	0.37	0.84	0.69
	SAN TX	0.13	0.40	1.03	0.94	0.09	0.35	0.80	0.72
	SDO CA	0.11	0.48	0.90	0.78	0.08	0.38	0.68	0.57
	SFO CA	0.05	0.24	0.71	0.58	0.04	0.23	0.66	0.52
	TAM FL	0.12	0.44	0.94	0.82	0.08	0.36	0.71	0.60
	TUL OK	0.17	0.48	1.12	1.10	0.10	0.36	0.80	0.74
	WAS DC	0.18	0.49	1.20	1.15	0.10	0.38	0.82	0.73

The results show that none of the three compounds studied for this program can be considered to be of negligible ozone impact under the ethane standard informally used by the EPA. Isopropyl acetate is the least reactive of the three compounds studied, but it still forms three to four times more ozone per gram emitted than does ethane. However, isopropyl acetate is still a relatively low reactivity compound, with an ozone impact on a mass basis that is less than half that of the base ROG mixture in most scenarios. The relative ozone impact of isopropyl acetate is lower in the MIR scale or in terms of impacts on the maximum 8-hour average ozone, being approximately 1/3 that of the base ROG by those measured. Since the base ROG represents the mixture of reactive VOC emissions from all sources, this means that regulation of isopropyl acetate emissions is 1/3 to 1/2 as effective in terms of ozone control as regulating emissions of all sources of reactive VOCs equally.

On the other hand, the two ketones studied for this program have comparable ozone impact as the base ROG mixture, suggesting that regulating emissions of these compounds is approximately no more or less effective than regulating emissions of all reactive VOC sources equally. The relative impacts on peak ozone increase slightly as NO_x levels are reduced, but the NO_x dependence is relatively small compared to many other compounds, and there is very little NO_x dependence in terms of impacts on maximum 8-hour average ozone. Clearly these compounds cannot be considered to be negligibly reactive, but it is also not appropriate to consider them as highly reactive and subject them to more stringent controls than other VOCs, at least in terms of ozone control.

The minor adjustments in the isopropyl acetate mechanism in this work compared to the version used to calculate the reactivity scale given by Carter (2000) resulted in about a 9% decrease in its calculated reactivity in the MIR scale, and a smaller change in the lower NO_x scenarios. This is probably due to the slight increase in the number of NO to NO₂ conversions resulting from the adjustment, which involves increasing the relative importance of reaction routes that involve multi-step mechanisms. This is apparently sufficient to offset the slight downward adjustment in the overall nitrate yield, which would tend to increase the predicted reactivity. These ≤10% changes are well within the uncertainty in the overall reactivity estimation method, and should not be regarded as significant.

The higher reactivities of the ketones compared to isopropyl acetate is due primarily to their higher OH radical rate constants, combined with the fact that they also undergo photolysis. The lower mass-based reactivity of 2-heptanone compared to 2-pentanone is due in part to its greater mass and in part to its higher nitrate yields and lower rate of photodecomposition to form radicals. This more than compensates for the fact that 2-heptanone has a slightly higher OH radical rate constant. As discussed by Carter and Atkinson (1989) the sensitivity of the reactivity of a compound to the OH rate constant is relatively low for compounds with relatively high rate constants.

CONCLUSIONS

This program has achieved its objectives in providing data needed to increase our confidence in our ability to predict the atmospheric ozone impacts of the subject compounds under various conditions. The atmospheric reaction mechanisms developed for isopropyl acetate, 2-pentanone and 2-heptanone were found to give good simulations of the effects of these compounds on O₃ formation, NO oxidation rates, and formation of formaldehyde and (for isopropyl acetate) acetone under varying simulated atmospheric conditions. Some adjustments had to be made to the overall nitrate yield in the reaction of OH with isopropyl acetate but the adjustments were small and well within the uncertainty in the estimates. The overall quantum yields for the photolyses of the ketones also had to be adjusted to fit the chamber data, but the adjustments were chemically reasonable, and, as discussed below, provided useful data for developing general estimation methods.

Based on these data, the ozone impacts of isopropyl acetate are estimated to be relatively low, ranging from about 1/2 to 1/3 of the impacts, on a mass basis, of the average of emitted reactive VOCs, depending somewhat on the scenarios and how O₃ impacts are quantified. However, isopropyl acetate would not be considered to have a “negligible” impact under the informal standard currently used by the EPA, since its impact on a mass basis is 3-4 times that of ethane, the compound whose reactivity is currently used as a standard in this regard. Its relative ozone impacts are slightly lower under high NO_x, MIR conditions or in terms of effects on maximum 8-hour average ozone, compared to impacts on peak O₃ yields in lower NO_x scenarios.

The ozone impacts of the two ketones studied for this project were found to be approximately the same, on a mass basis, as the average of emitted reactive VOCs. Their impacts tend to be somewhat less dependent on scenario conditions than most other VOCs, but like isopropyl acetate their relative impacts are slightly lower under high NO_x, MIR conditions or when considering impacts on 8-hour average ozone. Consistent with the trend observed for many homologous series of higher molecular weight compounds (Carter, 1994a, 2000), the mass-based ozone impacts of 2-heptanone are slightly lower than those of 2-pentanone, though only by about 10%.

In a broader perspective, the major contribution of this study has been to provide data that turned out to be useful in developing and evaluating general estimation methods that can be applied to deriving estimated mechanisms for compounds where data are unavailable or limited. Although it would have been better had duplicate experiments been carried out to verify the results, the nitrate yield adjustment for isopropyl acetate provided an additional data point for estimating overall nitrate yields from the reactions of NO with peroxy radicals formed from the reactions of esters and other oxygenated organic compounds. The relatively small adjustment that was made indicated that the SAPRC-99 estimation method performed reasonably well for this compound. These estimation methods also performed reasonably well in predicting apparent nitrate yields for the ketones that were studied, since the estimated nitrate yields did not have to be adjusted to obtain satisfactory fits of model simulations to the chamber data. Although

it might be argued that the adjustment of the overall quantum yield in the ketone photolysis may be compensating for possible errors in the nitrate yield estimates, the overall quantum yield adjustments were found to have relatively minor impacts on predicted results of the reactivity experiments that tend to be sensitive to assumed nitrate yields.

Perhaps the most useful contribution of this study has been to provide useful data for estimating overall quantum yields for radical input in the photolysis of various ketones. The actual mechanism for ketone photolysis in the atmosphere is probably complex and the representation of these processes in the current SAPRC-99 mechanism is almost certainly an oversimplification. However, in terms of the way the mechanism is used, what matters is the ability of the mechanism to overall impacts under atmospheric conditions. Very good fits of model simulations to results of ketone reactivity experiments can be obtained using the simple general ketone photolysis mechanism and an overall photodecomposition quantum yield adjusted to fit results of single ketone - NO_x - air experiments, which turn out to be the most sensitive to this parameter. But the overall photodecomposition quantum yield has to be estimated if there are no data are available for a particular ketone. Under CARB funding, we derived overall quantum yields of 0.15 and 0.05 for methyl ethyl ketone and methyl isobutyl ketone, respectively, which suggest that there may be an effect of the size of the molecule on the overall quantum yield. However, there may be other effects of structure that cannot be determined with only two data points. For this project, we obtained overall quantum yields of 0.1 for methyl propyl ketone and 0.02 for methyl pentyl ketone. Together these four data points indicate a monotonic decrease in overall quantum yield with the size of the molecule, and serve as a basis for the general estimation method incorporated in the SAPRC-99 mechanism. However, data for other ketones would be useful to further evaluate and refine these estimates, and to provide more comprehensive information concerning the photolysis rates and mechanisms of these higher ketones.

REFERENCES

- Atkinson, R. (1989): "Kinetics and Mechanisms of the Gas-Phase Reactions of the Hydroxyl Radical with Organic Compounds," J. Phys. Chem. Ref. Data, Monograph no 1.
- Atkinson, R. (1990): "Gas-Phase Tropospheric Chemistry of Organic Compounds: A Review," Atmos. Environ., 24A, 1-24.
- Atkinson, R. (1991): "Kinetics and Mechanisms of the Gas-Phase Reactions of the NO₃ Radical with Organic Compounds," J. Phys. Chem. Ref. Data, 20, 459-507.
- Atkinson, R. (1994): "Gas-Phase Tropospheric Chemistry of Organic Compounds," J. Phys. Chem. Ref. Data, Monograph No. 2.
- Atkinson, R. (1997): "Gas Phase Tropospheric Chemistry of Volatile Organic Compounds: 1. Alkanes and Alkenes," J. Phys. Chem. Ref. Data, 26, 215-290.
- Atkinson, R., S. M. Aschmann, W. P. L. Carter and J. N. Pitts, Jr. (1982): "Rate constants for the Gas-Phase Reaction of OH Radicals with a Series of Ketones at 299±2 K," Int J. Chem. Kinet. 14, 839, 1982.
- Atkinson, R. and W. P. L. Carter (1984): "Kinetics and Mechanisms of the Gas-Phase Reactions of Ozone with Organic Compounds under Atmospheric Conditions," Chem. Rev. 84, 437-470.
- Atkinson, R. and S. M. Aschmann (1988): J. Phys. Chem. 92, 4008.
- Atkinson, R., E. C. Tuazon and S. M. Aschmann (2000): "Atmospheric Chemistry of 2-pentanone and 2-heptanone," Environ. Sci. Technol., 34, 623-631.
- Baugues, K. (1990): "Preliminary Planning Information for Updating the Ozone Regulatory Impact Analysis Version of EKMA," Draft Document, Source Receptor Analysis Branch, Technical Support Division, U. S. Environmental Protection Agency, Research Triangle Park, NC, January.
- Calvert, J. G., and J. N. Pitts, Jr. (1966): "Photochemistry," John Wiley and Sons, New York.
- CARB (1999) California Air Resources Board, Proposed Regulation for Title 17, California Code of Regulations, Division 3, Chapter 1, Subchapter 8.5, Article 3.1, sections 94560- 94539.
- Carter, W. P. L. (1990): "A Detailed Mechanism for the Gas-Phase Atmospheric Reactions of Organic Compounds," Atmos. Environ., 24A, 481-518.
- Carter, W. P. L. (1994a): "Development of Ozone Reactivity Scales for Volatile Organic Compounds," J. Air & Waste Manage. Assoc., 44, 881-899.
- Carter, W. P. L. (1994b): "Calculation of Reactivity Scales Using an Updated Carbon Bond IV Mechanism," Report Prepared for Systems Applications International Under Funding from the Auto/Oil Air Quality Improvement Research Program, April 12. Available at <http://helium.ucr.edu/~carter/absts.htm#cb4rct>.

- Carter, W. P. L. (2000): "Documentation of the SAPRC-99 Chemical Mechanism for VOC Reactivity Assessment," Report to the California Air Resources Board, Contracts 92-329 and 95-308, May 8. Available at <http://helium.ucr.edu/~carter/absts.htm#saprc99>.
- Carter, W. P. L. and R. Atkinson (1987): "An Experimental Study of Incremental Hydrocarbon Reactivity," *Environ. Sci. Technol.*, 21, 670-679
- Carter, W. P. L. and R. Atkinson (1989): "A Computer Modeling Study of Incremental Hydrocarbon Reactivity", *Environ. Sci. Technol.*, 23, 864.
- Carter, W. P. L., and F. W. Lurmann (1990): "Evaluation of the RADM Gas-Phase Chemical Mechanism," Final Report, EPA-600/3-90-001.
- Carter, W. P. L. and F. W. Lurmann (1991): "Evaluation of a Detailed Gas-Phase Atmospheric Reaction Mechanism using Environmental Chamber Data," *Atm. Environ.* 25A, 2771-2806.
- Carter, W. P. L., J. A. Pierce, I. L. Malkina, D. Luo and W. D. Long (1993): "Environmental Chamber Studies of Maximum Incremental Reactivities of Volatile Organic Compounds," Report to Coordinating Research Council, Project No. ME-9, California Air Resources Board Contract No. A032-0692; South Coast Air Quality Management District Contract No. C91323, United States Environmental Protection Agency Cooperative Agreement No. CR-814396-01-0, University Corporation for Atmospheric Research Contract No. 59166, and Dow Corning Corporation. April 1. Available at <http://helium.ucr.edu/~carter/absts.htm#rct1rept>.
- Carter, W. P. L., J. A. Pierce, D. Luo, and I. L. Malkina (1995a): "Environmental Chamber Studies of Maximum Incremental Reactivities of Volatile Organic Compounds," *Atmos. Environ.* 29, 2499-2511.
- Carter, W. P. L., D. Luo, I. L. Malkina, and J. A. Pierce (1995b): "Environmental Chamber Studies of Atmospheric Reactivities of Volatile Organic Compounds. Effects of Varying ROG Surrogate and NO_x," Final report to Coordinating Research Council, Inc., Project ME-9, California Air Resources Board, Contract A032-0692, and South Coast Air Quality Management District, Contract C91323. March 24. Available at <http://helium.ucr.edu/~carter/absts.htm#rct2rept>.
- Carter, W. P. L., D. Luo, I. L. Malkina, and D. Fitz (1995c): "The University of California, Riverside Environmental Chamber Data Base for Evaluating Oxidant Mechanism. Indoor Chamber Experiments through 1993," Report submitted to the U. S. Environmental Protection Agency, EPA/AREAL, Research Triangle Park, NC., March 20. Available at <http://helium.ucr.edu/~carter/absts.htm#databas>.
- Carter, W. P. L., D. Luo, I. L. Malkina, and J. A. Pierce (1995d): "Environmental Chamber Studies of Atmospheric Reactivities of Volatile Organic Compounds. Effects of Varying Chamber and Light Source," Final report to National Renewable Energy Laboratory, Contract XZ-2-12075, Coordinating Research Council, Inc., Project M-9, California Air Resources Board, Contract A032-0692, and South Coast Air Quality Management District, Contract C91323, March 26. Available at <http://helium.ucr.edu/~carter/absts.htm#explrept>.
- Carter, W. P. L., D. Luo, and I. L. Malkina (1997): "Environmental Chamber Studies for Development of an Updated Photochemical Mechanism for VOC Reactivity Assessment," Final report to the California Air Resources Board, the Coordinating Research Council, and the National Renewable Energy Laboratory, November 26. Available at <http://helium.ucr.edu/~carter/absts.htm#rct3rept>.

- Carter, W. P. L., D. Luo and I. L. Malkina (2000): "Investigation of Atmospheric Reactivities of Selected Consumer Product VOCs," Report to California Air Resources Board, May 30. Available at <http://helium.ucr.edu/~carter/absts.htm#cpreport>.
- Chang, T. Y. and S. J. Rudy (1990): "Ozone-Forming Potential of Organic Emissions from Alternative-Fueled Vehicles," *Atmos. Environ.*, 24A, 2421-2430.
- Croes, B. E., Technical Support Division, California Air Resources Board, personal communication (1991).
- Croes, B. E., *et al.* (1994): "Southern California Air Quality Study Data Archive," Research Division, California Air Resources Board.
- Dasgupta, P. K, Dong, S. and Hwang, H. (1988): "Continuous Liquid Phase Fluorometry Coupled to a Diffusion Scrubber for the Determination of Atmospheric Formaldehyde, Hydrogen Peroxide, and Sulfur Dioxide," *Atmos. Environ.* 22, 949-963.
- Dasgupta, P.K, Dong, S. and Hwang, H. (1990): *Aerosol Science and Technology* 12, 98-104
- Dimitriades, B. (1999): "Scientific Basis of an Improved EPA Policy on Control of Organic Emissions for Ambient Ozone Reduction," *J. Air & Waste Manage. Assoc.* 49, 831-838
- Dodge, M. C. (1984): "Combined effects of organic reactivity and NMHC/NO_x ratio on photochemical oxidant formation -- a modeling study," *Atmos. Environ.*, 18, 1657.
- EPA (1984): "Guideline for Using the Carbon Bond Mechanism in City-Specific EKMA," EPA-450/4-84-005, February.
- Gery, M. W., R. D. Edmond and G. Z. Whitten (1987): "Tropospheric Ultraviolet Radiation. Assessment of Existing Data and Effects on Ozone Formation," Final Report, EPA-600/3-87-047, October.
- Gipson, G. L., W. P. Freas, R. A. Kelly and E. L. Meyer (1981): "Guideline for Use of City-Specific EKMA in Preparing Ozone SIPs, EPA-450/4-80-027, March.
- Gipson, G. L. and W. P. Freas (1983): "Use of City-Specific EKMA in the Ozone RIA," U. S. Environmental Protection Agency, July.
- Johnson, G. M. (1983): "Factors Affecting Oxidant Formation in Sydney Air," in "The Urban Atmosphere -- Sydney, a Case Study." Eds. J. N. Carras and G. M. Johnson (CSIRO, Melbourne), pp. 393-408.
- Jeffries, H. E. (1991): "UNC Solar Radiation Models," unpublished draft report for EPA Cooperative Agreements CR813107, CR813964 and CR815779".
- Jeffries, H. E., K. G. Sexton, J. R. Arnold, and T. L. Kale (1989): "Validation Testing of New Mechanisms with Outdoor Chamber Data. Volume 2: Analysis of VOC Data for the CB4 and CAL Photochemical Mechanisms," Final Report, EPA-600/3-89-010b.
- Jeffries, H. E. and R. Crouse (1991): "Scientific and Technical Issues Related to the Application of Incremental Reactivity. Part II: Explaining Mechanism Differences," Report prepared for Western States Petroleum Association, Glendale, CA, October.

- Kerr, J. A. and D. W. Stocker (1994): *J. Atmos. Chem.* 4, 253.
- Kwok, E. S. C., and R. Atkinson (1995): "Estimation of Hydroxyl Radical Reaction Rate Constants for Gas-Phase Organic Compounds Using a Structure-Reactivity Relationship: An Update," *Atmos. Environ* 29, 1685-1695.
- Kwok, E. S. C., S. Aschmann, and R. Atkinson (1996): "Rate Constants for the Gas-Phase Reactions of the OH Radical with Selected Carbamates and Lactates," *Environ. Sci. Technol* 30, 329-334.
- Lurmann, F. W. and H. H. Main (1992): "Analysis of the Ambient VOC Data Collected in the Southern California Air Quality Study," Final Report to California Air Resources Board Contract No. A832-130, February.
- McBride, S., M. Oravetz, and A.G. Russell. 1997. "Cost-Benefit and Uncertainty Issues Using Organic Reactivity to Regulate Urban Ozone." *Environ. Sci. Technol.* 35, A238-44.
- RRWG (1999): "VOC Reactivity Policy White Paper," Prepared by the Reactivity Research Work Group Policy Team, October 1. Available at <http://www.cgenv.com/Narsto/reactinfo.html>.
- Tuazon, E. C., S. M. Aschmann, R. Atkinson, and W. P. L. Carter (1998): "The reactions of Selected Acetates with the OH radical in the Presence of NO: Novel Rearrangement of Alkoxy Radicals of Structure RC(O)OCH(O.)R", *J. Phys. Chem A* 102, 2316-2321.
- Wallington, T. J. and M. J. Kurylo (1987): "Flash Photolysis Resonance Fluorescence Investigation of the Gas-Phase Reactions of OH Radicals with a Series of Aliphatic Ketones over the Temperature Range 240-440 K," *J. Phys. Chem* 91, 5050-5054.
- Wallington, T. J., P. Dagaut, R. Liu, and M. J. Kurylo (1988): "The Gas Phase Reactions of Hydroxyl Radicals with a Series of Esters Over the Temperature Range 240-440 K," *Int. J. Chem. Kinet.* 20, 177.
- Wirtz, K. (1999): "Determination of Photolysis Frequencies and Quantum Yields for Small Carbonyl Compounds using the EUPHORE Chamber," Presented at the US/German - Environmental Chamber Workshop, Riverside, California, October 4-6.
- Zafonte, L., P. L. Rieger, and J. R. Holmes (1977): "Nitrogen Dioxide Photolysis in the Los Angeles Atmosphere," *Environ. Sci. Technol.* 11, 483-487.

APPENDIX A.
MECHANISM LISTING AND TABULATIONS

This Appendix gives a complete listing of the mechanisms used in the model simulations in this report. Table A-1 contains a list of all the model species used in the mechanism, and Table A-2 lists the reactions and rate parameters, and Table A-3 lists the absorption cross sections and quantum yields for the photolysis reactions. In addition, Finally, Table A-4 gives the chamber-dependent parameters used in the model simulations of the chamber experiments.

Table A-1. Listing of the model species in the mechanism used in the model simulations discussed in this report.

Type and Name	Description
<u>Species used in Base Mechanism</u>	
<u>Constant Species.</u>	
O2	Oxygen
M	Air
H2O	Water
H2	Hydrogen Molecules
HV	Light
<u>Active Inorganic Species.</u>	
O3	Ozone
NO	Nitric Oxide
NO2	Nitrogen Dioxide
NO3	Nitrate Radical
N2O5	Nitrogen Pentoxide
HONO	Nitrous Acid
HNO3	Nitric Acid
HNO4	Peroxynitric Acid
HO2H	Hydrogen Peroxide
CO	Carbon Monoxide
SO2	Sulfur Dioxide
<u>Active Radical Species and Operators.</u>	
HO.	Hydroxyl Radicals
HO2.	Hydroperoxide Radicals
C-O2.	Methyl Peroxy Radicals
RO2-R.	Peroxy Radical Operator representing NO to NO2 conversion with HO2 formation.
R2O2.	Peroxy Radical Operator representing NO to NO2 conversion without HO2 formation.
RO2-N.	Peroxy Radical Operator representing NO consumption with organic nitrate formation.
CCO-O2.	Acetyl Peroxy Radicals
RCO-O2.	Peroxy Propionyl and higher peroxy acyl Radicals
BZCO-O2.	Peroxyacyl radical formed from Aromatic Aldehydes
MA-RCO3.	Peroxyacyl radicals formed from methacrolein and other acroleins.
<u>Steady State Radical Species</u>	
O3P	Ground State Oxygen Atoms
O*1D2	Excited Oxygen Atoms
TBU-O.	t-Butoxy Radicals
BZ-O.	Phenoxy Radicals
BZ(NO2)-O.	Nitro-substituted Phenoxy Radical
HOCOO.	Radical formed when Formaldehyde reacts with HO2
<u>PAN and PAN Analogues</u>	
PAN	Peroxy Acetyl Nitrate
PAN2	PPN and other higher alkyl PAN analogues
PBZN	PAN analogues formed from Aromatic Aldehydes
MA-PAN	PAN analogue formed from Methacrolein
<u>Explicit and Lumped Molecule Reactive Organic Product Species</u>	

Table A-1 (continued)

Type and Name	Description
HCHO	Formaldehyde
CCHO	Acetaldehyde
RCHO	Lumped C3+ Aldehydes
ACET	Acetone
MEK	Ketones and other non-aldehyde oxygenated products which react with OH radicals slower than $5 \times 10^{-12} \text{ cm}^3 \text{ molec}^{-2} \text{ sec}^{-1}$.
MEOH	Methanol
COOH	Methyl Hydroperoxide
ROOH	Lumped higher organic hydroperoxides
GLY	Glyoxal
MGLY	Methyl Glyoxal
BACL	Biacetyl
PHEN	Phenol
CRES	Cresols
NPHE	Nitrophenols
BALD	Aromatic aldehydes (e.g., benzaldehyde)
METHACRO	Methacrolein
MVK	Methyl Vinyl Ketone
ISO-PROD	Lumped isoprene product species
<u>Lumped Parameter Products</u>	
PROD2	Ketones and other non-aldehyde oxygenated products which react with OH radicals faster than $5 \times 10^{-12} \text{ cm}^3 \text{ molec}^{-2} \text{ sec}^{-1}$.
RNO3	Lumped Organic Nitrates
<u>Uncharacterized Reactive Aromatic Ring Fragmentation Products</u>	
DCB1	Reactive Aromatic Fragmentation Products that do not undergo significant photodecomposition to radicals.
DCB2	Reactive Aromatic Fragmentation Products which photolyze with alpha-dicarbonyl-like action spectrum.
DCB3	Reactive Aromatic Fragmentation Products which photolyze with acrolein action spectrum.
<u>Non-Reacting Species</u>	
CO2	Carbon Dioxide
XC	Lost Carbon
XN	Lost Nitrogen
SULF	Sulfates (SO_3 or H_2SO_4)
<u>Low Reactivity Compounds or Unknown Products Represented as Unreactive</u>	
H2	Hydrogen
HCOOH	Formic Acid
CCO-OH	Acetic Acid
RCO-OH	Higher organic acids
CCO-OOH	Peroxy Acetic Acid
RCO-OOH	Higher organic peroxy acids
NROG	Unspecified Unreactive Carbon

Table A-1 (continued)

Type and Name	Description
<u>Base ROG VOC Species used in the Chamber Simulations</u>	
N-C4	n-Butane
N-C6	n-Hexane
N-C8	n-Octane
ETHENE	Ethene
PROPENE	Propene
T-2-BUTE	<i>Trans</i> -2-Butene
TOLUENE	Toluene
M-XYLENE	m-Xylene
<u>Test Compounds Studied for this Project</u>	
IPR-ACET	Isopropyl Acetate
MPK	2-Pentanone (methyl propyl ketone)
C7-KET-2	2-Heptanone
<u>Major Reactive Products from 2-Heptanone not in Base Mechanism</u>	
PRD1	Aldehydes formed in the OH reaction. These are 23% CH ₃ CH(OH)CH ₂ CH ₂ CHO, 31% CH ₃ C(O)CH ₂ CHO, 19% CH ₃ CH ₂ CH ₂ CHO and 20% CH ₃ CH ₂ CH ₂ CH ₂ CHO
PRD2	Other reactive oxygenated products formed in the OH reaction. These are 65% CH ₃ C(O)CH ₂ C(O)CH ₂ CH ₂ CH ₂ OH, 21% CH ₃ CH ₂ C(O)CH ₂ CH ₂ C(O)CH ₃ , and 14% CH ₃ CH ₂ CH ₂ C(O)CH ₂ C(O)CH ₃
PRD3	CH ₃ CH(OH)CH ₂ CH ₂ CHO (Major photolysis product)
<u>Explicit and Lumped VOC Species used in the Ambient Simulations</u>	
<u>Primary Organics Represented explicitly</u>	
CH ₄	Methane
ETHENE	Ethene
ISOPRENE	Isoprene
<u>Example Test VOCs not in the Base Mechanism</u>	
ETHANE	Ethane
<u>Lumped Parameter Species</u>	
ALK1	Alkanes and other non-aromatic compounds that react only with OH, and have kOH < 5 x 10 ² ppm-1 min-1. (Primarily ethane)
ALK2	Alkanes and other non-aromatic compounds that react only with OH, and have kOH between 5 x 10 ² and 2.5 x 10 ³ ppm-1 min-1. (Primarily propane and acetylene)
ALK3	Alkanes and other non-aromatic compounds that react only with OH, and have kOH between 2.5 x 10 ³ and 5 x 10 ³ ppm-1 min-1.
ALK4	Alkanes and other non-aromatic compounds that react only with OH, and have kOH between 5 x 10 ³ and 1 x 10 ⁴ ppm-1 min-1.
ALK5	Alkanes and other non-aromatic compounds that react only with OH, and have kOH greater than 1 x 10 ⁴ ppm-1 min-1.
ARO1	Aromatics with kOH < 2x10 ⁴ ppm-1 min-1.
ARO2	Aromatics with kOH > 2x10 ⁴ ppm-1 min-1.
OLE1	Alkenes (other than ethene) with kOH < 7x10 ⁴ ppm-1 min-1.
OLE2	Alkenes with kOH > 7x10 ⁴ ppm-1 min-1.
TERP	Terpenes

Table A-2. Listing of the reactions in the mechanism used in the model simulations discussed in this report. See Carter (2000) for documentation.

Label	Rate Parameters [a]				Reaction and Products [b]
	k(298)	A	Ea	B	
<u>Inorganic Reactions</u>					
1		Phot Set= NO2			NO2 + HV = NO + O3P
2	5.79e-34	5.68e-34	0.00	-2.8	O3P + O2 + M = O3 + M
3	7.96e-15	8.00e-12	4.09		O3P + O3 = #2 O2
4	1.01e-31	1.00e-31	0.00	-1.6	O3P + NO + M = NO2 + M
5	9.72e-12	6.50e-12	-0.24		O3P + NO2 = NO + O2
6	1.82e-12	Falloff, F=0.80			O3P + NO2 = NO3 + M
		0: 9.00e-32	0.00	-2.0	
		inf: 2.20e-11	0.00	0.0	
8	1.81e-14	1.80e-12	2.72		O3 + NO = NO2 + O2
9	3.52e-17	1.40e-13	4.91		O3 + NO2 = O2 + NO3
10	2.60e-11	1.80e-11	-0.22		NO + NO3 = #2 NO2
11	1.95e-38	3.30e-39	-1.05		NO + NO + O2 = #2 NO2
12	1.54e-12	Falloff, F=0.45			NO2 + NO3 = N2O5
		0: 2.80e-30	0.00	-3.5	
		inf: 2.00e-12	0.00	0.2	
13	5.28e-2	Falloff, F=0.45			N2O5 = NO2 + NO3
		0: 1.00e-3	21.86	-3.5	
		inf: 9.70e+14	22.02	0.1	
14	2.60e-22	2.60e-22			N2O5 + H2O = #2 HNO3
15		(Slow)			N2O5 + HV = NO3 + NO + O3P
16		(Slow)			N2O5 + HV = NO3 + NO2
17	6.56e-16	4.50e-14	2.50		NO2 + NO3 = NO + NO2 + O2
18		Phot Set= NO3NO			NO3 + HV = NO + O2
19		Phot Set= NO3NO2			NO3 + HV = NO2 + O3P
20		Phot Set= O3O3P			O3 + HV = O3P + O2
21		Phot Set= O3O1D			O3 + HV = O*1D2 + O2
22	2.20e-10	2.20e-10			O*1D2 + H2O = #2 HO.
23	2.87e-11	2.09e-11	-0.19		O*1D2 + M = O3P + M
24	7.41e-12	Falloff, F=0.60			HO. + NO = HONO
		0: 7.00e-31	0.00	-2.6	
		inf: 3.60e-11	0.00	-0.1	
25		Phot Set= HONO-NO			HONO + HV = HO. + NO
26		Phot Set= HONO-NO2			HONO + HV = HO2. + NO2
27	6.46e-12	2.70e-12	-0.52		HO. + HONO = H2O + NO2
28	8.98e-12	Falloff, F=0.60			HO. + NO2 = HNO3
		0: 2.43e-30	0.00	-3.1	
		inf: 1.67e-11	0.00	-2.1	
29	2.00e-11	2.00e-11			HO. + NO3 = HO2. + NO2
30	1.47e-13	k = k0+k3M/(1+k3M/k2)			HO. + HNO3 = H2O + NO3
		k0: 7.20e-15	-1.56	0.0	
		k2: 4.10e-16	-2.86	0.0	
		k3: 1.90e-33	-1.44	0.0	
31		Phot Set= HNO3			HNO3 + HV = HO. + NO2
32	2.09e-13	k = k1 + k2 [M]			HO. + CO = HO2. + CO2
		k1: 1.30e-13	0.00	0.0	
		k2: 3.19e-33	0.00	0.0	
33	6.63e-14	1.90e-12	1.99		HO. + O3 = HO2. + O2

Table A-2 (continued)

Label	Rate Parameters [a]				Reaction and Products [b]
	k(298)	A	Ea	B	
34	8.41e-12	3.40e-12	-0.54		HO2. + NO = HO. + NO2
35	1.38e-12	Falloff, F=0.60			HO2. + NO2 = HNO4
		0: 1.80e-31	0.00	-3.2	
		inf: 4.70e-12	0.00	0.0	
36	7.55e-2	Falloff, F=0.50			HNO4 = HO2. + NO2
		0: 4.10e-5	21.16	0.0	
		inf: 5.70e+15	22.20	0.0	
37		Phot Set= HO2NO2			HNO4 + HV = #.61 {HO2. + NO2} + #.39 {HO. + NO3}
38	5.02e-12	1.50e-12	-0.72		HNO4 + HO. = H2O + NO2 + O2
39	1.87e-15	1.40e-14	1.19		HO2. + O3 = HO. + #2 O2
40A	2.87e-12	k = k1 + k2 [M]			HO2. + HO2. = HO2H + O2
		k1: 2.20e-13	-1.19	0.0	
		k2: 1.85e-33	-1.95	0.0	
40B	6.46e-30	k = k1 + k2 [M]			HO2. + HO2. + H2O = HO2H + O2 + H2O
		k1: 3.08e-34	-5.56	0.0	
		k2: 2.59e-54	-6.32	0.0	
41	4.00e-12	4.00e-12			NO3 + HO2. = #.8 {HO. + NO2 + O2} + #.2 {HNO3 + O2}
42	2.28e-16	8.50e-13	4.87		NO3 + NO3 = #2 NO2 + O2
43		Phot Set= H2O2			HO2H + HV = #2 HO.
44	1.70e-12	2.90e-12	0.32		HO2H + HO. = HO2. + H2O
45	1.11e-10	4.80e-11	-0.50		HO. + HO2. = H2O + O2
S2OH	9.77e-13	Falloff, F=0.45			HO. + SO2 = HO2. + SULF
		0: 4.00e-31	0.00	-3.3	
		inf: 2.00e-12	0.00	0.0	
H2OH	6.70e-15	7.70e-12	4.17		HO. + H2 = HO2. + H2O
<u>Methyl peroxy and methoxy reactions</u>					
MER1	7.29e-12	2.80e-12	-0.57		C-O2. + NO = NO2 + HCHO + HO2.
MER4	5.21e-12	3.80e-13	-1.55		C-O2. + HO2. = COOH + O2
MEN3	1.30e-12	1.30e-12			C-O2. + NO3 = HCHO + HO2. + NO2
MER5	2.65e-13	2.45e-14	-1.41		C-O2. + C-O2. = MEOH + HCHO + O2
MER6	1.07e-13	5.90e-13	1.01		C-O2. + C-O2. = #2 {HCHO + HO2.}
<u>Peroxy Radical Operators</u>					
RRNO	9.04e-12	2.70e-12	-0.72		RO2-R. + NO = NO2 + HO2.
RRH2	1.49e-11	1.90e-13	-2.58		RO2-R. + HO2. = ROOH + O2 + #-3 XC
RRN3	2.30e-12	2.30e-12			RO2-R. + NO3 = NO2 + O2 + HO2.
RRME	2.00e-13	2.00e-13			RO2-R. + C-O2. = HO2. + #.75 HCHO + #.25 MEOH
RRR2	3.50e-14	3.50e-14			RO2-R. + RO2-R. = HO2.
R2NO	Same k as rxn RRNO				R2O2. + NO = NO2
R2H2	Same k as rxn RRH2				R2O2. + HO2. = HO2.
R2N3	Same k as rxn RRN3				R2O2. + NO3 = NO2
R2ME	Same k as rxn RRME				R2O2. + C-O2. = C-O2.
R2RR	Same k as rxn RRR2				R2O2. + RO2-R. = RO2-R.
R2R3	Same k as rxn RRR2				R2O2. + R2O2. =
RNNO	Same k as rxn RRNO				RO2-N. + NO = RNO3
RNH2	Same k as rxn RRH2				RO2-N. + HO2. = ROOH + #3 XC
RNME	Same k as rxn RRME				RO2-N. + C-O2. = HO2. + #.25 MEOH + #.5 {MEK + PROD2} + #.75 HCHO + XC
RNN3	Same k as rxn RRN3				RO2-N. + NO3 = NO2 + O2 + HO2. + MEK + #2 XC

Table A-2 (continued)

Label	Rate Parameters [a]			B	Reaction and Products [b]
	k(298)	A	Ea		
RNRR		Same k as rxn RRR2			RO2-N. + RO2-R. = HO2. + #.5 {MEK + PROD2} + O2 + XC
RNR2		Same k as rxn RRR2			RO2-N. + R2O2. = RO2-N.
RNRN		Same k as rxn RRR2			RO2-N. + RO2-N. = MEK + HO2. + PROD2 + O2 + #2 XC
APN2	1.05e-11	Falloff, F=0.30			CCO-O2. + NO2 = PAN
		0:	2.70e-28	0.00	-7.1
		inf:	1.20e-11	0.00	-0.9
DPAN	5.21e-4	Falloff, F=0.30			PAN = CCO-O2. + NO2
		0:	4.90e-3	24.05	0.0
		inf:	4.00e+16	27.03	0.0
APNO	2.13e-11	7.80e-12	-0.60		CCO-O2. + NO = C-O2. + CO2 + NO2
APH2	1.41e-11	4.30e-13	-2.07		CCO-O2. + HO2. = #.75 {CCO-OOH + O2} + #.25 {CCO-OH + O3}
APN3	4.00e-12	4.00e-12			CCO-O2. + NO3 = C-O2. + CO2 + NO2 + O2
APME	9.64e-12	1.80e-12	-0.99		CCO-O2. + C-O2. = CCO-OH + HCHO + O2
APRR	7.50e-12	7.50e-12			CCO-O2. + RO2-R. = CCO-OH
APR2		Same k as rxn APRR			CCO-O2. + R2O2. = CCO-O2.
APRN		Same k as rxn APRR			CCO-O2. + RO2-N. = CCO-OH + PROD2
APAP	1.55e-11	2.90e-12	-0.99		CCO-O2. + CCO-O2. = #2 {C-O2. + CO2} + O2
PPN2	1.21e-11	1.20e-11	0.00	-0.9	RCO-O2. + NO2 = PAN2
PAN2	4.43e-4	2.00e+15	25.44		PAN2 = RCO-O2. + NO2
PPNO	2.80e-11	1.25e-11	-0.48		RCO-O2. + NO = NO2 + CCHO + RO2-R. + CO2
PPH2		Same k as rxn APH2			RCO-O2. + HO2. = #.75 {RCO-OOH + O2} + #.25 {RCO-OH + O3}
PPN3		Same k as rxn APN3			RCO-O2. + NO3 = NO2 + CCHO + RO2-R. + CO2 + O2
PPME		Same k as rxn APME			RCO-O2. + C-O2. = RCO-OH + HCHO + O2
PPRR		Same k as rxn APRR			RCO-O2. + RO2-R. = RCO-OH + O2
PPR2		Same k as rxn APRR			RCO-O2. + R2O2. = RCO-O2.
PPRN		Same k as rxn APRR			RCO-O2. + RO2-N. = RCO-OH + PROD2 + O2
PPAP		Same k as rxn APAP			RCO-O2. + CCO-O2. = #2 CO2 + C-O2. + CCHO + RO2-R. + O2
PPPP		Same k as rxn APAP			RCO-O2. + RCO-O2. = #2 {CCHO + RO2-R. + CO2}
BPN2	1.37e-11	1.37e-11			BZCO-O2. + NO2 = PBZN
BPAN	3.12e-4	7.90e+16	27.82		PBZN = BZCO-O2. + NO2
BPNO		Same k as rxn PPNO			BZCO-O2. + NO = NO2 + CO2 + BZ-O. + R2O2.
BPH2		Same k as rxn APH2			BZCO-O2. + HO2. = #.75 {RCO-OOH + O2} + #.25 {RCO-OH + O3} + #4 XC
BPN3		Same k as rxn APN3			BZCO-O2. + NO3 = NO2 + CO2 + BZ-O. + R2O2. + O2
BPME		Same k as rxn APME			BZCO-O2. + C-O2. = RCO-OH + HCHO + O2 + #4 XC
BPRR		Same k as rxn APRR			BZCO-O2. + RO2-R. = RCO-OH + O2 + #4 XC
BPR2		Same k as rxn APRR			BZCO-O2. + R2O2. = BZCO-O2.
BPRN		Same k as rxn APRR			BZCO-O2. + RO2-N. = RCO-OH + PROD2 + O2 + #4 XC
BPAP		Same k as rxn APAP			BZCO-O2. + CCO-O2. = #2 CO2 + C-O2. + BZ-O. + R2O2.
BPPP		Same k as rxn APAP			BZCO-O2. + RCO-O2. = #2 CO2 + CCHO + RO2-R. + BZ-O. + R2O2.
BPBP		Same k as rxn APAP			BZCO-O2. + BZCO-O2. = #2 {BZ-O. + R2O2. + CO2}
MPN2		Same k as rxn PPN2			MA-RCO3. + NO2 = MA-PAN
MPPN	3.55e-4	1.60e+16	26.80		MA-PAN = MA-RCO3. + NO2
MPNO		Same k as rxn PPNO			MA-RCO3. + NO = NO2 + CO2 + HCHO + CCO-O2.
MPH2		Same k as rxn APH2			MA-RCO3. + HO2. = #.75 {RCO-OOH + O2} + #.25 {RCO-OH + O3} + XC

Table A-2 (continued)

Label	Rate Parameters [a]			B	Reaction and Products [b]
	k(298)	A	Ea		
MPN3		Same k as rxn APN3			MA-RCO3. + NO3 = NO2 + CO2 + HCHO + CCO-O2. + O2
MPME		Same k as rxn APME			MA-RCO3. + C-O2. = RCO-OH + HCHO + XC + O2
MPRR		Same k as rxn APRR			MA-RCO3. + RO2-R. = RCO-OH + XC
MPR2		Same k as rxn APRR			MA-RCO3. + R2O2. = MA-RCO3.
MPRN		Same k as rxn APRR			MA-RCO3. + RO2-N. = #2 RCO-OH + O2 + #4 XC
MPAP		Same k as rxn APAP			MA-RCO3. + CCO-O2. = #2 CO2 + C-O2. + HCHO + CCO-O2. + O2
MPPP		Same k as rxn APAP			MA-RCO3. + RCO-O2. = HCHO + CCO-O2. + CCHO + RO2-R. + #2 CO2
MPBP		Same k as rxn APAP			MA-RCO3. + BZCO-O2. = HCHO + CCO-O2. + BZ-O. + R2O2. + #2 CO2
MPMP		Same k as rxn APAP			MA-RCO3. + MA-RCO3. = #2 {HCHO + CCO-O2. + CO2}
<u>Other Organic Radical Species</u>					
TBON	2.40e-11	2.40e-11			TBU-O. + NO2 = RNO3 + #-2 XC
TBOD	9.87e+2	7.50e+14	16.20		TBU-O. = ACET + C-O2.
BRN2	3.80e-11	2.30e-11	-0.30		BZ-O. + NO2 = NPHE
BRH2		Same k as rxn RRH2			BZ-O. + HO2. = PHEN
BRXX	1.00e-3	1.00e-3			BZ-O. = PHEN
BNN2		Same k as rxn BRN2			BZ(NO2)-O. + NO2 = #2 XN + #6 XC
BNH2		Same k as rxn RRH2			BZ(NO2)-O. + HO2. = NPHE
BNXX		Same k as rxn BRXX			BZ(NO2)-O. = NPHE
<u>Explicit and Lumped Molecule Organic Products</u>					
FAHV		Phot Set= HCHO_R			HCHO + HV = #2 HO2. + CO
FAVS		Phot Set= HCHO_M			HCHO + HV = H2 + CO
FAOH	9.20e-12	8.60e-12	-0.04		HCHO + HO. = HO2. + CO + H2O
FAH2	7.90e-14	9.70e-15	-1.24		HCHO + HO2. = HOCOO.
FAHR	1.51e+2	2.40e+12	13.91		HOCOO. = HO2. + HCHO
FAHN		Same k as rxn MER1			HOCOO. + NO = HCOOH + NO2 + HO2.
FAN3	5.74e-16	2.00e-12	4.83		HCHO + NO3 = HNO3 + HO2. + CO
AAOH	1.58e-11	5.60e-12	-0.62		CCHO + HO. = CCO-O2. + H2O
AAHV		Phot Set= CCHO_R			CCHO + HV = CO + HO2. + C-O2.
AAN3	2.73e-15	1.40e-12	3.70		CCHO + NO3 = HNO3 + CCO-O2.
PAOH	2.00e-11	2.00e-11			RCHO + HO. = #.034 RO2-R. + #.001 RO2-N. + #.965 RCO-O2. + #.034 CO + #.034 CCHO + #.0003 XC
PAHV		Phot Set= C2CHO			RCHO + HV = CCHO + RO2-R. + CO + HO2.
PAN3	3.67e-15	1.40e-12	3.52		RCHO + NO3 = HNO3 + RCO-O2.
K3OH	1.92e-13	1.10e-12	1.03		ACET + HO. = HCHO + CCO-O2. + R2O2.
K3HV		Phot Set= ACETONE			ACET + HV = CCO-O2. + C-O2.
K4OH	1.18e-12	1.30e-12	0.05	2.0	MEK + HO. = #.37 RO2-R. + #.042 RO2-N. + #.616 R2O2. + #.492 CCO-O2. + #.096 RCO-O2. + #.115 HCHO + #.482 CCHO + #.37 RCHO + #.287 XC
K4HV		Phot Set= KETONE, qy= 1.5e-1			MEK + HV = CCO-O2. + CCHO + RO2-R.
MeOH	9.14e-13	3.10e-12	0.72	2.0	MEOH + HO. = HCHO + HO2.
MER9	5.49e-12	2.90e-12	-0.38		COOH + HO. = H2O + #.35 {HCHO + HO.} + #.65 C-O2.
MERA		Phot Set= COOH			COOH + HV = HCHO + HO2. + HO.

Table A-2 (continued)

Label	Rate Parameters [a]				Reaction and Products [b]
	k(298)	A	Ea	B	
LPR9	1.10e-11	1.10e-11			ROOH + HO. = H2O + RCHO + #.34 RO2-R. + #.66 HO.
LPRA		Phot Set= COOH			ROOH + HV = RCHO + HO2. + HO.
GLHV		Phot Set= GLY_R			GLY + HV = #2 {CO + HO2.}
GLVM		Phot Set= GLY_ABS, qy= 6.0e-3			GLY + HV = HCHO + CO
GLOH	1.10e-11	1.10e-11			GLY + HO. = #.63 HO2. + #1.26 CO + #.37 RCO-O2. + #-.37 XC
GLN3	9.63e-16	2.80e-12	4.72		GLY + NO3 = HNO3 + #.63 HO2. + #1.26 CO + #.37 RCO-O2. + #-.37 XC
MGHV		Phot Set= MGLY_ADJ			MGLY + HV = HO2. + CO + CCO-O2.
MGOH	1.50e-11	1.50e-11			MGLY + HO. = CO + CCO-O2.
MGN3	2.43e-15	1.40e-12	3.77		MGLY + NO3 = HNO3 + CO + CCO-O2.
BAHV		Phot Set= BAACL_ADJ			BAACL + HV = #2 CCO-O2.
PHOH	2.63e-11	2.63e-11			PHEN + HO. = #.24 BZ-O. + #.76 RO2-R. + #.23 GLY + #4.1 XC
PHN3	3.78e-12	3.78e-12			PHEN + NO3 = HNO3 + BZ-O.
CROH	4.20e-11	4.20e-11			CRES + HO. = #.24 BZ-O. + #.76 RO2-R. + #.23 MGLY + #4.87 XC
CRN3	1.37e-11	1.37e-11			CRES + NO3 = HNO3 + BZ-O. + XC
NPN3		Same k as rxn PHN3			NPHE + NO3 = HNO3 + BZ(NO2)-O.
BZOH	1.29e-11	1.29e-11			BALD + HO. = BZCO-O2.
BZHV		Phot Set= BZCHO, qy= 5.0e-2			BALD + HV = #7 XC
BZNT	2.62e-15	1.40e-12	3.72		BALD + NO3 = HNO3 + BZCO-O2.
MAOH	3.36e-11	1.86e-11	-0.35		METHACRO + HO. = #.5 RO2-R. + #.416 CO + #.084 HCHO + #.416 MEK + #.084 MGLY + #.5 MA-RCO3. + #-.0416 XC
MAO3	1.13e-18	1.36e-15	4.20		METHACRO + O3 = #.008 HO2. + #.1 RO2-R. + #.208 HO. + #.1 RCO-O2. + #.45 CO + #.117 CO2 + #.2 HCHO + #.9 MGLY + #.333 HCOOH + #-.0.1 XC
MAN3	4.58e-15	1.50e-12	3.43		METHACRO + NO3 = #.5 {HNO3 + RO2-R. + CO + MA-RCO3.} + #1.5 XC + #.5 XN
MAOP	6.34e-12	6.34e-12			METHACRO + O3P = RCHO + XC
MAHV		Phot Set= ACROLEIN, qy= 4.1e-3			METHACRO + HV = #.34 HO2. + #.33 RO2-R. + #.33 HO. + #.67 CCO-O2. + #.67 CO + #.67 HCHO + #.33 MA-RCO3. + #-.0 XC
MVOH	1.89e-11	4.14e-12	-0.90		MVK + HO. = #.3 RO2-R. + #.025 RO2-N. + #.675 R2O2. + #.675 CCO-O2. + #.3 HCHO + #.675 RCHO + #.3 MGLY + #-.0.725 XC
MVO3	4.58e-18	7.51e-16	3.02		MVK + O3 = #.064 HO2. + #.05 RO2-R. + #.164 HO. + #.05 RCO-O2. + #.475 CO + #.124 CO2 + #.1 HCHO + #.95 MGLY + #.351 HCOOH + #-.0.05 XC
MVN3		(Slow)			MVK + NO3 = #4 XC + XN
MVOP	4.32e-12	4.32e-12			MVK + O3P = #.45 RCHO + #.55 MEK + #.45 XC
MVHV		Phot Set= ACROLEIN, qy= 2.1e-3			MVK + HV = #.3 C-O2. + #.7 CO + #.7 PROD2 + #.3 MA-RCO3. + #-.2.4 XC
IPOH	6.19e-11	6.19e-11			ISO-PROD + HO. = #.67 RO2-R. + #.041 RO2-N. + #.289 MA-RCO3. + #.336 CO + #.055 HCHO + #.129 CCHO + #.013 RCHO + #.15 MEK + #.332 PROD2 + #.15 GLY + #.174 MGLY + #-.0.504 XC

Table A-2 (continued)

Label	Rate Parameters [a]				Reaction and Products [b]
	k(298)	A	Ea	B	
IPO3	4.18e-18	4.18e-18			ISO-PROD + O3 = #.4 HO2. + #.048 RO2-R. + #.048 RCO-O2. + #.285 HO. + #.498 CO + #.14 CO2 + #.125 HCHO + #.047 CCHO + #.21 MEK + #.023 GLY + #.742 MGLY + #.1 HCOOH + #.372 RCO-OH + #.33 XC
IPN3	1.00e-13	1.00e-13			ISO-PROD + NO3 = #.799 RO2-R. + #.051 RO2-N. + #.15 MA-RCO3. + #.572 CO + #.15 HNO3 + #.227 HCHO + #.218 RCHO + #.008 MGLY + #.572 RNO3 + #.28 XN + #.815 XC
IPHV	Phot Set= ACROLEIN, qy= 4.1e-3				ISO-PROD + HV = #1.233 HO2. + #.467 CCO-O2. + #.3 RCO-O2. + #1.233 CO + #.3 HCHO + #.467 CCHO + #.233 MEK + #.233 XC
<u>Lumped Parameter Organic Products</u>					
K6OH	1.50e-11	1.50e-11			PROD2 + HO. = #.379 HO2. + #.473 RO2-R. + #.07 RO2-N. + #.029 CCO-O2. + #.049 RCO-O2. + #.213 HCHO + #.084 CCHO + #.558 RCHO + #.115 MEK + #.329 PROD2 + #.886 XC
K6HV	Phot Set= KETONE, qy= 2.0e-2				PROD2 + HV = #.96 RO2-R. + #.04 RO2-N. + #.515 R2O2. + #.667 CCO-O2. + #.333 RCO-O2. + #.506 HCHO + #.246 CCHO + #.71 RCHO + #.299 XC
RNOH	7.80e-12	7.80e-12			RNO3 + HO. = #.338 NO2 + #.113 HO2. + #.376 RO2-R. + #.173 RO2-N. + #.596 R2O2. + #.01 HCHO + #.439 CCHO + #.213 RCHO + #.006 ACET + #.177 MEK + #.048 PROD2 + #.31 RNO3 + #.351 XN + #.56 XC
RNHV	Phot Set= IC3ONO2				RNO3 + HV = NO2 + #.341 HO2. + #.564 RO2-R. + #.095 RO2-N. + #.152 R2O2. + #.134 HCHO + #.431 CCHO + #.147 RCHO + #.02 ACET + #.243 MEK + #.435 PROD2 + #.35 XC
<u>Uncharacterized Reactive Aromatic Ring Fragmentation Products</u>					
D1OH	5.00e-11	5.00e-11			DCB1 + HO. = RCHO + RO2-R. + CO
D1HV			(Slow)		DCB1 + HV = HO2. + #2 CO + RO2-R. + GLY + R2O2.
D1O3	2.00e-18	2.00e-18			DCB1 + O3 = #1.5 HO2. + #.5 HO. + #1.5 CO + #.5 CO2 + GLY
D2OH	5.00e-11	5.00e-11			DCB2 + HO. = R2O2. + RCHO + CCO-O2.
D2HV	Phot Set= MGLY_ABS, qy= 3.7e-1				DCB2 + HV = RO2-R. + #.5 {CCO-O2. + HO2.} + CO + R2O2. + #.5 {GLY + MGLY + XC}
D3OH	5.00e-11	5.00e-11			DCB3 + HO. = R2O2. + RCHO + CCO-O2.
D3HV	Phot Set= ACROLEIN, qy= 7.3e+0				DCB3 + HV = RO2-R. + #.5 {CCO-O2. + HO2.} + CO + R2O2. + #.5 {GLY + MGLY + XC}
<u>Base ROG VOCs Used in the Chamber Simulations and Explicit VOCs in the Ambient Simulations</u>					
c1OH	6.37e-15	2.15e-12	3.45		CH4 + HO. = H2O + C-O2.
c2OH	2.54e-13	1.37e-12	0.99	2.0	ETHANE + HO. = RO2-R. + CCHO
c4OH	2.44e-12	1.52e-12	-0.29	2.0	N-C4 + HO. = #.921 RO2-R. + #.079 RO2-N. + #.413 R2O2. + #.632 CCHO + #.12 RCHO + #.485 MEK + #.038 XC
c6OH	5.47e-12	1.38e-12	-0.82	2.0	N-C6 + HO. = #.775 RO2-R. + #.225 RO2-N. + #.787 R2O2. + #.011 CCHO + #.113 RCHO + #.688 PROD2 + #.162 XC
c8OH	8.70e-12	2.48e-12	-0.75	2.0	N-C8 + HO. = #.646 RO2-R. + #.354 RO2-N. + #.786 R2O2. + #.024 RCHO + #.622 PROD2 + #2.073 XC
etOH	8.52e-12	1.96e-12	-0.87		ETHENE + HO. = RO2-R. + #1.61 HCHO + #.195 CCHO
etO3	1.59e-18	9.14e-15	5.13		ETHENE + O3 = #.12 HO. + #.12 HO2. + #.5 CO + #.13 CO2 + HCHO + #.37 HCOOH
etN3	2.05e-16	4.39e-13	4.53	2.0	ETHENE + NO3 = RO2-R. + RCHO + #-1 XC + XN

Table A-2 (continued)

Label	Rate Parameters [a]			Reaction and Products [b]	
	k(298)	A	Ea		
etOA	7.29e-13	1.04e-11	1.57		ETHENE + O3P = #.5 HO2. + #.2 RO2-R. + #.3 C-O2. + #.491 CO + #.191 HCHO + #.25 CCHO + #.009 GLY + #.5 XC
prOH	2.63e-11	4.85e-12	-1.00		PROPENE + HO. = #.984 RO2-R. + #.016 RO2-N. + #.984 HCHO + #.984 CCHO + #-0.048 XC
prO3	1.01e-17	5.51e-15	3.73		PROPENE + O3 = #.32 HO. + #.06 HO2. + #.26 C-O2. + #.51 CO + #.135 CO2 + #.5 HCHO + #.5 CCHO + #.185 HCOOH + #.17 CCO-OH + #.07 INERT + #.07 XC
prN3	9.49e-15	4.59e-13	2.30		PROPENE + NO3 = #.949 RO2-R. + #.051 RO2-N. + #.2.693 XC + XN
prOP	3.98e-12	1.18e-11	0.64		PROPENE + O3P = #.45 RCHO + #.55 MEK + #-0.55 XC
t2OH	6.40e-11	1.01e-11	-1.09		T-2-BUTE + HO. = #.965 RO2-R. + #.035 RO2-N. + #1.93 CCHO + #-0.07 XC
t2O3	1.90e-16	6.64e-15	2.10		T-2-BUTE + O3 = #.52 HO. + #.52 C-O2. + #.52 CO + #.14 CO2 + CCHO + #.34 CCO-OH + #.14 INERT + #.14 XC
t2N3	3.91e-13	1.10e-13	-0.76	2.0	T-2-BUTE + NO3 = #.705 NO2 + #.215 RO2-R. + #.08 RO2-N. + #.705 R2O2. + #1.41 CCHO + #.215 RNO3 + #-0.59 XC + #.08 XN
t2OP	2.18e-11	2.18e-11			T-2-BUTE + O3P = MEK
isOH	9.82e-11	2.50e-11	-0.81		ISOPRENE + HO. = #.907 RO2-R. + #.093 RO2-N. + #.079 R2O2. + #.624 HCHO + #.23 METHACRO + #.32 MVK + #.357 ISO-PROD + #-0.167 XC
isO3	1.28e-17	7.86e-15	3.80		ISOPRENE + O3 = #.266 HO. + #.066 RO2-R. + #.008 RO2-N. + #.126 R2O2. + #.192 MA-RCO3. + #.275 CO + #.122 CO2 + #.592 HCHO + #.1 PROD2 + #.39 METHACRO + #.16 MVK + #.204 HCOOH + #.15 RCO-OH + #-0.259 XC
isN3	6.74e-13	3.03e-12	0.89		ISOPRENE + NO3 = #.187 NO2 + #.749 RO2-R. + #.064 RO2-N. + #.187 R2O2. + #.936 ISO-PROD + #-0.064 XC + #.813 XN
isOP	3.60e-11	3.60e-11			ISOPRENE + O3P = #.01 RO2-N. + #.24 R2O2. + #.25 C-O2. + #.24 MA-RCO3. + #.24 HCHO + #.75 PROD2 + #-1.01 XC
t1OH	5.95e-12	1.81e-12	-0.71	0.0	TOLUENE + HO. = #.234 HO2. + #.758 RO2-R. + #.008 RO2-N. + #.116 GLY + #.135 MGLY + #.234 CRES + #.085 BALD + #.46 DCB1 + #.156 DCB2 + #.057 DCB3 + #1.178 XC
mxOH	2.36e-11	2.36e-11	0.00	0.0	M-XYLENE + HO. = #.21 HO2. + #.782 RO2-R. + #.008 RO2-N. + #.107 GLY + #.335 MGLY + #.21 CRES + #.037 BALD + #.347 DCB1 + #.29 DCB2 + #.108 DCB3 + #1.628 XC
Lumped Organic Species used in the Ambient Reactivity Simulations					
t1OH	8.27e-11	1.83e-11	-0.89		TERP + HO. = #.75 RO2-R. + #.25 RO2-N. + #.5 R2O2. + #.276 HCHO + #.474 RCHO + #.276 PROD2 + #5.146 XC
t1O3	6.88e-17	1.08e-15	1.63		TERP + O3 = #.567 HO. + #.033 HO2. + #.031 RO2-R. + #.18 RO2-N. + #.729 R2O2. + #.123 CCO-O2. + #.201 RCO-O2. + #.157 CO + #.037 CO2 + #.235 HCHO + #.205 RCHO + #.13 ACET + #.276 PROD2 + #.001 GLY + #.031 BACL + #.103 HCOOH + #.189 RCO-OH + #4.183 XC
t1N3	6.57e-12	3.66e-12	-0.35		TERP + NO3 = #.474 NO2 + #.276 RO2-R. + #.25 RO2-N. + #.75 R2O2. + #.474 RCHO + #.276 RNO3 + #5.421 XC + #.25 XN
t1OP	3.27e-11	3.27e-11			TERP + O3P = #.147 RCHO + #.853 PROD2 + #4.441 XC
a1OH	2.54e-13	1.37e-12	0.99	2.0	ALK1 + HO. = RO2-R. + CCHO

Table A-2 (continued)

Label	Rate Parameters [a]			B	Reaction and Products [b]
	k(298)	A	Ea		
a2OH	1.04e-12	9.87e-12	1.33		ALK2 + HO. = #.246 HO. + #.121 HO2. + #.612 RO2-R. + #.021 RO2-N. + #.16 CO + #.039 HCHO + #.155 RCHO + #.417 ACET + #.248 GLY + #.121 HCOOH + #0.338 XC
a3OH	2.38e-12	1.02e-11	0.86		ALK3 + HO. = #.695 RO2-R. + #.07 RO2-N. + #.559 R2O2. + #.236 TBU-O. + #.026 HCHO + #.445 CCHO + #.122 RCHO + #.024 ACET + #.332 MEK + #-0.05 XC
a4OH	4.39e-12	5.95e-12	0.18		ALK4 + HO. = #.835 RO2-R. + #.143 RO2-N. + #.936 R2O2. + #.011 C-O2. + #.011 CCO-O2. + #.002 CO + #.024 HCHO + #.455 CCHO + #.244 RCHO + #.452 ACET + #.11 MEK + #.125 PROD2 + #-0.105 XC
a5OH	9.34e-12	1.11e-11	0.10		ALK5 + HO. = #.653 RO2-R. + #.347 RO2-N. + #.948 R2O2. + #.026 HCHO + #.099 CCHO + #.204 RCHO + #.072 ACET + #.089 MEK + #.417 PROD2 + #2.008 XC
b1OH	5.95e-12	1.81e-12	-0.71		ARO1 + HO. = #.224 HO2. + #.765 RO2-R. + #.011 RO2-N. + #.055 PROD2 + #.118 GLY + #.119 MGLY + #.017 PHEN + #.207 CRES + #.059 BALD + #.491 DCB1 + #.108 DCB2 + #.051 DCB3 + #1.288 XC
b2OH	2.64e-11	2.64e-11	0.00		ARO2 + HO. = #.187 HO2. + #.804 RO2-R. + #.009 RO2-N. + #.097 GLY + #.287 MGLY + #.087 BA CL + #.187 CRES + #.05 BALD + #.561 DCB1 + #.099 DCB2 + #.093 DCB3 + #1.68 XC
o1OH	3.23e-11	7.10e-12	-0.90		OLE1 + HO. = #.91 RO2-R. + #.09 RO2-N. + #.205 R2O2. + #.732 HCHO + #.294 CCHO + #.497 RCHO + #.005 ACET + #.119 PROD2 + #.92 XC
o1O3	1.06e-17	2.62e-15	3.26		OLE1 + O3 = #.155 HO. + #.056 HO2. + #.022 RO2-R. + #.001 RO2-N. + #.076 C-O2. + #.345 CO + #.086 CO2 + #.5 HCHO + #.154 CCHO + #.363 RCHO + #.001 ACET + #.215 PROD2 + #.185 HCOOH + #.05 CCO-OH + #.119 RCO-OH + #.654 XC
o1N3	1.26e-14	4.45e-14	0.75		OLE1 + NO3 = #.824 RO2-R. + #.176 RO2-N. + #.488 R2O2. + #.009 CCHO + #.037 RCHO + #.024 ACET + #.511 RNO3 + #.677 XC + #.489 XN
o1OP	4.90e-12	1.07e-11	0.47		OLE1 + O3P = #.45 RCHO + #.437 MEK + #.113 PROD2 + #1.224 XC
o2OH	6.33e-11	1.74e-11	-0.76		OLE2 + HO. = #.918 RO2-R. + #.082 RO2-N. + #.001 R2O2. + #.244 HCHO + #.732 CCHO + #.511 RCHO + #.127 ACET + #.072 MEK + #.061 BALD + #.025 METHACRO + #.025 ISO-PROD + #-0.054 XC
o2O3	1.07e-16	5.02e-16	0.92		OLE2 + O3 = #.378 HO. + #.003 HO2. + #.033 RO2-R. + #.002 RO2-N. + #.137 R2O2. + #.197 C-O2. + #.137 CCO-O2. + #.006 RCO-O2. + #.265 CO + #.07 CO2 + #.269 HCHO + #.456 CCHO + #.305 RCHO + #.045 ACET + #.026 MEK + #.006 PROD2 + #.042 BALD + #.026 METHACRO + #.073 HCOOH + #.129 CCO-OH + #.303 RCO-OH + #.155 XC
o2N3	7.27e-13	7.27e-13	0.00		OLE2 + NO3 = #.391 NO2 + #.442 RO2-R. + #.136 RO2-N. + #.711 R2O2. + #.03 C-O2. + #.079 HCHO + #.507 CCHO + #.151 RCHO + #.102 ACET + #.001 MEK + #.015 BALD + #.048 MVK + #.321 RNO3 + #.075 XC + #.288 XN
o2OP	2.09e-11	2.09e-11			OLE2 + O3P = #.013 HO2. + #.012 RO2-R. + #.001 RO2-N. + #.012 CO + #.069 RCHO + #.659 MEK + #.259 PROD2 + #.012 METHACRO + #.537 XC

Table A-2 (continued)

Label	Rate Parameters [a]			Reaction and Products [b]
	k(298)	A	Ea B	
<u>Test Compounds Studied for This Project [c]</u>				
	3.40e-12	3.40e-12		IPR-ACET + HO. = #.015 RO2-R. + #.055 RO2-N. + #1.034 R2O2. + #.845 C-O2. + #.085 CCO-O2. + #.203 CO2 + #.093 HCHO + #.203 ACET + #.011 MGLY + #.085 CCO-OH + #.647 INERT + #1.902 XC
	4.56e-12	4.56e-12		MPK + HO. = #.154 RO2-R. + #.065 RO2-N. + #1.373 R2O2. + #.761 CCO-O2. + #.02 RCO-O2. + #.612 HCHO + #.591 CCHO + #.203 RCHO + #.12 MEK + #.142 XC
			PF=KETONE QY = 0.10	MPK + HV = #.98 RO2-R. + #.02 RO2-N. + CCO-O2. + #.98 RCHO + #.06 XC
	1.17e-11	1.17e-11		C7-KET-2 + HO. = #.513 RO2-R. + #.193 RO2-N. + #.936 R2O2. + #.283 CCO-O2. + #.011 RCO-O2. + #.099 HCHO + #.013 CCHO + #.14 RCHO + #1.265 XC + #.449 PRD1 + #.347 PRD2
			PF=KETONE QY = 0.02	C7-KET-2 + HV = #.874 RO2-R. + #.126 RO2-N. + #.935 R2O2. + CCO-O2. + #1.623 XC + #.874 PRD3
<u>Major Reactive Products from 2-Heptanone [d]</u>				
	3.85e-11	3.85e-11		PRD1 + HO. = #.069 HO2. + #.056 RO2-R. + #.007 RO2-N. + #.02 R2O2. + #.869 RCO-O2. + #.026 CO + #.005 HCHO + #.019 CCHO + #.12 RCHO + #.001 MGLY + #.08 XC
	3.80e-15	3.80e-15	PF=C2CHO	PRD1 + NO3 = RCO-O2. + #.0 XC + XN
				PRD1 + HV = #.311 HO2. + #1.323 RO2-R. + #.037 RO2-N. + #.329 CCO-O2. + CO + #.329 HCHO + #.634 RCHO + #.111 XC
	8.79e-12	8.79e-12		PRD2 + HO. = #.185 HO2. + #.398 RO2-R. + #.102 RO2-N. + #.266 R2O2. + #.1 CCO-O2. + #.216 RCO-O2. + #.281 HCHO + #.041 CCHO + #.747 RCHO + #.053 MEK + #.047 MGLY + #1.585 XC
			PF=KETONE QY = 0.014	PRD2 + HV = #.189 RO2-R. + #.037 RO2-N. + #.782 R2O2. + #.897 CCO-O2. + #.876 RCO-O2. + #.769 HCHO + #.007 CCHO + #.189 RCHO + #.004 XC
	3.01e-11	3.01e-11		PRD3 + HO. = #.276 HO2. + #.074 RO2-R. + #.005 RO2-N. + #.645 RCO-O2. + #.025 CO + #.045 CCHO + #.348 RCHO + #.001 MGLY + #.013 XC
	3.80e-15	3.80e-15	PF=C2CHO	PRD3 + NO3 = RCO-O2. + XN
				PRD3 + HV = #.215 HO2. + #1.715 RO2-R. + #.07 RO2-N. + CO + #.93 RCHO + #.1.211 XC

[a] Except as indicated, the rate constants are given by $k(T) = A \cdot (T/300)^B \cdot e^{-E_a/RT}$, where the units of k and A are $\text{cm}^3 \text{molec}^{-1} \text{s}^{-1}$, E_a are kcal mol^{-1} , T is $^{\circ}\text{K}$, and $R=0.0019872 \text{ kcal mol}^{-1} \text{ deg}^{-1}$. The following special rate constant expressions are used:

Phot Set = name: The absorption cross sections and quantum yields for the photolysis reaction are given in Table A-5, where “name” indicates the photolysis set used. If a “ $qy=number$ ” notation is given, the number given is the overall quantum yield, which is assumed to be wavelength independent.

Falloff: The rate constant as a function of temperature and pressure is calculated using $k(T,M) = \{k_0(T) \cdot [M] / [1 + k_0(T) \cdot [M] / k_{inf}(T)]\} \cdot F^Z$, where $Z = \{1 + [\log_{10}\{k_0(T) \cdot [M] / k_{inf}(T)\}]^2\}^{-1}$, [M] is the total pressure in molecules cm^{-3} , F is as indicated on the table, and the temperature dependences of k_0 and k_{inf} are as indicated on the table.

(Slow): The reaction is assumed to be negligible and is not included in the mechanism. It is shown on the listing for documentation purposes only.

Table A-2 (continued)

$k = k_0 + k_3 M(1 + k_3 M/k_2)$: The rate constant as a function of temperature and pressure is calculated using $k(T, M) = k_0(T) + k_3(T) \cdot [M] \cdot (1 + k_3(T) \cdot [M]/k_2(T))$, where $[M]$ is the total bath gas (air) concentration in molecules cm^{-3} , and the temperature dependences for k_0 , k_2 and k_3 are as indicated on the table.

$k = k_1 + k_2 [M]$: The rate constant as a function of temperature and pressure is calculated using $k(T, M) = k_1(T) + k_2(T) \cdot [M]$, where $[M]$ is the total bath gas (air) concentration in molecules cm^{-3} , and the temperature dependences for k_1 , and k_2 are as indicated on the table.

Same k as Rxn label: The rate constant is the same as the reaction with the indicated label.

- [b] Format of reaction listing: “=” separates reactants from products; “#number” indicates stoichiometric coefficient, “#coefficient { product list }” means that the stoichiometric coefficient is applied to all the products listed. See Table A-1 for a listing of the model species used.
- [c] Best fit or adjusted mechanisms derived as discussed in the text.
- [d] Mechanisms are derived by weighted averages of the estimated mechanisms derived for the product compounds using the SAPRC-99 mechanism generation system (Carter, 2000). See Carter (2000) for a discussion of adjusted product mechanisms.

Table A-3. Listing of the absorption cross sections and quantum yields for the photolysis reactions.

WL (nm)	Abs (cm ²)	QY	WL (nm)	Abs (cm ²)	QY	WL (nm)	Abs (cm ²)	QY	WL (nm)	Abs (cm ²)	QY	WL (nm)	Abs (cm ²)	QY
<u>NO2</u>														
205.0	4.31e-19	1.000	210.0	4.72e-19	1.000	215.0	4.95e-19	1.000	220.0	4.56e-19	1.000	225.0	3.79e-19	1.000
230.0	2.74e-19	1.000	235.0	1.67e-19	1.000	240.0	9.31e-20	1.000	245.0	4.74e-20	1.000	250.0	2.48e-20	1.000
255.0	1.95e-20	1.000	260.0	2.24e-20	1.000	265.0	2.73e-20	1.000	270.0	4.11e-20	1.000	275.0	4.90e-20	1.000
280.0	5.92e-20	1.000	285.0	7.39e-20	1.000	290.0	9.00e-20	1.000	295.0	1.09e-19	1.000	300.0	1.31e-19	1.000
305.0	1.57e-19	1.000	310.0	1.86e-19	1.000	315.0	2.15e-19	0.990	320.0	2.48e-19	0.990	325.0	2.81e-19	0.990
330.0	3.13e-19	0.990	335.0	3.43e-19	0.990	340.0	3.80e-19	0.990	345.0	4.07e-19	0.990	350.0	4.31e-19	0.990
355.0	4.72e-19	0.990	360.0	4.83e-19	0.980	365.0	5.17e-19	0.980	370.0	5.32e-19	0.980	375.0	5.51e-19	0.980
380.0	5.64e-19	0.970	385.0	5.76e-19	0.970	390.0	5.93e-19	0.960	395.0	5.85e-19	0.935	400.0	6.02e-19	0.820
405.0	5.78e-19	0.355	410.0	6.00e-19	0.130	411.0	5.93e-19	0.110	412.0	5.86e-19	0.094	413.0	5.79e-19	0.083
414.0	5.72e-19	0.070	415.0	5.65e-19	0.059	416.0	5.68e-19	0.048	417.0	5.71e-19	0.039	418.0	5.75e-19	0.030
419.0	5.78e-19	0.023	420.0	5.81e-19	0.018	421.0	5.72e-19	0.012	422.0	5.64e-19	0.008	423.0	5.55e-19	0.004
424.0	5.47e-19	0.000												
<u>NO3NO</u>														
585.0	2.89e-18	0.000	586.0	3.32e-18	0.050	587.0	4.16e-18	0.100	588.0	5.04e-18	0.150	589.0	6.13e-18	0.200
590.0	5.96e-18	0.250	591.0	5.44e-18	0.280	592.0	5.11e-18	0.310	593.0	4.58e-18	0.340	594.0	4.19e-18	0.370
595.0	4.29e-18	0.400	596.0	4.62e-18	0.370	597.0	4.36e-18	0.340	598.0	3.67e-18	0.310	599.0	3.10e-18	0.280
600.0	2.76e-18	0.250	601.0	2.86e-18	0.240	602.0	3.32e-18	0.230	603.0	3.80e-18	0.220	604.0	4.37e-18	0.210
605.0	4.36e-18	0.200	606.0	3.32e-18	0.200	607.0	2.40e-18	0.200	608.0	1.85e-18	0.200	609.0	1.71e-18	0.200
610.0	1.77e-18	0.200	611.0	1.91e-18	0.180	612.0	2.23e-18	0.160	613.0	2.63e-18	0.140	614.0	2.55e-18	0.120
615.0	2.26e-18	0.100	616.0	2.09e-18	0.100	617.0	2.11e-18	0.100	618.0	2.39e-18	0.100	619.0	2.56e-18	0.100
620.0	3.27e-18	0.100	621.0	5.24e-18	0.090	622.0	1.02e-17	0.080	623.0	1.47e-17	0.070	624.0	1.21e-17	0.060
625.0	8.38e-18	0.050	626.0	7.30e-18	0.050	627.0	7.53e-18	0.050	628.0	7.37e-18	0.050	629.0	6.98e-18	0.050
630.0	6.76e-18	0.050	631.0	4.84e-18	0.046	632.0	3.27e-18	0.042	633.0	2.17e-18	0.038	634.0	1.64e-18	0.034
635.0	1.44e-18	0.030	636.0	1.69e-18	0.024	637.0	2.07e-18	0.018	638.0	2.03e-18	0.012	639.0	1.58e-18	0.006
640.0	1.23e-18	0.000												
<u>NO3NO2</u>														
400.0	0.00e+00	1.000	401.0	0.00e+00	1.000	402.0	0.00e+00	1.000	403.0	2.00e-20	1.000	404.0	0.00e+00	1.000
405.0	3.00e-20	1.000	406.0	2.00e-20	1.000	407.0	1.00e-20	1.000	408.0	3.00e-20	1.000	409.0	0.00e+00	1.000
410.0	1.00e-20	1.000	411.0	2.00e-20	1.000	412.0	5.00e-20	1.000	413.0	5.00e-20	1.000	414.0	2.00e-20	1.000
415.0	6.00e-20	1.000	416.0	6.00e-20	1.000	417.0	7.00e-20	1.000	418.0	5.00e-20	1.000	419.0	8.00e-20	1.000
420.0	8.00e-20	1.000	421.0	8.00e-20	1.000	422.0	9.00e-20	1.000	423.0	1.10e-19	1.000	424.0	9.00e-20	1.000
425.0	7.00e-20	1.000	426.0	1.40e-19	1.000	427.0	1.40e-19	1.000	428.0	1.20e-19	1.000	429.0	1.10e-19	1.000
430.0	1.70e-19	1.000	431.0	1.30e-19	1.000	432.0	1.50e-19	1.000	433.0	1.80e-19	1.000	434.0	1.80e-19	1.000
435.0	1.60e-19	1.000	436.0	1.50e-19	1.000	437.0	1.80e-19	1.000	438.0	2.10e-19	1.000	439.0	2.00e-19	1.000
440.0	1.90e-19	1.000	441.0	1.80e-19	1.000	442.0	2.10e-19	1.000	443.0	1.80e-19	1.000	444.0	1.90e-19	1.000
445.0	2.00e-19	1.000	446.0	2.40e-19	1.000	447.0	2.90e-19	1.000	448.0	2.40e-19	1.000	449.0	2.80e-19	1.000
450.0	2.90e-19	1.000	451.0	3.00e-19	1.000	452.0	3.30e-19	1.000	453.0	3.10e-19	1.000	454.0	3.60e-19	1.000
455.0	3.60e-19	1.000	456.0	3.60e-19	1.000	457.0	4.00e-19	1.000	458.0	3.70e-19	1.000	459.0	4.20e-19	1.000
460.0	4.00e-19	1.000	461.0	3.90e-19	1.000	462.0	4.00e-19	1.000	463.0	4.10e-19	1.000	464.0	4.80e-19	1.000
465.0	5.10e-19	1.000	466.0	5.40e-19	1.000	467.0	5.70e-19	1.000	468.0	5.60e-19	1.000	469.0	5.80e-19	1.000
470.0	5.90e-19	1.000	471.0	6.20e-19	1.000	472.0	6.40e-19	1.000	473.0	6.20e-19	1.000	474.0	6.20e-19	1.000
475.0	6.80e-19	1.000	476.0	7.80e-19	1.000	477.0	7.70e-19	1.000	478.0	7.30e-19	1.000	479.0	7.30e-19	1.000
480.0	7.00e-19	1.000	481.0	7.10e-19	1.000	482.0	7.10e-19	1.000	483.0	7.20e-19	1.000	484.0	7.70e-19	1.000
485.0	8.20e-19	1.000	486.0	9.10e-19	1.000	487.0	9.20e-19	1.000	488.0	9.50e-19	1.000	489.0	9.60e-19	1.000
490.0	1.03e-18	1.000	491.0	9.90e-19	1.000	492.0	9.90e-19	1.000	493.0	1.01e-18	1.000	494.0	1.01e-18	1.000
495.0	1.06e-18	1.000	496.0	1.21e-18	1.000	497.0	1.22e-18	1.000	498.0	1.20e-18	1.000	499.0	1.17e-18	1.000
500.0	1.13e-18	1.000	501.0	1.11e-18	1.000	502.0	1.11e-18	1.000	503.0	1.11e-18	1.000	504.0	1.26e-18	1.000
505.0	1.28e-18	1.000	506.0	1.34e-18	1.000	507.0	1.28e-18	1.000	508.0	1.27e-18	1.000	509.0	1.35e-18	1.000
510.0	1.51e-18	1.000	511.0	1.73e-18	1.000	512.0	1.77e-18	1.000	513.0	1.60e-18	1.000	514.0	1.58e-18	1.000
515.0	1.58e-18	1.000	516.0	1.56e-18	1.000	517.0	1.49e-18	1.000	518.0	1.44e-18	1.000	519.0	1.54e-18	1.000
520.0	1.68e-18	1.000	521.0	1.83e-18	1.000	522.0	1.93e-18	1.000	523.0	1.77e-18	1.000	524.0	1.64e-18	1.000
525.0	1.58e-18	1.000	526.0	1.63e-18	1.000	527.0	1.81e-18	1.000	528.0	2.10e-18	1.000	529.0	2.39e-18	1.000
530.0	2.23e-18	1.000	531.0	2.09e-18	1.000	532.0	2.02e-18	1.000	533.0	1.95e-18	1.000	534.0	2.04e-18	1.000
535.0	2.30e-18	1.000	536.0	2.57e-18	1.000	537.0	2.58e-18	1.000	538.0	2.34e-18	1.000	539.0	2.04e-18	1.000
540.0	2.10e-18	1.000	541.0	2.04e-18	1.000	542.0	1.88e-18	1.000	543.0	1.68e-18	1.000	544.0	1.70e-18	1.000
545.0	1.96e-18	1.000	546.0	2.42e-18	1.000	547.0	2.91e-18	1.000	548.0	2.98e-18	1.000	549.0	2.71e-18	1.000
550.0	2.48e-18	1.000	551.0	2.43e-18	1.000	552.0	2.47e-18	1.000	553.0	2.53e-18	1.000	554.0	2.78e-18	1.000
555.0	3.11e-18	1.000	556.0	3.26e-18	1.000	557.0	3.29e-18	1.000	558.0	3.51e-18	1.000	559.0	3.72e-18	1.000
560.0	3.32e-18	1.000	561.0	2.98e-18	1.000	562.0	2.90e-18	1.000	563.0	2.80e-18	1.000	564.0	2.72e-18	1.000
565.0	2.73e-18	1.000	566.0	2.85e-18	1.000	567.0	2.81e-18	1.000	568.0	2.85e-18	1.000	569.0	2.89e-18	1.000
570.0	2.79e-18	1.000	571.0	2.76e-18	1.000	572.0	2.74e-18	1.000	573.0	2.78e-18	1.000	574.0	2.86e-18	1.000
575.0	3.08e-18	1.000	576.0	3.27e-18	1.000	577.0	3.38e-18	1.000	578.0	3.31e-18	1.000	579.0	3.24e-18	1.000
580.0	3.34e-18	1.000	581.0	3.55e-18	1.000	582.0	3.28e-18	1.000	583.0	2.93e-18	1.000	584.0	2.82e-18	1.000
585.0	2.89e-18	1.000	586.0	3.32e-18	0.950	587.0	4.16e-18	0.900	588.0	5.04e-18	0.850	589.0	6.13e-18	0.800
590.0	5.96e-18	0.750	591.0	5.44e-18	0.720	592.0	5.11e-18	0.690	593.0	4.58e-18	0.660	594.0	4.19e-18	0.630
595.0	4.29e-18	0.600	596.0	4.62e-18	0.590	597.0	4.36e-18	0.580	598.0	3.67e-18	0.570	599.0	3.10e-18	0.560
600.0	2.76e-18	0.550	601.0	2.86e-18	0.540	602.0	3.32e-18	0.530	603.0	3.80e-18	0.520	604.0	4.37e-18	0.510
605.0	4.36e-18	0.400	606.0	3.32e-18	0.380	607.0	2.40e-18	0.360	608.0	1.85e-18	0.340	609.0	1.71e-18	0.320

Table A-3 (continued)

WL (nm)	Abs (cm ²)	QY	WL (nm)	Abs (cm ²)	QY	WL (nm)	Abs (cm ²)	QY	WL (nm)	Abs (cm ²)	QY	WL (nm)	Abs (cm ²)	QY
610.0	1.77e-18	0.300	611.0	1.91e-18	0.290	612.0	2.23e-18	0.280	613.0	2.63e-18	0.270	614.0	2.55e-18	0.260
615.0	2.26e-18	0.250	616.0	2.09e-18	0.240	617.0	2.11e-18	0.230	618.0	2.39e-18	0.220	619.0	2.56e-18	0.210
620.0	3.27e-18	0.200	621.0	5.24e-18	0.190	622.0	1.02e-17	0.180	623.0	1.47e-17	0.170	624.0	1.21e-17	0.160
625.0	8.38e-18	0.150	626.0	7.30e-18	0.130	627.0	7.53e-18	0.110	628.0	7.37e-18	0.090	629.0	6.98e-18	0.070
630.0	6.76e-18	0.050	631.0	4.84e-18	0.040	632.0	3.27e-18	0.030	633.0	2.17e-18	0.020	634.0	1.64e-18	0.010
635.0	1.44e-18	0.000												
<u>O3O3P</u>														
280.0	3.94e-18	0.095	281.0	3.62e-18	0.093	282.0	3.31e-18	0.090	283.0	2.99e-18	0.088	284.0	2.70e-18	0.086
285.0	2.46e-18	0.084	286.0	2.22e-18	0.082	287.0	1.98e-18	0.079	288.0	1.75e-18	0.077	289.0	1.59e-18	0.075
290.0	1.42e-18	0.073	291.0	1.25e-18	0.070	292.0	1.09e-18	0.068	293.0	9.81e-19	0.066	294.0	8.73e-19	0.064
295.0	7.65e-19	0.061	296.0	6.58e-19	0.059	297.0	5.81e-19	0.057	298.0	5.18e-19	0.055	299.0	4.55e-19	0.052
300.0	3.92e-19	0.050	301.0	3.35e-19	0.035	302.0	3.01e-19	0.025	303.0	2.66e-19	0.015	304.0	2.32e-19	0.010
305.0	1.97e-19	0.020	306.0	1.73e-19	0.050	307.0	1.55e-19	0.123	308.0	1.37e-19	0.227	309.0	1.18e-19	0.333
310.0	9.98e-20	0.400	311.0	8.92e-20	0.612	312.0	7.94e-20	0.697	313.0	6.96e-20	0.738	314.0	5.99e-20	0.762
315.0	5.01e-20	0.765	316.0	4.51e-20	0.779	317.0	4.00e-20	0.791	318.0	3.50e-20	0.806	319.0	2.99e-20	0.822
320.0	2.49e-20	0.852	321.0	2.23e-20	0.879	322.0	1.97e-20	0.903	323.0	1.72e-20	0.908	324.0	1.46e-20	0.920
325.0	1.20e-20	0.930	326.0	1.08e-20	0.934	327.0	9.67e-21	0.938	328.0	8.50e-21	0.942	329.0	7.34e-21	0.946
330.0	6.17e-21	0.950	331.0	5.48e-21	0.950	332.0	4.80e-21	0.950	333.0	4.11e-21	0.950	334.0	3.43e-21	0.950
335.0	2.74e-21	0.950	336.0	2.43e-21	0.960	337.0	2.11e-21	0.970	338.0	1.80e-21	0.980	339.0	1.48e-21	0.990
340.0	1.17e-21	1.000	350.0	0.00e+00	1.000	400.0	0.00e+00	1.000	410.0	1.20e-23	1.000	420.0	2.20e-23	1.000
440.0	1.12e-22	1.000	460.0	3.28e-22	1.000	480.0	6.84e-22	1.000	500.0	1.22e-21	1.000	520.0	1.82e-21	1.000
540.0	2.91e-21	1.000	560.0	3.94e-21	1.000	580.0	4.59e-21	1.000	600.0	5.11e-21	1.000	620.0	4.00e-21	1.000
640.0	2.96e-21	1.000	660.0	2.09e-21	1.000	680.0	1.36e-21	1.000	700.0	9.10e-22	1.000	750.0	3.20e-22	1.000
800.0	1.60e-22	1.000	900.0	0.00e+00	1.000									
<u>O3O1D</u>														
280.0	3.94e-18	0.905	281.0	3.62e-18	0.907	282.0	3.31e-18	0.910	283.0	2.99e-18	0.912	284.0	2.70e-18	0.914
285.0	2.46e-18	0.916	286.0	2.22e-18	0.918	287.0	1.98e-18	0.921	288.0	1.75e-18	0.923	289.0	1.59e-18	0.925
290.0	1.42e-18	0.927	291.0	1.25e-18	0.930	292.0	1.09e-18	0.932	293.0	9.81e-19	0.934	294.0	8.73e-19	0.936
295.0	7.65e-19	0.939	296.0	6.58e-19	0.941	297.0	5.81e-19	0.943	298.0	5.18e-19	0.945	299.0	4.55e-19	0.948
300.0	3.92e-19	0.950	301.0	3.35e-19	0.965	302.0	3.01e-19	0.975	303.0	2.66e-19	0.985	304.0	2.32e-19	0.990
305.0	1.97e-19	0.980	306.0	1.73e-19	0.950	307.0	1.55e-19	0.877	308.0	1.37e-19	0.773	309.0	1.18e-19	0.667
310.0	9.98e-20	0.600	311.0	8.92e-20	0.388	312.0	7.94e-20	0.303	313.0	6.96e-20	0.262	314.0	5.99e-20	0.238
315.0	5.01e-20	0.235	316.0	4.51e-20	0.221	317.0	4.00e-20	0.209	318.0	3.50e-20	0.194	319.0	2.99e-20	0.178
320.0	2.49e-20	0.148	321.0	2.23e-20	0.121	322.0	1.97e-20	0.097	323.0	1.72e-20	0.092	324.0	1.46e-20	0.080
325.0	1.20e-20	0.070	326.0	1.08e-20	0.066	327.0	9.67e-21	0.062	328.0	8.50e-21	0.058	329.0	7.34e-21	0.054
330.0	6.17e-21	0.050	331.0	5.48e-21	0.050	332.0	4.80e-21	0.050	333.0	4.11e-21	0.050	334.0	3.43e-21	0.050
335.0	2.74e-21	0.050	336.0	2.43e-21	0.040	337.0	2.11e-21	0.030	338.0	1.80e-21	0.020	339.0	1.48e-21	0.010
340.0	1.17e-21	0.000												
<u>HONO-NO</u>														
309.0	0.00e+00	0.410	310.0	1.30e-20	0.410	311.0	1.90e-20	0.411	312.0	2.80e-20	0.421	313.0	2.20e-20	0.432
314.0	3.60e-20	0.443	315.0	3.00e-20	0.454	316.0	1.40e-20	0.464	317.0	3.10e-20	0.475	318.0	5.60e-20	0.486
319.0	3.60e-20	0.496	320.0	4.90e-20	0.507	321.0	7.80e-20	0.518	322.0	4.90e-20	0.529	323.0	5.10e-20	0.539
324.0	7.10e-20	0.550	325.0	5.00e-20	0.561	326.0	2.90e-20	0.571	327.0	6.60e-20	0.582	328.0	1.17e-19	0.593
329.0	6.10e-20	0.604	330.0	1.11e-19	0.614	331.0	1.79e-19	0.625	332.0	8.70e-20	0.636	333.0	7.60e-20	0.646
334.0	9.60e-20	0.657	335.0	9.60e-20	0.668	336.0	7.20e-20	0.679	337.0	5.30e-20	0.689	338.0	1.00e-19	0.700
339.0	1.88e-19	0.711	340.0	1.00e-19	0.721	341.0	1.70e-19	0.732	342.0	3.86e-19	0.743	343.0	1.49e-19	0.754
344.0	9.70e-20	0.764	345.0	1.09e-19	0.775	346.0	1.23e-19	0.786	347.0	1.04e-19	0.796	348.0	9.10e-20	0.807
349.0	7.90e-20	0.818	350.0	1.12e-19	0.829	351.0	2.12e-19	0.839	352.0	1.55e-19	0.850	353.0	1.91e-19	0.861
354.0	5.81e-19	0.871	355.0	3.64e-19	0.882	356.0	1.41e-19	0.893	357.0	1.17e-19	0.904	358.0	1.20e-19	0.914
359.0	1.04e-19	0.925	360.0	9.00e-20	0.936	361.0	8.30e-20	0.946	362.0	8.00e-20	0.957	363.0	9.60e-20	0.968
364.0	1.46e-19	0.979	365.0	1.68e-19	0.989	366.0	1.83e-19	1.000	367.0	3.02e-19	1.000	368.0	5.20e-19	1.000
369.0	3.88e-19	1.000	370.0	1.78e-19	1.000	371.0	1.13e-19	1.000	372.0	1.00e-19	1.000	373.0	7.70e-20	1.000
374.0	6.20e-20	1.000	375.0	5.30e-20	1.000	376.0	5.30e-20	1.000	377.0	5.00e-20	1.000	378.0	5.80e-20	1.000
379.0	8.00e-20	1.000	380.0	9.60e-20	1.000	381.0	1.13e-19	1.000	382.0	1.59e-19	1.000	383.0	2.10e-19	1.000
384.0	2.41e-19	1.000	385.0	2.03e-19	1.000	386.0	1.34e-19	1.000	387.0	9.00e-20	1.000	388.0	5.60e-20	1.000
389.0	3.40e-20	1.000	390.0	2.70e-20	1.000	391.0	2.00e-20	1.000	392.0	1.50e-20	1.000	393.0	1.10e-20	1.000
394.0	6.00e-21	1.000	395.0	1.00e-20	1.000	396.0	4.00e-21	1.000	400.0	0.00e+00	1.000			
<u>HONO-NO2</u>														
309.0	0.00e+00	0.590	310.0	1.30e-20	0.590	311.0	1.90e-20	0.589	312.0	2.80e-20	0.579	313.0	2.20e-20	0.568
314.0	3.60e-20	0.557	315.0	3.00e-20	0.546	316.0	1.40e-20	0.536	317.0	3.10e-20	0.525	318.0	5.60e-20	0.514
319.0	3.60e-20	0.504	320.0	4.90e-20	0.493	321.0	7.80e-20	0.482	322.0	4.90e-20	0.471	323.0	5.10e-20	0.461
324.0	7.10e-20	0.450	325.0	5.00e-20	0.439	326.0	2.90e-20	0.429	327.0	6.60e-20	0.418	328.0	1.17e-19	0.407
329.0	6.10e-20	0.396	330.0	1.11e-19	0.386	331.0	1.79e-19	0.375	332.0	8.70e-20	0.364	333.0	7.60e-20	0.354
334.0	9.60e-20	0.343	335.0	9.60e-20	0.332	336.0	7.20e-20	0.321	337.0	5.30e-20	0.311	338.0	1.00e-19	0.300
339.0	1.88e-19	0.289	340.0	1.00e-19	0.279	341.0	1.70e-19	0.268	342.0	3.86e-19	0.257	343.0	1.49e-19	0.246
344.0	9.70e-20	0.236	345.0	1.09e-19	0.225	346.0	1.23e-19	0.214	347.0	1.04e-19	0.204	348.0	9.10e-20	0.193
349.0	7.90e-20	0.182	350.0	1.12e-19	0.171	351.0	2.12e-19	0.161	352.0	1.55e-19	0.150	353.0	1.91e-19	0.139
354.0	5.81e-19	0.129	355.0	3.64e-19	0.118	356.0	1.41e-19	0.107	357.0	1.17e-19	0.096	358.0	1.20e-19	0.086
359.0	1.04e-19	0.075	360.0	9.00e-20	0.064	361.0	8.30e-20	0.054	362.0	8.00e-20	0.043	363.0	9.60e-20	0.032

Table A-3 (continued)

WL (nm)	Abs (cm ²)	QY	WL (nm)	Abs (cm ²)	QY	WL (nm)	Abs (cm ²)	QY	WL (nm)	Abs (cm ²)	QY	WL (nm)	Abs (cm ²)	QY
364.0	1.46e-19	0.021	365.0	1.68e-19	0.011	366.0	1.83e-19	0.000						
<u>HNO3</u>														
190.0	1.36e-17	1.000	195.0	1.02e-17	1.000	200.0	5.88e-18	1.000	205.0	2.80e-18	1.000	210.0	1.04e-18	1.000
215.0	3.65e-19	1.000	220.0	1.49e-19	1.000	225.0	8.81e-20	1.000	230.0	5.75e-20	1.000	235.0	3.75e-20	1.000
240.0	2.58e-20	1.000	245.0	2.11e-20	1.000	250.0	1.97e-20	1.000	255.0	1.95e-20	1.000	260.0	1.91e-20	1.000
265.0	1.80e-20	1.000	270.0	1.62e-20	1.000	275.0	1.38e-20	1.000	280.0	1.12e-20	1.000	285.0	8.58e-21	1.000
290.0	6.15e-21	1.000	295.0	4.12e-21	1.000	300.0	2.63e-21	1.000	305.0	1.50e-21	1.000	310.0	8.10e-22	1.000
315.0	4.10e-22	1.000	320.0	2.00e-22	1.000	325.0	9.50e-23	1.000	330.0	4.30e-23	1.000	335.0	2.20e-23	1.000
340.0	1.00e-23	1.000	345.0	6.00e-24	1.000	350.0	4.00e-24	1.000	355.0	0.00e+00	1.000			
<u>HO2NO2</u>														
190.0	1.01e-17	1.000	195.0	8.16e-18	1.000	200.0	5.63e-18	1.000	205.0	3.67e-18	1.000	210.0	2.39e-18	1.000
215.0	1.61e-18	1.000	220.0	1.18e-18	1.000	225.0	9.32e-19	1.000	230.0	7.88e-19	1.000	235.0	6.80e-19	1.000
240.0	5.79e-19	1.000	245.0	4.97e-19	1.000	250.0	4.11e-19	1.000	255.0	3.49e-19	1.000	260.0	2.84e-19	1.000
265.0	2.29e-19	1.000	270.0	1.80e-19	1.000	275.0	1.33e-19	1.000	280.0	9.30e-20	1.000	285.0	6.20e-20	1.000
290.0	3.90e-20	1.000	295.0	2.40e-20	1.000	300.0	1.40e-20	1.000	305.0	8.50e-21	1.000	310.0	5.30e-21	1.000
315.0	3.90e-21	1.000	320.0	2.40e-21	1.000	325.0	1.50e-21	1.000	330.0	9.00e-22	1.000	335.0	0.00e+00	1.000
<u>H2O2</u>														
190.0	6.72e-19	1.000	195.0	5.63e-19	1.000	200.0	4.75e-19	1.000	205.0	4.08e-19	1.000	210.0	3.57e-19	1.000
215.0	3.07e-19	1.000	220.0	2.58e-19	1.000	225.0	2.17e-19	1.000	230.0	1.82e-19	1.000	235.0	1.50e-19	1.000
240.0	1.24e-19	1.000	245.0	1.02e-19	1.000	250.0	8.30e-20	1.000	255.0	6.70e-20	1.000	260.0	5.30e-20	1.000
265.0	4.20e-20	1.000	270.0	3.30e-20	1.000	275.0	2.60e-20	1.000	280.0	2.00e-20	1.000	285.0	1.50e-20	1.000
290.0	1.20e-20	1.000	295.0	9.00e-21	1.000	300.0	6.80e-21	1.000	305.0	5.10e-21	1.000	310.0	3.90e-21	1.000
315.0	2.90e-21	1.000	320.0	2.20e-21	1.000	325.0	1.60e-21	1.000	330.0	1.30e-21	1.000	335.0	1.00e-21	1.000
340.0	7.00e-22	1.000	345.0	5.00e-22	1.000	350.0	4.00e-22	1.000	355.0	0.00e+00	1.000			
<u>HCHO R</u>														
240.0	6.40e-22	0.270	241.0	5.60e-22	0.272	242.0	1.05e-21	0.274	243.0	1.15e-21	0.276	244.0	8.20e-22	0.278
245.0	1.03e-21	0.280	246.0	9.80e-22	0.282	247.0	1.35e-21	0.284	248.0	1.91e-21	0.286	249.0	2.82e-21	0.288
250.0	2.05e-21	0.290	251.0	1.70e-21	0.291	252.0	2.88e-21	0.292	253.0	2.55e-21	0.293	254.0	2.55e-21	0.294
255.0	3.60e-21	0.295	256.0	5.09e-21	0.296	257.0	3.39e-21	0.297	258.0	2.26e-21	0.298	259.0	5.04e-21	0.299
260.0	5.05e-21	0.300	261.0	5.49e-21	0.308	262.0	5.20e-21	0.316	263.0	9.33e-21	0.324	264.0	8.23e-21	0.332
265.0	4.30e-21	0.340	266.0	4.95e-21	0.348	267.0	1.24e-20	0.356	268.0	1.11e-20	0.364	269.0	8.78e-21	0.372
270.0	9.36e-21	0.380	271.0	1.79e-20	0.399	272.0	1.23e-20	0.418	273.0	6.45e-21	0.437	274.0	6.56e-21	0.456
275.0	2.23e-20	0.475	276.0	2.42e-20	0.494	277.0	1.40e-20	0.513	278.0	1.05e-20	0.532	279.0	2.55e-20	0.551
280.0	2.08e-20	0.570	281.0	1.48e-20	0.586	282.0	8.81e-21	0.602	283.0	1.07e-20	0.618	284.0	4.49e-20	0.634
285.0	3.59e-20	0.650	286.0	1.96e-20	0.666	287.0	1.30e-20	0.682	288.0	3.36e-20	0.698	289.0	2.84e-20	0.714
290.0	1.30e-20	0.730	291.0	1.75e-20	0.735	292.0	8.32e-21	0.740	293.0	3.73e-20	0.745	294.0	6.54e-20	0.750
295.0	3.95e-20	0.755	296.0	2.33e-20	0.760	297.0	1.51e-20	0.765	298.0	4.04e-20	0.770	299.0	2.87e-20	0.775
300.0	8.71e-21	0.780	301.0	1.72e-20	0.780	302.0	1.06e-20	0.780	303.0	3.20e-20	0.780	304.0	6.90e-20	0.780
305.0	4.91e-20	0.780	306.0	4.63e-20	0.780	307.0	2.10e-20	0.780	308.0	1.49e-20	0.780	309.0	3.41e-20	0.780
310.0	1.95e-20	0.780	311.0	5.21e-21	0.764	312.0	1.12e-20	0.748	313.0	1.12e-20	0.732	314.0	4.75e-20	0.716
315.0	5.25e-20	0.700	316.0	2.90e-20	0.684	317.0	5.37e-20	0.668	318.0	2.98e-20	0.652	319.0	9.18e-21	0.636
320.0	1.26e-20	0.620	321.0	1.53e-20	0.585	322.0	6.69e-21	0.550	323.0	3.45e-21	0.515	324.0	8.16e-21	0.480
325.0	1.85e-20	0.445	326.0	5.95e-20	0.410	327.0	3.49e-20	0.375	328.0	1.09e-20	0.340	329.0	3.35e-20	0.305
330.0	3.32e-20	0.270	331.0	1.07e-20	0.243	332.0	2.89e-21	0.216	333.0	2.15e-21	0.189	334.0	1.71e-21	0.162
335.0	1.43e-21	0.135	336.0	1.94e-21	0.108	337.0	4.17e-21	0.081	338.0	2.36e-20	0.054	339.0	4.71e-20	0.027
340.0	2.48e-20	0.000												
<u>HCHO M</u>														
240.0	6.40e-22	0.490	241.0	5.60e-22	0.490	242.0	1.05e-21	0.490	243.0	1.15e-21	0.490	244.0	8.20e-22	0.490
245.0	1.03e-21	0.490	246.0	9.80e-22	0.490	247.0	1.35e-21	0.490	248.0	1.91e-21	0.490	249.0	2.82e-21	0.490
250.0	2.05e-21	0.490	251.0	1.70e-21	0.490	252.0	2.88e-21	0.490	253.0	2.55e-21	0.490	254.0	2.55e-21	0.490
255.0	3.60e-21	0.490	256.0	5.09e-21	0.490	257.0	3.39e-21	0.490	258.0	2.26e-21	0.490	259.0	5.04e-21	0.490
260.0	5.05e-21	0.490	261.0	5.49e-21	0.484	262.0	5.20e-21	0.478	263.0	9.33e-21	0.472	264.0	8.23e-21	0.466
265.0	4.30e-21	0.460	266.0	4.95e-21	0.454	267.0	1.24e-20	0.448	268.0	1.11e-20	0.442	269.0	8.78e-21	0.436
270.0	9.36e-21	0.430	271.0	1.79e-20	0.419	272.0	1.23e-20	0.408	273.0	6.45e-21	0.397	274.0	6.56e-21	0.386
275.0	2.23e-20	0.375	276.0	2.42e-20	0.364	277.0	1.40e-20	0.353	278.0	1.05e-20	0.342	279.0	2.55e-20	0.331
280.0	2.08e-20	0.320	281.0	1.48e-20	0.312	282.0	8.81e-21	0.304	283.0	1.07e-20	0.296	284.0	4.49e-20	0.288
285.0	3.59e-20	0.280	286.0	1.96e-20	0.272	287.0	1.30e-20	0.264	288.0	3.36e-20	0.256	289.0	2.84e-20	0.248
290.0	1.30e-20	0.240	291.0	1.75e-20	0.237	292.0	8.32e-21	0.234	293.0	3.73e-20	0.231	294.0	6.54e-20	0.228
295.0	3.95e-20	0.225	296.0	2.33e-20	0.222	297.0	1.51e-20	0.219	298.0	4.04e-20	0.216	299.0	2.87e-20	0.213
300.0	8.71e-21	0.210	301.0	1.72e-20	0.211	302.0	1.06e-20	0.212	303.0	3.20e-20	0.213	304.0	6.90e-20	0.214
305.0	4.91e-20	0.215	306.0	4.63e-20	0.216	307.0	2.10e-20	0.217	308.0	1.49e-20	0.218	309.0	3.41e-20	0.219
310.0	1.95e-20	0.220	311.0	5.21e-21	0.236	312.0	1.12e-20	0.252	313.0	1.12e-20	0.268	314.0	4.75e-20	0.284
315.0	5.25e-20	0.300	316.0	2.90e-20	0.316	317.0	5.37e-20	0.332	318.0	2.98e-20	0.348	319.0	9.18e-21	0.364
320.0	1.26e-20	0.380	321.0	1.53e-20	0.408	322.0	6.69e-21	0.436	323.0	3.45e-21	0.464	324.0	8.16e-21	0.492
325.0	1.85e-20	0.520	326.0	5.95e-20	0.548	327.0	3.49e-20	0.576	328.0	1.09e-20	0.604	329.0	3.35e-20	0.632
330.0	3.32e-20	0.660	331.0	1.07e-20	0.650	332.0	2.89e-21	0.640	333.0	2.15e-21	0.630	334.0	1.71e-21	0.620
335.0	1.43e-21	0.610	336.0	1.94e-21	0.600	337.0	4.17e-21	0.590	338.0	2.36e-20	0.580	339.0	4.71e-20	0.570
340.0	2.48e-20	0.560	341.0	7.59e-21	0.525	342.0	6.81e-21	0.490	343.0	1.95e-20	0.455	344.0	1.14e-20	0.420
345.0	3.23e-21	0.385	346.0	1.13e-21	0.350	347.0	6.60e-22	0.315	348.0	1.22e-21	0.280	349.0	3.20e-22	0.245

Table A-3 (continued)

WL (nm)	Abs (cm ²)	QY	WL (nm)	Abs (cm ²)	QY	WL (nm)	Abs (cm ²)	QY	WL (nm)	Abs (cm ²)	QY	WL (nm)	Abs (cm ²)	QY
350.0	3.80e-22	0.210	351.0	1.04e-21	0.192	352.0	7.13e-21	0.174	353.0	2.21e-20	0.156	354.0	1.54e-20	0.138
355.0	6.76e-21	0.120	356.0	1.35e-21	0.102	357.0	3.60e-22	0.084	358.0	5.70e-23	0.066	359.0	5.80e-22	0.048
360.0	8.20e-22	0.000												
<u>CCHO_R</u>														
262.0	2.44e-20	0.326	266.0	3.05e-20	0.358	270.0	3.42e-20	0.390	274.0	4.03e-20	0.466	278.0	4.19e-20	0.542
280.0	4.50e-20	0.580	281.0	4.69e-20	0.575	282.0	4.72e-20	0.570	283.0	4.75e-20	0.565	284.0	4.61e-20	0.560
285.0	4.49e-20	0.555	286.0	4.44e-20	0.550	287.0	4.59e-20	0.545	288.0	4.72e-20	0.540	289.0	4.77e-20	0.535
290.0	4.89e-20	0.530	291.0	4.78e-20	0.520	292.0	4.68e-20	0.510	293.0	4.53e-20	0.500	294.0	4.33e-20	0.490
295.0	4.27e-20	0.480	296.0	4.24e-20	0.470	297.0	4.38e-20	0.460	298.0	4.41e-20	0.450	299.0	4.26e-20	0.440
300.0	4.16e-20	0.430	301.0	3.99e-20	0.418	302.0	3.86e-20	0.406	303.0	3.72e-20	0.394	304.0	3.48e-20	0.382
305.0	3.42e-20	0.370	306.0	3.42e-20	0.354	307.0	3.36e-20	0.338	308.0	3.33e-20	0.322	309.0	3.14e-20	0.306
310.0	2.93e-20	0.290	311.0	2.76e-20	0.266	312.0	2.53e-20	0.242	313.0	2.47e-20	0.218	314.0	2.44e-20	0.194
315.0	2.20e-20	0.170	316.0	2.04e-20	0.156	317.0	2.07e-20	0.142	318.0	1.98e-20	0.128	319.0	1.87e-20	0.114
320.0	1.72e-20	0.100	321.0	1.48e-20	0.088	322.0	1.40e-20	0.076	323.0	1.24e-20	0.064	324.0	1.09e-20	0.052
325.0	1.14e-20	0.040	326.0	1.07e-20	0.032	327.0	8.58e-21	0.024	328.0	7.47e-21	0.016	329.0	7.07e-21	0.008
<u>C2CHO</u>														
294.0	5.80e-20	0.890	295.0	5.57e-20	0.885	296.0	5.37e-20	0.880	297.0	5.16e-20	0.875	298.0	5.02e-20	0.870
299.0	5.02e-20	0.865	300.0	5.04e-20	0.860	301.0	5.09e-20	0.855	302.0	5.07e-20	0.850	303.0	4.94e-20	0.818
304.0	4.69e-20	0.786	305.0	4.32e-20	0.755	306.0	4.04e-20	0.723	307.0	3.81e-20	0.691	308.0	3.65e-20	0.659
309.0	3.62e-20	0.627	310.0	3.60e-20	0.596	311.0	3.53e-20	0.564	312.0	3.50e-20	0.532	313.0	3.32e-20	0.500
314.0	3.06e-20	0.480	315.0	2.77e-20	0.460	316.0	2.43e-20	0.440	317.0	2.18e-20	0.420	318.0	2.00e-20	0.400
319.0	1.86e-20	0.380	320.0	1.83e-20	0.360	321.0	1.78e-20	0.340	322.0	1.66e-20	0.320	323.0	1.58e-20	0.300
324.0	1.49e-20	0.280	325.0	1.30e-20	0.260	326.0	1.13e-20	0.248	327.0	9.96e-21	0.236	328.0	8.28e-21	0.223
329.0	6.85e-21	0.211	330.0	5.75e-21	0.199	331.0	4.94e-21	0.187	332.0	4.66e-21	0.174	333.0	4.30e-21	0.162
334.0	3.73e-21	0.150	335.0	3.25e-21	0.133	336.0	2.80e-21	0.117	337.0	2.30e-21	0.100	338.0	1.85e-21	0.083
339.0	1.66e-21	0.067	340.0	1.55e-21	0.050	341.0	1.19e-21	0.033	342.0	7.60e-22	0.017	343.0	4.50e-22	0.000
<u>ACETONE</u>														
250.0	2.47e-20	0.760	254.0	3.04e-20	0.776	258.0	3.61e-20	0.792	262.0	4.15e-20	0.768	266.0	4.58e-20	0.704
270.0	4.91e-20	0.640	274.0	5.06e-20	0.604	278.0	5.07e-20	0.568	280.0	5.05e-20	0.550	281.0	5.01e-20	0.525
282.0	4.94e-20	0.500	283.0	4.86e-20	0.475	284.0	4.76e-20	0.450	285.0	4.68e-20	0.425	286.0	4.58e-20	0.400
287.0	4.50e-20	0.375	288.0	4.41e-20	0.350	289.0	4.29e-20	0.325	290.0	4.19e-20	0.302	291.0	4.08e-20	0.284
292.0	3.94e-20	0.266	293.0	3.81e-20	0.249	294.0	3.67e-20	0.232	295.0	3.52e-20	0.217	296.0	3.35e-20	0.201
297.0	3.20e-20	0.187	298.0	3.07e-20	0.173	299.0	2.91e-20	0.160	300.0	2.77e-20	0.147	301.0	2.66e-20	0.135
302.0	2.53e-20	0.124	303.0	2.37e-20	0.114	304.0	2.24e-20	0.104	305.0	2.11e-20	0.095	306.0	1.95e-20	0.086
307.0	1.80e-20	0.078	308.0	1.66e-20	0.071	309.0	1.54e-20	0.064	310.0	1.41e-20	0.057	311.0	1.28e-20	0.052
312.0	1.17e-20	0.046	313.0	1.08e-20	0.042	314.0	9.67e-21	0.037	315.0	8.58e-21	0.033	316.0	7.77e-21	0.029
317.0	6.99e-21	0.026	318.0	6.08e-21	0.023	319.0	5.30e-21	0.020	320.0	4.67e-21	0.018	321.0	4.07e-21	0.016
322.0	3.44e-21	0.014	323.0	2.87e-21	0.012	324.0	2.43e-21	0.011	325.0	2.05e-21	0.009	326.0	1.68e-21	0.008
327.0	1.35e-21	0.007	328.0	1.08e-21	0.006	329.0	8.60e-22	0.005	330.0	6.70e-22	0.005	331.0	5.10e-22	0.004
332.0	4.00e-22	0.003	333.0	3.10e-22	0.003	334.0	2.60e-22	0.002	335.0	1.70e-22	0.002	336.0	1.40e-22	0.002
337.0	1.10e-22	0.002	338.0	9.00e-23	0.001	339.0	6.00e-23	0.001	340.0	5.00e-23	0.001	341.0	5.00e-23	0.001
342.0	3.00e-23	0.001	343.0	4.00e-23	0.001	344.0	2.00e-23	0.000						
<u>KETONE</u>														
198.5	3.95e-19	1.000	199.0	1.61e-19	1.000	199.5	7.75e-20	1.000	200.0	3.76e-20	1.000	200.5	2.51e-20	1.000
201.0	1.83e-20	1.000	201.5	1.36e-20	1.000	202.0	1.16e-20	1.000	202.5	8.97e-21	1.000	203.0	4.62e-21	1.000
203.5	3.18e-21	1.000	204.0	2.42e-21	1.000	204.5	2.01e-21	1.000	205.0	1.77e-21	1.000	205.5	1.64e-21	1.000
206.0	1.54e-21	1.000	206.5	1.52e-21	1.000	207.0	1.54e-21	1.000	207.5	1.62e-21	1.000	208.0	1.64e-21	1.000
208.5	1.60e-21	1.000	209.0	1.57e-21	1.000	209.5	1.49e-21	1.000	210.0	1.47e-21	1.000	210.5	1.52e-21	1.000
211.0	1.50e-21	1.000	211.5	1.62e-21	1.000	212.0	1.81e-21	1.000	212.5	2.10e-21	1.000	213.0	2.23e-21	1.000
213.5	2.06e-21	1.000	214.0	1.69e-21	1.000	214.5	1.49e-21	1.000	215.0	1.42e-21	1.000	215.5	1.42e-21	1.000
216.0	1.42e-21	1.000	216.5	1.48e-21	1.000	217.0	1.48e-21	1.000	217.5	1.53e-21	1.000	218.0	1.56e-21	1.000
218.5	1.67e-21	1.000	219.0	1.68e-21	1.000	219.5	1.78e-21	1.000	220.0	1.85e-21	1.000	220.5	1.92e-21	1.000
221.0	2.01e-21	1.000	221.5	2.11e-21	1.000	222.0	2.23e-21	1.000	222.5	2.33e-21	1.000	223.0	2.48e-21	1.000
223.5	2.60e-21	1.000	224.0	2.74e-21	1.000	224.5	2.85e-21	1.000	225.0	3.04e-21	1.000	225.5	3.15e-21	1.000
226.0	3.33e-21	1.000	226.5	3.55e-21	1.000	227.0	3.73e-21	1.000	227.5	3.93e-21	1.000	228.0	4.11e-21	1.000
228.5	4.34e-21	1.000	229.0	4.56e-21	1.000	229.5	4.75e-21	1.000	230.0	5.01e-21	1.000	230.5	5.27e-21	1.000
231.0	5.53e-21	1.000	231.5	5.83e-21	1.000	232.0	6.15e-21	1.000	232.5	6.45e-21	1.000	233.0	6.73e-21	1.000
233.5	7.02e-21	1.000	234.0	7.42e-21	1.000	234.5	7.83e-21	1.000	235.0	8.11e-21	1.000	235.5	8.45e-21	1.000
236.0	8.82e-21	1.000	236.5	9.21e-21	1.000	237.0	9.65e-21	1.000	237.5	1.00e-20	1.000	238.0	1.05e-20	1.000
238.5	1.10e-20	1.000	239.0	1.15e-20	1.000	239.5	1.20e-20	1.000	240.0	1.23e-20	1.000	240.5	1.28e-20	1.000
241.0	1.32e-20	1.000	241.5	1.38e-20	1.000	242.0	1.44e-20	1.000	242.5	1.50e-20	1.000	243.0	1.57e-20	1.000
243.5	1.63e-20	1.000	244.0	1.68e-20	1.000	244.5	1.75e-20	1.000	245.0	1.81e-20	1.000	245.5	1.88e-20	1.000
246.0	1.96e-20	1.000	246.5	2.03e-20	1.000	247.0	2.11e-20	1.000	247.5	2.19e-20	1.000	248.0	2.25e-20	1.000
248.5	2.33e-20	1.000	249.0	2.40e-20	1.000	249.5	2.48e-20	1.000	250.0	2.56e-20	1.000	250.5	2.64e-20	1.000
251.0	2.73e-20	1.000	251.5	2.81e-20	1.000	252.0	2.88e-20	1.000	252.5	2.98e-20	1.000	253.0	3.07e-20	1.000
253.5	3.16e-20	1.000	254.0	3.25e-20	1.000	254.5	3.34e-20	1.000	255.0	3.43e-20	1.000	255.5	3.51e-20	1.000
256.0	3.59e-20	1.000	256.5	3.67e-20	1.000	257.0	3.75e-20	1.000	257.5	3.84e-20	1.000	258.0	3.94e-20	1.000
258.5	4.03e-20	1.000	259.0	4.13e-20	1.000	259.5	4.22e-20	1.000	260.0	4.28e-20	1.000	260.5	4.33e-20	1.000
261.0	4.41e-20	1.000	261.5	4.49e-20	1.000	262.0	4.57e-20	1.000	262.5	4.65e-20	1.000	263.0	4.72e-20	1.000
263.5	4.78e-20	1.000	264.0	4.85e-20	1.000	264.5	4.92e-20	1.000	265.0	4.99e-20	1.000	265.5	5.04e-20	1.000
266.0	5.12e-20	1.000	266.5	5.22e-20	1.000	267.0	5.28e-20	1.000	267.5	5.34e-20	1.000	268.0	5.41e-20	1.000

Table A-3 (continued)

WL (nm)	Abs (cm ²)	QY	WL (nm)	Abs (cm ²)	QY	WL (nm)	Abs (cm ²)	QY	WL (nm)	Abs (cm ²)	QY	WL (nm)	Abs (cm ²)	QY
268.5	5.46e-20	1.000	269.0	5.51e-20	1.000	269.5	5.55e-20	1.000	270.0	5.59e-20	1.000	270.5	5.63e-20	1.000
271.0	5.66e-20	1.000	271.5	5.70e-20	1.000	272.0	5.74e-20	1.000	272.5	5.78e-20	1.000	273.0	5.81e-20	1.000
273.5	5.86e-20	1.000	274.0	5.90e-20	1.000	274.5	5.93e-20	1.000	275.0	5.96e-20	1.000	275.5	5.97e-20	1.000
276.0	5.98e-20	1.000	276.5	5.98e-20	1.000	277.0	5.99e-20	1.000	277.5	5.99e-20	1.000	278.0	5.98e-20	1.000
278.5	5.96e-20	1.000	279.0	5.96e-20	1.000	279.5	5.95e-20	1.000	280.0	5.94e-20	1.000	280.5	5.92e-20	1.000
281.0	5.90e-20	1.000	281.5	5.88e-20	1.000	282.0	5.86e-20	1.000	282.5	5.83e-20	1.000	283.0	5.79e-20	1.000
283.5	5.75e-20	1.000	284.0	5.71e-20	1.000	284.5	5.67e-20	1.000	285.0	5.61e-20	1.000	285.5	5.56e-20	1.000
286.0	5.51e-20	1.000	286.5	5.45e-20	1.000	287.0	5.41e-20	1.000	287.5	5.37e-20	1.000	288.0	5.33e-20	1.000
288.5	5.27e-20	1.000	289.0	5.21e-20	1.000	289.5	5.15e-20	1.000	290.0	5.08e-20	1.000	290.5	4.99e-20	1.000
291.0	4.89e-20	1.000	291.5	4.82e-20	1.000	292.0	4.73e-20	1.000	292.5	4.62e-20	1.000	293.0	4.53e-20	1.000
293.5	4.41e-20	1.000	294.0	4.32e-20	1.000	294.5	4.23e-20	1.000	295.0	4.15e-20	1.000	295.5	4.11e-20	1.000
296.0	4.01e-20	1.000	296.5	3.94e-20	1.000	297.0	3.88e-20	1.000	297.5	3.77e-20	1.000	298.0	3.69e-20	1.000
298.5	3.63e-20	1.000	299.0	3.54e-20	1.000	299.5	3.46e-20	1.000	300.0	3.36e-20	1.000	300.5	3.24e-20	1.000
301.0	3.16e-20	1.000	301.5	3.06e-20	1.000	302.0	2.95e-20	1.000	302.5	2.82e-20	1.000	303.0	2.70e-20	1.000
303.5	2.59e-20	1.000	304.0	2.49e-20	1.000	304.5	2.42e-20	1.000	305.0	2.34e-20	1.000	305.5	2.28e-20	1.000
306.0	2.19e-20	1.000	306.5	2.11e-20	1.000	307.0	2.04e-20	1.000	307.5	1.93e-20	1.000	308.0	1.88e-20	1.000
308.5	1.80e-20	1.000	309.0	1.73e-20	1.000	309.5	1.66e-20	1.000	310.0	1.58e-20	1.000	310.5	1.48e-20	1.000
311.0	1.42e-20	1.000	311.5	1.34e-20	1.000	312.0	1.26e-20	1.000	312.5	1.17e-20	1.000	313.0	1.13e-20	1.000
313.5	1.08e-20	1.000	314.0	1.04e-20	1.000	314.5	9.69e-21	1.000	315.0	8.91e-21	1.000	315.5	8.61e-21	1.000
316.0	7.88e-21	1.000	316.5	7.25e-21	1.000	317.0	6.92e-21	1.000	317.5	6.43e-21	1.000	318.0	6.07e-21	1.000
318.5	5.64e-21	1.000	319.0	5.19e-21	1.000	319.5	4.66e-21	1.000	320.0	4.36e-21	1.000	320.5	3.95e-21	1.000
321.0	3.64e-21	1.000	321.5	3.38e-21	1.000	322.0	3.17e-21	1.000	322.5	2.80e-21	1.000	323.0	2.62e-21	1.000
323.5	2.29e-21	1.000	324.0	2.13e-21	1.000	324.5	1.93e-21	1.000	325.0	1.70e-21	1.000	325.5	1.58e-21	1.000
326.0	1.48e-21	1.000	326.5	1.24e-21	1.000	327.0	1.20e-21	1.000	327.5	1.04e-21	1.000	328.0	9.51e-22	1.000
328.5	8.44e-22	1.000	329.0	7.26e-22	1.000	329.5	6.70e-22	1.000	330.0	6.08e-22	1.000	330.5	5.15e-22	1.000
331.0	4.56e-22	1.000	331.5	4.13e-22	1.000	332.0	3.56e-22	1.000	332.5	3.30e-22	1.000	333.0	2.97e-22	1.000
333.5	2.67e-22	1.000	334.0	2.46e-22	1.000	334.5	2.21e-22	1.000	335.0	1.93e-22	1.000	335.5	1.56e-22	1.000
336.0	1.47e-22	1.000	336.5	1.37e-22	1.000	337.0	1.27e-22	1.000	337.5	1.19e-22	1.000	338.0	1.09e-22	1.000
338.5	1.01e-22	1.000	339.0	9.09e-23	1.000	339.5	8.22e-23	1.000	340.0	7.66e-23	1.000	340.5	7.43e-23	1.000
341.0	6.83e-23	1.000	341.5	6.72e-23	1.000	342.0	6.04e-23	1.000	342.5	4.78e-23	1.000	343.0	0.00e+00	1.000
COOH														
210.0	3.12e-19	1.000	215.0	2.09e-19	1.000	220.0	1.54e-19	1.000	225.0	1.22e-19	1.000	230.0	9.62e-20	1.000
235.0	7.61e-20	1.000	240.0	6.05e-20	1.000	245.0	4.88e-20	1.000	250.0	3.98e-20	1.000	255.0	3.23e-20	1.000
260.0	2.56e-20	1.000	265.0	2.11e-20	1.000	270.0	1.70e-20	1.000	275.0	1.39e-20	1.000	280.0	1.09e-20	1.000
285.0	8.63e-21	1.000	290.0	6.91e-21	1.000	295.0	5.51e-21	1.000	300.0	4.13e-21	1.000	305.0	3.13e-21	1.000
310.0	2.39e-21	1.000	315.0	1.82e-21	1.000	320.0	1.37e-21	1.000	325.0	1.05e-21	1.000	330.0	7.90e-22	1.000
335.0	6.10e-22	1.000	340.0	4.70e-22	1.000	345.0	3.50e-22	1.000	350.0	2.70e-22	1.000	355.0	2.10e-22	1.000
360.0	1.60e-22	1.000	365.0	1.20e-22	1.000	370.0	0.00e+00	1.000						
GLY R														
230.0	2.87e-21	1.000	235.0	2.87e-21	1.000	240.0	4.30e-21	1.000	245.0	5.73e-21	1.000	250.0	8.60e-21	1.000
255.0	1.15e-20	1.000	260.0	1.43e-20	1.000	265.0	1.86e-20	1.000	270.0	2.29e-20	1.000	275.0	2.58e-20	1.000
280.0	2.87e-20	1.000	285.0	3.30e-20	1.000	290.0	3.15e-20	1.000	295.0	3.30e-20	1.000	300.0	3.58e-20	1.000
305.0	2.72e-20	1.000	310.0	2.72e-20	1.000	312.5	2.87e-20	1.000	315.0	2.29e-20	1.000	320.0	1.43e-20	1.000
325.0	1.15e-20	1.000	327.5	1.43e-20	1.000	330.0	1.15e-20	1.000	335.0	2.87e-21	1.000	340.0	0.00e+00	1.000
345.0	0.00e+00	1.000	350.0	0.00e+00	1.000	355.0	0.00e+00	1.000	360.0	2.29e-21	1.000	365.0	2.87e-21	1.000
370.0	8.03e-21	1.000	375.0	1.00e-20	1.000	380.0	1.72e-20	0.972	382.0	1.58e-20	0.855	384.0	1.49e-20	0.737
386.0	1.49e-20	0.619	388.0	2.87e-20	0.502	390.0	3.15e-20	0.384	391.0	3.24e-20	0.326	392.0	3.04e-20	0.267
393.0	2.23e-20	0.208	394.0	2.63e-20	0.149	395.0	3.04e-20	0.090	396.0	2.63e-20	0.032	397.0	2.43e-20	0.000
398.0	3.24e-20	0.000	399.0	3.04e-20	0.000	400.0	2.84e-20	0.000	401.0	3.24e-20	0.000	402.0	4.46e-20	0.000
403.0	5.27e-20	0.000	404.0	4.26e-20	0.000	405.0	3.04e-20	0.000	406.0	3.04e-20	0.000	407.0	2.84e-20	0.000
408.0	2.43e-20	0.000	409.0	2.84e-20	0.000	410.0	6.08e-20	0.000	411.0	5.07e-20	0.000	411.5	6.08e-20	0.000
412.0	4.86e-20	0.000	413.0	8.31e-20	0.000	413.5	6.48e-20	0.000	414.0	7.50e-20	0.000	414.5	8.11e-20	0.000
415.0	8.11e-20	0.000	415.5	6.89e-20	0.000	416.0	4.26e-20	0.000	417.0	4.86e-20	0.000	418.0	5.88e-20	0.000
GLY ABS														
230.0	2.87e-21	1.000	235.0	2.87e-21	1.000	240.0	4.30e-21	1.000	245.0	5.73e-21	1.000	250.0	8.60e-21	1.000
255.0	1.15e-20	1.000	260.0	1.43e-20	1.000	265.0	1.86e-20	1.000	270.0	2.29e-20	1.000	275.0	2.58e-20	1.000
280.0	2.87e-20	1.000	285.0	3.30e-20	1.000	290.0	3.15e-20	1.000	295.0	3.30e-20	1.000	300.0	3.58e-20	1.000
305.0	2.72e-20	1.000	310.0	2.72e-20	1.000	312.5	2.87e-20	1.000	315.0	2.29e-20	1.000	320.0	1.43e-20	1.000
325.0	1.15e-20	1.000	327.5	1.43e-20	1.000	330.0	1.15e-20	1.000	335.0	2.87e-21	1.000	340.0	0.00e+00	1.000
355.0	0.00e+00	1.000	360.0	2.29e-21	1.000	365.0	2.87e-21	1.000	370.0	8.03e-21	1.000	375.0	1.00e-20	1.000
380.0	1.72e-20	1.000	382.0	1.58e-20	1.000	384.0	1.49e-20	1.000	386.0	1.49e-20	1.000	388.0	2.87e-20	1.000
390.0	3.15e-20	1.000	391.0	3.24e-20	1.000	392.0	3.04e-20	1.000	393.0	2.23e-20	1.000	394.0	2.63e-20	1.000
395.0	3.04e-20	1.000	396.0	2.63e-20	1.000	397.0	2.43e-20	1.000	398.0	3.24e-20	1.000	399.0	3.04e-20	1.000
400.0	2.84e-20	1.000	401.0	3.24e-20	1.000	402.0	4.46e-20	1.000	403.0	5.27e-20	1.000	404.0	4.26e-20	1.000
405.0	3.04e-20	1.000	406.0	3.04e-20	1.000	407.0	2.84e-20	1.000	408.0	2.43e-20	1.000	409.0	2.84e-20	1.000
410.0	6.08e-20	1.000	411.0	5.07e-20	1.000	411.5	6.08e-20	1.000	412.0	4.86e-20	1.000	413.0	8.31e-20	1.000
413.5	6.48e-20	1.000	414.0	7.50e-20	1.000	414.5	8.11e-20	1.000	415.0	8.11e-20	1.000	415.5	6.89e-20	1.000
416.0	4.26e-20	1.000	417.0	4.86e-20	1.000	418.0	5.88e-20	1.000	419.0	6.69e-20	1.000	420.0	3.85e-20	1.000
421.0	5.67e-20	1.000	421.5	4.46e-20	1.000	422.0	5.27e-20	1.000	422.5	1.05e-19	1.000	423.0	8.51e-20	1.000
424.0	6.08e-20	1.000	425.0	7.29e-20	1.000	426.0	1.18e-19	1.000	426.5	1.30e-19	1.000	427.0	1.07e-19	1.000
428.0	1.66e-19	1.000	429.0	4.05e-20	1.000	430.0	5.07e-20	1.000	431.0	4.86e-20	1.000	432.0	4.05e-20	1.000

Table A-3 (continued)

WL (nm)	Abs (cm ²)	QY	WL (nm)	Abs (cm ²)	QY	WL (nm)	Abs (cm ²)	QY	WL (nm)	Abs (cm ²)	QY	WL (nm)	Abs (cm ²)	QY
433.0	3.65e-20	1.000	434.0	4.05e-20	1.000	434.5	6.08e-20	1.000	435.0	5.07e-20	1.000	436.0	8.11e-20	1.000
436.5	1.13e-19	1.000	437.0	5.27e-20	1.000	438.0	1.01e-19	1.000	438.5	1.38e-19	1.000	439.0	7.70e-20	1.000
440.0	2.47e-19	1.000	441.0	8.11e-20	1.000	442.0	6.08e-20	1.000	443.0	7.50e-20	1.000	444.0	9.32e-20	1.000
445.0	1.13e-19	1.000	446.0	5.27e-20	1.000	447.0	2.43e-20	1.000	448.0	2.84e-20	1.000	449.0	3.85e-20	1.000
450.0	6.08e-20	1.000	451.0	1.09e-19	1.000	451.5	9.32e-20	1.000	452.0	1.22e-19	1.000	453.0	2.39e-19	1.000
454.0	1.70e-19	1.000	455.0	3.40e-19	1.000	455.5	4.05e-19	1.000	456.0	1.01e-19	1.000	457.0	1.62e-20	1.000
458.0	1.22e-20	1.000	458.5	1.42e-20	1.000	459.0	4.05e-21	1.000	460.0	4.05e-21	1.000	460.5	6.08e-21	1.000
461.0	2.03e-21	1.000	462.0	0.00e+00	1.000									
MGLY ADJ														
219.0	9.84e-21	1.000	219.5	1.04e-20	1.000	220.0	1.06e-20	1.000	220.5	1.11e-20	1.000	221.0	1.15e-20	1.000
221.5	1.18e-20	1.000	222.0	1.22e-20	1.000	222.5	1.24e-20	1.000	223.0	1.26e-20	1.000	223.5	1.26e-20	1.000
224.0	1.25e-20	1.000	224.5	1.24e-20	1.000	225.0	1.25e-20	1.000	225.5	1.27e-20	1.000	226.0	1.27e-20	1.000
226.5	1.29e-20	1.000	227.0	1.31e-20	1.000	227.5	1.32e-20	1.000	228.0	1.35e-20	1.000	228.5	1.37e-20	1.000
229.0	1.40e-20	1.000	229.5	1.42e-20	1.000	230.0	1.48e-20	1.000	230.5	1.53e-20	1.000	231.0	1.57e-20	1.000
231.5	1.59e-20	1.000	232.0	1.61e-20	1.000	232.5	1.62e-20	1.000	233.0	1.61e-20	1.000	233.5	1.68e-20	1.000
234.0	1.74e-20	1.000	234.5	1.80e-20	1.000	235.0	1.84e-20	1.000	235.5	1.87e-20	1.000	236.0	1.89e-20	1.000
236.5	1.91e-20	1.000	237.0	1.93e-20	1.000	237.5	1.94e-20	1.000	238.0	1.96e-20	1.000	238.5	1.96e-20	1.000
239.0	2.01e-20	1.000	239.5	2.04e-20	1.000	240.0	2.08e-20	1.000	240.5	2.10e-20	1.000	241.0	2.14e-20	1.000
241.5	2.16e-20	1.000	242.0	2.19e-20	1.000	242.5	2.20e-20	1.000	243.0	2.23e-20	1.000	243.5	2.26e-20	1.000
244.0	2.28e-20	1.000	244.5	2.29e-20	1.000	245.0	2.30e-20	1.000	245.5	2.32e-20	1.000	246.0	2.33e-20	1.000
246.5	2.35e-20	1.000	247.0	2.38e-20	1.000	247.5	2.41e-20	1.000	248.0	2.46e-20	1.000	248.5	2.51e-20	1.000
249.0	2.57e-20	1.000	249.5	2.61e-20	1.000	250.0	2.65e-20	1.000	250.5	2.67e-20	1.000	251.0	2.69e-20	1.000
251.5	2.69e-20	1.000	252.0	2.71e-20	1.000	252.5	2.72e-20	1.000	253.0	2.73e-20	1.000	253.5	2.74e-20	1.000
254.0	2.76e-20	1.000	254.5	2.78e-20	1.000	255.0	2.82e-20	1.000	255.5	2.87e-20	1.000	256.0	2.93e-20	1.000
256.5	2.98e-20	1.000	257.0	3.07e-20	1.000	257.5	3.12e-20	1.000	258.0	3.17e-20	1.000	258.5	3.21e-20	1.000
259.0	3.26e-20	1.000	259.5	3.28e-20	1.000	260.0	3.29e-20	1.000	260.5	3.31e-20	1.000	261.0	3.33e-20	1.000
261.5	3.34e-20	1.000	262.0	3.36e-20	1.000	262.5	3.38e-20	1.000	263.0	3.42e-20	1.000	263.5	3.44e-20	1.000
264.0	3.48e-20	1.000	264.5	3.54e-20	1.000	265.0	3.59e-20	1.000	265.5	3.65e-20	1.000	266.0	3.73e-20	1.000
266.5	3.80e-20	1.000	267.0	3.87e-20	1.000	267.5	3.95e-20	1.000	268.0	4.02e-20	1.000	268.5	4.08e-20	1.000
269.0	4.13e-20	1.000	269.5	4.17e-20	1.000	270.0	4.20e-20	1.000	270.5	4.22e-20	1.000	271.0	4.22e-20	1.000
271.5	4.22e-20	1.000	272.0	4.23e-20	1.000	272.5	4.24e-20	1.000	273.0	4.27e-20	1.000	273.5	4.29e-20	1.000
274.0	4.31e-20	1.000	274.5	4.33e-20	1.000	275.0	4.37e-20	1.000	275.5	4.42e-20	1.000	276.0	4.48e-20	1.000
276.5	4.56e-20	1.000	277.0	4.64e-20	1.000	277.5	4.71e-20	1.000	278.0	4.78e-20	1.000	278.5	4.83e-20	1.000
279.0	4.87e-20	1.000	279.5	4.90e-20	1.000	280.0	4.92e-20	1.000	280.5	4.93e-20	1.000	281.0	4.94e-20	1.000
281.5	4.92e-20	1.000	282.0	4.90e-20	1.000	282.5	4.86e-20	1.000	283.0	4.83e-20	1.000	283.5	4.79e-20	1.000
284.0	4.76e-20	1.000	284.5	4.72e-20	1.000	285.0	4.70e-20	1.000	285.5	4.68e-20	1.000	286.0	4.66e-20	1.000
286.5	4.65e-20	1.000	287.0	4.65e-20	1.000	287.5	4.68e-20	1.000	288.0	4.73e-20	1.000	288.5	4.78e-20	1.000
289.0	4.84e-20	1.000	289.5	4.89e-20	1.000	290.0	4.92e-20	1.000	290.5	4.92e-20	1.000	291.0	4.90e-20	1.000
291.5	4.86e-20	1.000	292.0	4.81e-20	1.000	292.5	4.75e-20	1.000	293.0	4.70e-20	1.000	293.5	4.65e-20	1.000
294.0	4.58e-20	1.000	294.5	4.48e-20	1.000	295.0	4.38e-20	1.000	295.5	4.27e-20	1.000	296.0	4.17e-20	1.000
296.5	4.07e-20	1.000	297.0	3.99e-20	1.000	297.5	3.94e-20	1.000	298.0	3.88e-20	1.000	298.5	3.82e-20	1.000
299.0	3.76e-20	1.000	299.5	3.72e-20	1.000	300.0	3.69e-20	1.000	300.5	3.68e-20	1.000	301.0	3.70e-20	1.000
301.5	3.72e-20	1.000	302.0	3.74e-20	1.000	302.5	3.74e-20	1.000	303.0	3.75e-20	1.000	303.5	3.71e-20	1.000
304.0	3.62e-20	1.000	304.5	3.51e-20	1.000	305.0	3.38e-20	1.000	305.5	3.25e-20	1.000	306.0	3.15e-20	1.000
306.5	3.04e-20	1.000	307.0	2.92e-20	1.000	307.5	2.80e-20	1.000	308.0	2.71e-20	1.000	308.5	2.63e-20	1.000
309.0	2.52e-20	1.000	309.5	2.43e-20	1.000	310.0	2.34e-20	1.000	310.5	2.25e-20	1.000	311.0	2.19e-20	1.000
311.5	2.12e-20	1.000	312.0	2.06e-20	1.000	312.5	2.02e-20	1.000	313.0	1.96e-20	1.000	313.5	1.92e-20	1.000
314.0	1.91e-20	1.000	314.5	1.88e-20	1.000	315.0	1.86e-20	1.000	315.5	1.85e-20	1.000	316.0	1.86e-20	1.000
316.5	1.87e-20	1.000	317.0	1.87e-20	1.000	317.5	1.87e-20	1.000	318.0	1.83e-20	1.000	318.5	1.75e-20	1.000
319.0	1.69e-20	1.000	319.5	1.60e-20	1.000	320.0	1.50e-20	1.000	320.5	1.41e-20	1.000	321.0	1.34e-20	1.000
321.5	1.27e-20	1.000	322.0	1.21e-20	1.000	322.5	1.18e-20	1.000	323.0	1.14e-20	1.000	323.5	1.08e-20	1.000
324.0	1.01e-20	1.000	324.5	9.62e-21	1.000	325.0	9.28e-21	1.000	325.5	8.75e-21	1.000	326.0	8.49e-21	1.000
326.5	8.21e-21	1.000	327.0	7.71e-21	1.000	327.5	7.38e-21	1.000	328.0	7.18e-21	1.000	328.5	6.86e-21	1.000
329.0	6.71e-21	1.000	329.5	6.63e-21	1.000	330.0	6.46e-21	1.000	330.5	6.29e-21	1.000	331.0	6.21e-21	1.000
331.5	6.18e-21	1.000	332.0	6.20e-21	1.000	332.5	5.49e-21	1.000	333.0	5.21e-21	1.000	333.5	5.38e-21	1.000
334.0	5.35e-21	1.000	334.5	5.04e-21	1.000	335.0	4.94e-21	1.000	335.5	4.90e-21	1.000	336.0	4.52e-21	1.000
336.5	4.26e-21	1.000	337.0	4.11e-21	1.000	337.5	3.76e-21	1.000	338.0	3.61e-21	1.000	338.5	3.58e-21	1.000
339.0	3.47e-21	1.000	339.5	3.32e-21	1.000	340.0	3.22e-21	1.000	340.5	3.10e-21	1.000	341.0	3.00e-21	1.000
341.5	2.94e-21	1.000	342.0	2.89e-21	1.000	342.5	2.86e-21	1.000	343.0	2.88e-21	1.000	343.5	2.88e-21	1.000
344.0	2.89e-21	0.992	344.5	2.91e-21	0.984	345.0	2.95e-21	0.976	345.5	3.00e-21	0.968	346.0	3.08e-21	0.960
346.5	3.18e-21	0.953	347.0	3.25e-21	0.945	347.5	3.30e-21	0.937	348.0	3.39e-21	0.929	348.5	3.51e-21	0.921
349.0	3.63e-21	0.913	349.5	3.73e-21	0.905	350.0	3.85e-21	0.897	350.5	3.99e-21	0.889	351.0	4.27e-21	0.881
351.5	4.47e-21	0.873	352.0	4.63e-21	0.865	352.5	4.78e-21	0.858	353.0	4.92e-21	0.850	353.5	5.07e-21	0.842
354.0	5.23e-21	0.834	354.5	5.39e-21	0.826	355.0	5.56e-21	0.818	355.5	5.77e-21	0.810	356.0	5.97e-21	0.802
356.5	6.15e-21	0.794	357.0	6.35e-21	0.786	357.5	6.56e-21	0.778	358.0	6.76e-21	0.770	358.5	6.95e-21	0.763
359.0	7.20e-21	0.755	359.5	7.44e-21	0.747	360.0	7.64e-21	0.739	360.5	7.89e-21	0.731	361.0	8.15e-21	0.723
361.5	8.43e-21	0.715	362.0	8.71e-21	0.707	362.5	9.02e-21	0.699	363.0	9.33e-21	0.691	363.5	9.65e-21	0.683
364.0	1.00e-20	0.675	364.5	1.04e-20	0.668	365.0	1.08e-20	0.660	365.5	1.11e-20	0.652	366.0	1.15e-20	0.644
366.5	1.19e-20	0.636	367.0	1.23e-20	0.628	367.5	1.27e-20	0.620	368.0	1.31e-20	0.612	368.5	1.35e-20	0.604
369.0	1.40e-20	0.596	369.5	1.44e-20	0.588	370.0	1.47e-20	0.580	370.5	1.51e-20	0.573	371.0	1.55e-20	0.565
371.5	1.59e-20	0.557	372.0	1.64e-20	0.549	372.5	1.70e-20	0.541	373.0	1.73e-20	0.533	373.5	1.77e-20	0.525
374.0	1.81e-20	0.517	374.5	1.86e-20	0.509	375.0	1.90e-20	0.501	375.5	1.96e-20	0.493	376.0	2.02e-20	0.486

Table A-3 (continued)

WL (nm)	Abs (cm ²)	QY	WL (nm)	Abs (cm ²)	QY	WL (nm)	Abs (cm ²)	QY	WL (nm)	Abs (cm ²)	QY	WL (nm)	Abs (cm ²)	QY
376.5	2.06e-20	0.478	377.0	2.10e-20	0.470	377.5	2.14e-20	0.462	378.0	2.18e-20	0.454	378.5	2.24e-20	0.446
379.0	2.30e-20	0.438	379.5	2.37e-20	0.430	380.0	2.42e-20	0.422	380.5	2.47e-20	0.414	381.0	2.54e-20	0.406
381.5	2.62e-20	0.398	382.0	2.69e-20	0.391	382.5	2.79e-20	0.383	383.0	2.88e-20	0.375	383.5	2.96e-20	0.367
384.0	3.02e-20	0.359	384.5	3.10e-20	0.351	385.0	3.20e-20	0.343	385.5	3.29e-20	0.335	386.0	3.39e-20	0.327
386.5	3.51e-20	0.319	387.0	3.62e-20	0.311	387.5	3.69e-20	0.303	388.0	3.70e-20	0.296	388.5	3.77e-20	0.288
389.0	3.88e-20	0.280	389.5	3.97e-20	0.272	390.0	4.03e-20	0.264	390.5	4.12e-20	0.256	391.0	4.22e-20	0.248
391.5	4.29e-20	0.240	392.0	4.30e-20	0.232	392.5	4.38e-20	0.224	393.0	4.47e-20	0.216	393.5	4.55e-20	0.208
394.0	4.56e-20	0.201	394.5	4.59e-20	0.193	395.0	4.67e-20	0.185	395.5	4.80e-20	0.177	396.0	4.87e-20	0.169
396.5	4.96e-20	0.161	397.0	5.08e-20	0.153	397.5	5.19e-20	0.145	398.0	5.23e-20	0.137	398.5	5.39e-20	0.129
399.0	5.46e-20	0.121	399.5	5.54e-20	0.113	400.0	5.59e-20	0.106	400.5	5.77e-20	0.098	401.0	5.91e-20	0.090
401.5	5.99e-20	0.082	402.0	6.06e-20	0.074	402.5	6.20e-20	0.066	403.0	6.35e-20	0.058	403.5	6.52e-20	0.050
404.0	6.54e-20	0.042	404.5	6.64e-20	0.034	405.0	6.93e-20	0.026	405.5	7.15e-20	0.018	406.0	7.19e-20	0.011
406.5	7.32e-20	0.003	407.0	7.58e-20	0.000	407.5	7.88e-20	0.000	408.0	7.97e-20	0.000	408.5	7.91e-20	0.000
409.0	8.11e-20	0.000	409.5	8.41e-20	0.000	410.0	8.53e-20	0.000	410.5	8.59e-20	0.000	411.0	8.60e-20	0.000
411.5	8.80e-20	0.000	412.0	9.04e-20	0.000	412.5	9.45e-20	0.000	413.0	9.34e-20	0.000	413.5	9.37e-20	0.000
414.0	9.63e-20	0.000	414.5	9.71e-20	0.000	415.0	9.70e-20	0.000	415.5	9.65e-20	0.000	416.0	9.69e-20	0.000
416.5	9.89e-20	0.000	417.0	1.00e-19	0.000	417.5	1.02e-19	0.000	418.0	1.00e-19	0.000	418.5	1.02e-19	0.000
419.0	1.01e-19	0.000	419.5	1.01e-19	0.000	420.0	1.03e-19	0.000	420.5	1.01e-19	0.000	421.0	1.04e-19	0.000
BACL ADJ														
230.0	1.30e-20	1.000	232.5	1.46e-20	1.000	235.0	1.68e-20	1.000	237.5	1.84e-20	1.000	240.0	2.16e-20	1.000
242.5	2.49e-20	1.000	245.0	2.65e-20	1.000	247.5	2.71e-20	1.000	250.0	3.03e-20	1.000	252.5	3.46e-20	1.000
255.0	3.46e-20	1.000	257.5	3.57e-20	1.000	260.0	3.95e-20	1.000	262.5	4.17e-20	1.000	265.0	4.17e-20	1.000
267.5	4.22e-20	1.000	270.0	4.60e-20	1.000	272.5	4.54e-20	1.000	275.0	4.33e-20	1.000	277.5	4.22e-20	1.000
280.0	4.44e-20	1.000	282.5	4.33e-20	1.000	285.0	3.90e-20	1.000	287.5	3.57e-20	1.000	290.0	3.25e-20	1.000
292.5	2.92e-20	1.000	295.0	2.60e-20	1.000	297.5	2.16e-20	1.000	300.0	1.79e-20	1.000	302.5	1.73e-20	1.000
305.0	1.46e-20	1.000	307.5	1.08e-20	1.000	310.0	9.20e-21	1.000	312.5	7.03e-21	1.000	315.0	6.49e-21	1.000
317.5	5.41e-21	1.000	320.0	5.41e-21	1.000	322.5	5.41e-21	1.000	325.0	4.33e-21	1.000	327.5	3.25e-21	1.000
330.0	3.79e-21	1.000	332.5	3.79e-21	1.000	335.0	4.33e-21	1.000	337.5	4.87e-21	1.000	340.0	5.41e-21	1.000
342.5	5.95e-21	1.000	345.0	6.49e-21	1.000	347.5	7.03e-21	1.000	350.0	8.12e-21	0.995	352.5	7.57e-21	0.960
355.0	9.20e-21	0.925	357.5	9.74e-21	0.890	360.0	1.08e-20	0.855	362.5	1.19e-20	0.820	365.0	1.41e-20	0.785
367.5	1.51e-20	0.750	370.0	1.79e-20	0.715	372.5	2.00e-20	0.680	375.0	2.11e-20	0.645	377.5	2.33e-20	0.610
380.0	2.60e-20	0.575	382.5	2.81e-20	0.540	385.0	3.14e-20	0.505	387.5	3.46e-20	0.470	390.0	3.90e-20	0.435
392.5	4.11e-20	0.399	395.0	4.33e-20	0.364	397.5	4.38e-20	0.329	400.0	4.65e-20	0.294	402.5	4.81e-20	0.259
405.0	5.19e-20	0.224	407.5	5.84e-20	0.189	410.0	6.06e-20	0.154	412.5	6.49e-20	0.119	415.0	6.92e-20	0.084
417.5	6.87e-20	0.049	420.0	6.82e-20	0.014	422.5	6.71e-20	0.000	425.0	6.49e-20	0.000	427.5	5.95e-20	0.000
430.0	5.73e-20	0.000	432.5	6.28e-20	0.000	435.0	6.01e-20	0.000	437.5	5.84e-20	0.000	440.0	5.95e-20	0.000
442.5	6.49e-20	0.000	445.0	5.95e-20	0.000	447.5	4.98e-20	0.000	450.0	3.79e-20	0.000	452.5	2.81e-20	0.000
455.0	1.73e-20	0.000	457.5	1.08e-20	0.000	460.0	5.41e-21	0.000	462.5	3.79e-21	0.000	465.0	2.16e-21	0.000
467.5	1.08e-21	0.000	470.0	1.08e-21	0.000	472.5	0.00e+00	0.000						
BZCHO														
299.0	1.78e-19	1.000	304.0	7.40e-20	1.000	306.0	6.91e-20	1.000	309.0	6.41e-20	1.000	313.0	6.91e-20	1.000
314.0	6.91e-20	1.000	318.0	6.41e-20	1.000	325.0	8.39e-20	1.000	332.0	7.65e-20	1.000	338.0	8.88e-20	1.000
342.0	8.88e-20	1.000	346.0	7.89e-20	1.000	349.0	7.89e-20	1.000	354.0	9.13e-20	1.000	355.0	8.14e-20	1.000
364.0	5.67e-20	1.000	368.0	6.66e-20	1.000	369.0	8.39e-20	1.000	370.0	8.39e-20	1.000	372.0	3.45e-20	1.000
374.0	3.21e-20	1.000	376.0	2.47e-20	1.000	377.0	2.47e-20	1.000	380.0	3.58e-20	1.000	382.0	9.90e-21	1.000
386.0	0.00e+00	1.000												
ACROLEIN														
250.0	1.80e-21	1.000	252.0	2.05e-21	1.000	253.0	2.20e-21	1.000	254.0	2.32e-21	1.000	255.0	2.45e-21	1.000
256.0	2.56e-21	1.000	257.0	2.65e-21	1.000	258.0	2.74e-21	1.000	259.0	2.83e-21	1.000	260.0	2.98e-21	1.000
261.0	3.24e-21	1.000	262.0	3.47e-21	1.000	263.0	3.58e-21	1.000	264.0	3.93e-21	1.000	265.0	4.67e-21	1.000
266.0	5.10e-21	1.000	267.0	5.38e-21	1.000	268.0	5.73e-21	1.000	269.0	6.13e-21	1.000	270.0	6.64e-21	1.000
271.0	7.20e-21	1.000	272.0	7.77e-21	1.000	273.0	8.37e-21	1.000	274.0	8.94e-21	1.000	275.0	9.55e-21	1.000
276.0	1.04e-20	1.000	277.0	1.12e-20	1.000	278.0	1.19e-20	1.000	279.0	1.27e-20	1.000	280.0	1.27e-20	1.000
281.0	1.26e-20	1.000	282.0	1.26e-20	1.000	283.0	1.28e-20	1.000	284.0	1.33e-20	1.000	285.0	1.38e-20	1.000
286.0	1.44e-20	1.000	287.0	1.50e-20	1.000	288.0	1.57e-20	1.000	289.0	1.63e-20	1.000	290.0	1.71e-20	1.000
291.0	1.78e-20	1.000	292.0	1.86e-20	1.000	293.0	1.95e-20	1.000	294.0	2.05e-20	1.000	295.0	2.15e-20	1.000
296.0	2.26e-20	1.000	297.0	2.37e-20	1.000	298.0	2.48e-20	1.000	299.0	2.60e-20	1.000	300.0	2.73e-20	1.000
301.0	2.85e-20	1.000	302.0	2.99e-20	1.000	303.0	3.13e-20	1.000	304.0	3.27e-20	1.000	305.0	3.39e-20	1.000
306.0	3.51e-20	1.000	307.0	3.63e-20	1.000	308.0	3.77e-20	1.000	309.0	3.91e-20	1.000	310.0	4.07e-20	1.000
311.0	4.25e-20	1.000	312.0	4.39e-20	1.000	313.0	4.44e-20	1.000	314.0	4.50e-20	1.000	315.0	4.59e-20	1.000
316.0	4.75e-20	1.000	317.0	4.90e-20	1.000	318.0	5.05e-20	1.000	319.0	5.19e-20	1.000	320.0	5.31e-20	1.000
321.0	5.43e-20	1.000	322.0	5.52e-20	1.000	323.0	5.60e-20	1.000	324.0	5.67e-20	1.000	325.0	5.67e-20	1.000
326.0	5.62e-20	1.000	327.0	5.63e-20	1.000	328.0	5.71e-20	1.000	329.0	5.76e-20	1.000	330.0	5.80e-20	1.000
331.0	5.95e-20	1.000	332.0	6.23e-20	1.000	333.0	6.39e-20	1.000	334.0	6.38e-20	1.000	335.0	6.24e-20	1.000
336.0	6.01e-20	1.000	337.0	5.79e-20	1.000	338.0	5.63e-20	1.000	339.0	5.56e-20	1.000	340.0	5.52e-20	1.000
341.0	5.54e-20	1.000	342.0	5.53e-20	1.000	343.0	5.47e-20	1.000	344.0	5.41e-20	1.000	345.0	5.40e-20	1.000
346.0	5.48e-20	1.000	347.0	5.90e-20	1.000	348.0	6.08e-20	1.000	349.0	6.00e-20	1.000	350.0	5.53e-20	1.000
351.0	5.03e-20	1.000	352.0	4.50e-20	1.000	353.0	4.03e-20	1.000	354.0	3.75e-20	1.000	355.0	3.55e-20	1.000
356.0	3.45e-20	1.000	357.0	3.46e-20	1.000	358.0	3.49e-20	1.000	359.0	3.41e-20	1.000	360.0	3.23e-20	1.000
361.0	2.95e-20	1.000	362.0	2.81e-20	1.000	363.0	2.91e-20	1.000	364.0	3.25e-20	1.000	365.0	3.54e-20	1.000
366.0	3.30e-20	1.000	367.0	2.78e-20	1.000	368.0	2.15e-20	1.000	369.0	1.59e-20	1.000	370.0	1.19e-20	1.000

Table A-3 (continued)

WL (nm)	Abs (cm ²)	QY	WL (nm)	Abs (cm ²)	QY	WL (nm)	Abs (cm ²)	QY	WL (nm)	Abs (cm ²)	QY	WL (nm)	Abs (cm ²)	QY
371.0	8.99e-21	1.000	372.0	7.22e-21	1.000	373.0	5.86e-21	1.000	374.0	4.69e-21	1.000	375.0	3.72e-21	1.000
376.0	3.57e-21	1.000	377.0	3.55e-21	1.000	378.0	2.83e-21	1.000	379.0	1.69e-21	1.000	380.0	8.29e-24	1.000
381.0	0.00e+00	1.000												
IC3ONO2														
185.0	1.79e-17	1.000	188.0	1.81e-17	1.000	190.0	1.79e-17	1.000	195.0	1.61e-17	1.000	200.0	1.26e-17	1.000
205.0	8.67e-18	1.000	210.0	4.98e-18	1.000	215.0	2.47e-18	1.000	220.0	1.17e-18	1.000	225.0	5.80e-19	1.000
230.0	3.10e-19	1.000	235.0	1.80e-19	1.000	240.0	1.10e-19	1.000	245.0	7.00e-20	1.000	250.0	5.70e-20	1.000
255.0	5.20e-20	1.000	260.0	4.90e-20	1.000	265.0	4.60e-20	1.000	270.0	4.10e-20	1.000	275.0	3.60e-20	1.000
280.0	2.90e-20	1.000	285.0	2.30e-20	1.000	290.0	1.70e-20	1.000	295.0	1.20e-20	1.000	300.0	8.10e-21	1.000
305.0	5.20e-21	1.000	310.0	3.20e-21	1.000	315.0	1.90e-21	1.000	320.0	1.10e-21	1.000	325.0	6.10e-22	1.000
330.0	3.70e-22	1.000	335.0	0.00e+00	1.000									
MGLY ABS														
219.0	9.84e-21	1.000	219.5	1.04e-20	1.000	220.0	1.06e-20	1.000	220.5	1.11e-20	1.000	221.0	1.15e-20	1.000
221.5	1.18e-20	1.000	222.0	1.22e-20	1.000	222.5	1.24e-20	1.000	223.0	1.26e-20	1.000	223.5	1.26e-20	1.000
224.0	1.25e-20	1.000	224.5	1.24e-20	1.000	225.0	1.25e-20	1.000	225.5	1.27e-20	1.000	226.0	1.27e-20	1.000
226.5	1.29e-20	1.000	227.0	1.31e-20	1.000	227.5	1.32e-20	1.000	228.0	1.35e-20	1.000	228.5	1.37e-20	1.000
229.0	1.40e-20	1.000	229.5	1.42e-20	1.000	230.0	1.48e-20	1.000	230.5	1.53e-20	1.000	231.0	1.57e-20	1.000
231.5	1.59e-20	1.000	232.0	1.61e-20	1.000	232.5	1.62e-20	1.000	233.0	1.61e-20	1.000	233.5	1.68e-20	1.000
234.0	1.74e-20	1.000	234.5	1.80e-20	1.000	235.0	1.84e-20	1.000	235.5	1.87e-20	1.000	236.0	1.89e-20	1.000
236.5	1.91e-20	1.000	237.0	1.93e-20	1.000	237.5	1.94e-20	1.000	238.0	1.96e-20	1.000	238.5	1.96e-20	1.000
239.0	2.01e-20	1.000	239.5	2.04e-20	1.000	240.0	2.08e-20	1.000	240.5	2.10e-20	1.000	241.0	2.14e-20	1.000
241.5	2.16e-20	1.000	242.0	2.19e-20	1.000	242.5	2.20e-20	1.000	243.0	2.23e-20	1.000	243.5	2.26e-20	1.000
244.0	2.28e-20	1.000	244.5	2.29e-20	1.000	245.0	2.30e-20	1.000	245.5	2.32e-20	1.000	246.0	2.33e-20	1.000
246.5	2.35e-20	1.000	247.0	2.38e-20	1.000	247.5	2.41e-20	1.000	248.0	2.46e-20	1.000	248.5	2.51e-20	1.000
249.0	2.57e-20	1.000	249.5	2.61e-20	1.000	250.0	2.65e-20	1.000	250.5	2.67e-20	1.000	251.0	2.69e-20	1.000
251.5	2.69e-20	1.000	252.0	2.71e-20	1.000	252.5	2.72e-20	1.000	253.0	2.73e-20	1.000	253.5	2.74e-20	1.000
254.0	2.76e-20	1.000	254.5	2.78e-20	1.000	255.0	2.82e-20	1.000	255.5	2.87e-20	1.000	256.0	2.93e-20	1.000
256.5	2.98e-20	1.000	257.0	3.07e-20	1.000	257.5	3.12e-20	1.000	258.0	3.17e-20	1.000	258.5	3.21e-20	1.000
259.0	3.26e-20	1.000	259.5	3.28e-20	1.000	260.0	3.29e-20	1.000	260.5	3.31e-20	1.000	261.0	3.33e-20	1.000
261.5	3.34e-20	1.000	262.0	3.36e-20	1.000	262.5	3.38e-20	1.000	263.0	3.42e-20	1.000	263.5	3.44e-20	1.000
264.0	3.48e-20	1.000	264.5	3.54e-20	1.000	265.0	3.59e-20	1.000	265.5	3.65e-20	1.000	266.0	3.73e-20	1.000
266.5	3.80e-20	1.000	267.0	3.87e-20	1.000	267.5	3.95e-20	1.000	268.0	4.02e-20	1.000	268.5	4.08e-20	1.000
269.0	4.13e-20	1.000	269.5	4.17e-20	1.000	270.0	4.20e-20	1.000	270.5	4.22e-20	1.000	271.0	4.22e-20	1.000
271.5	4.22e-20	1.000	272.0	4.23e-20	1.000	272.5	4.24e-20	1.000	273.0	4.27e-20	1.000	273.5	4.29e-20	1.000
274.0	4.31e-20	1.000	274.5	4.33e-20	1.000	275.0	4.37e-20	1.000	275.5	4.42e-20	1.000	276.0	4.48e-20	1.000
276.5	4.56e-20	1.000	277.0	4.64e-20	1.000	277.5	4.71e-20	1.000	278.0	4.78e-20	1.000	278.5	4.83e-20	1.000
279.0	4.87e-20	1.000	279.5	4.90e-20	1.000	280.0	4.92e-20	1.000	280.5	4.93e-20	1.000	281.0	4.94e-20	1.000
281.5	4.92e-20	1.000	282.0	4.90e-20	1.000	282.5	4.86e-20	1.000	283.0	4.83e-20	1.000	283.5	4.79e-20	1.000
284.0	4.76e-20	1.000	284.5	4.72e-20	1.000	285.0	4.70e-20	1.000	285.5	4.68e-20	1.000	286.0	4.66e-20	1.000
286.5	4.65e-20	1.000	287.0	4.65e-20	1.000	287.5	4.68e-20	1.000	288.0	4.73e-20	1.000	288.5	4.78e-20	1.000
289.0	4.84e-20	1.000	289.5	4.89e-20	1.000	290.0	4.92e-20	1.000	290.5	4.92e-20	1.000	291.0	4.90e-20	1.000
291.5	4.86e-20	1.000	292.0	4.81e-20	1.000	292.5	4.75e-20	1.000	293.0	4.70e-20	1.000	293.5	4.65e-20	1.000
294.0	4.58e-20	1.000	294.5	4.48e-20	1.000	295.0	4.38e-20	1.000	295.5	4.27e-20	1.000	296.0	4.17e-20	1.000
296.5	4.07e-20	1.000	297.0	3.99e-20	1.000	297.5	3.94e-20	1.000	298.0	3.88e-20	1.000	298.5	3.82e-20	1.000
299.0	3.76e-20	1.000	299.5	3.72e-20	1.000	300.0	3.69e-20	1.000	300.5	3.68e-20	1.000	301.0	3.70e-20	1.000
301.5	3.72e-20	1.000	302.0	3.74e-20	1.000	302.5	3.74e-20	1.000	303.0	3.75e-20	1.000	303.5	3.71e-20	1.000
304.0	3.62e-20	1.000	304.5	3.51e-20	1.000	305.0	3.38e-20	1.000	305.5	3.25e-20	1.000	306.0	3.15e-20	1.000
306.5	3.04e-20	1.000	307.0	2.92e-20	1.000	307.5	2.80e-20	1.000	308.0	2.71e-20	1.000	308.5	2.63e-20	1.000
309.0	2.52e-20	1.000	309.5	2.43e-20	1.000	310.0	2.34e-20	1.000	310.5	2.25e-20	1.000	311.0	2.19e-20	1.000
311.5	2.12e-20	1.000	312.0	2.06e-20	1.000	312.5	2.02e-20	1.000	313.0	1.96e-20	1.000	313.5	1.92e-20	1.000
314.0	1.91e-20	1.000	314.5	1.88e-20	1.000	315.0	1.86e-20	1.000	315.5	1.85e-20	1.000	316.0	1.86e-20	1.000
316.5	1.87e-20	1.000	317.0	1.87e-20	1.000	317.5	1.87e-20	1.000	318.0	1.83e-20	1.000	318.5	1.75e-20	1.000
319.0	1.69e-20	1.000	319.5	1.60e-20	1.000	320.0	1.50e-20	1.000	320.5	1.41e-20	1.000	321.0	1.34e-20	1.000
321.5	1.27e-20	1.000	322.0	1.21e-20	1.000	322.5	1.18e-20	1.000	323.0	1.14e-20	1.000	323.5	1.08e-20	1.000
324.0	1.01e-20	1.000	324.5	9.62e-21	1.000	325.0	9.28e-21	1.000	325.5	8.75e-21	1.000	326.0	8.49e-21	1.000
326.5	8.21e-21	1.000	327.0	7.71e-21	1.000	327.5	7.38e-21	1.000	328.0	7.18e-21	1.000	328.5	6.86e-21	1.000
329.0	6.71e-21	1.000	329.5	6.63e-21	1.000	330.0	6.46e-21	1.000	330.5	6.29e-21	1.000	331.0	6.21e-21	1.000
331.5	6.18e-21	1.000	332.0	6.20e-21	1.000	332.5	5.49e-21	1.000	333.0	5.21e-21	1.000	333.5	5.38e-21	1.000
334.0	5.35e-21	1.000	334.5	5.04e-21	1.000	335.0	4.94e-21	1.000	335.5	4.90e-21	1.000	336.0	4.52e-21	1.000
336.5	4.26e-21	1.000	337.0	4.11e-21	1.000	337.5	3.76e-21	1.000	338.0	3.61e-21	1.000	338.5	3.58e-21	1.000
339.0	3.47e-21	1.000	339.5	3.32e-21	1.000	340.0	3.22e-21	1.000	340.5	3.10e-21	1.000	341.0	3.00e-21	1.000
341.5	2.94e-21	1.000	342.0	2.89e-21	1.000	342.5	2.86e-21	1.000	343.0	2.88e-21	1.000	343.5	2.88e-21	1.000
344.0	2.89e-21	1.000	344.5	2.91e-21	1.000	345.0	2.95e-21	1.000	345.5	3.00e-21	1.000	346.0	3.08e-21	1.000
346.5	3.18e-21	1.000	347.0	3.25e-21	1.000	347.5	3.30e-21	1.000	348.0	3.39e-21	1.000	348.5	3.51e-21	1.000
349.0	3.63e-21	1.000	349.5	3.73e-21	1.000	350.0	3.85e-21	1.000	350.5	3.99e-21	1.000	351.0	4.27e-21	1.000
351.5	4.47e-21	1.000	352.0	4.63e-21	1.000	352.5	4.78e-21	1.000	353.0	4.92e-21	1.000	353.5	5.07e-21	1.000
354.0	5.23e-21	1.000	354.5	5.39e-21	1.000	355.0	5.56e-21	1.000	355.5	5.77e-21	1.000	356.0	5.97e-21	1.000
356.5	6.15e-21	1.000	357.0	6.35e-21	1.000	357.5	6.56e-21	1.000	358.0	6.76e-21	1.000	358.5	6.95e-21	1.000
359.0	7.20e-21	1.000	359.5	7.44e-21	1.000	360.0	7.64e-21	1.000	360.5	7.89e-21	1.000	361.0	8.15e-21	1.000
361.5	8.43e-21	1.000	362.0	8.71e-21	1.000	362.5	9.02e-21	1.000	363.0	9.33e-21	1.000	363.5	9.65e-21	1.000
364.0	1.00e-20	1.000	364.5	1.04e-20	1.000	365.0	1.08e-20	1.000	365.5	1.11e-20	1.000	366.0		

Table A-3 (continued)

WL (nm)	Abs (cm ²)	QY	WL (nm)	Abs (cm ²)	QY	WL (nm)	Abs (cm ²)	QY	WL (nm)	Abs (cm ²)	QY	WL (nm)	Abs (cm ²)	QY
366.5	1.19e-20	1.000	367.0	1.23e-20	1.000	367.5	1.27e-20	1.000	368.0	1.31e-20	1.000	368.5	1.35e-20	1.000
369.0	1.40e-20	1.000	369.5	1.44e-20	1.000	370.0	1.47e-20	1.000	370.5	1.51e-20	1.000	371.0	1.55e-20	1.000
371.5	1.59e-20	1.000	372.0	1.64e-20	1.000	372.5	1.70e-20	1.000	373.0	1.73e-20	1.000	373.5	1.77e-20	1.000
374.0	1.81e-20	1.000	374.5	1.86e-20	1.000	375.0	1.90e-20	1.000	375.5	1.96e-20	1.000	376.0	2.02e-20	1.000
376.5	2.06e-20	1.000	377.0	2.10e-20	1.000	377.5	2.14e-20	1.000	378.0	2.18e-20	1.000	378.5	2.24e-20	1.000
379.0	2.30e-20	1.000	379.5	2.37e-20	1.000	380.0	2.42e-20	1.000	380.5	2.47e-20	1.000	381.0	2.54e-20	1.000
381.5	2.62e-20	1.000	382.0	2.69e-20	1.000	382.5	2.79e-20	1.000	383.0	2.88e-20	1.000	383.5	2.96e-20	1.000
384.0	3.02e-20	1.000	384.5	3.10e-20	1.000	385.0	3.20e-20	1.000	385.5	3.29e-20	1.000	386.0	3.39e-20	1.000
386.5	3.51e-20	1.000	387.0	3.62e-20	1.000	387.5	3.69e-20	1.000	388.0	3.70e-20	1.000	388.5	3.77e-20	1.000
389.0	3.88e-20	1.000	389.5	3.97e-20	1.000	390.0	4.03e-20	1.000	390.5	4.12e-20	1.000	391.0	4.22e-20	1.000
391.5	4.29e-20	1.000	392.0	4.30e-20	1.000	392.5	4.38e-20	1.000	393.0	4.47e-20	1.000	393.5	4.55e-20	1.000
394.0	4.56e-20	1.000	394.5	4.59e-20	1.000	395.0	4.67e-20	1.000	395.5	4.80e-20	1.000	396.0	4.87e-20	1.000
396.5	4.96e-20	1.000	397.0	5.08e-20	1.000	397.5	5.19e-20	1.000	398.0	5.23e-20	1.000	398.5	5.39e-20	1.000
399.0	5.46e-20	1.000	399.5	5.54e-20	1.000	400.0	5.59e-20	1.000	400.5	5.77e-20	1.000	401.0	5.91e-20	1.000
401.5	5.99e-20	1.000	402.0	6.06e-20	1.000	402.5	6.20e-20	1.000	403.0	6.35e-20	1.000	403.5	6.52e-20	1.000
404.0	6.54e-20	1.000	404.5	6.64e-20	1.000	405.0	6.93e-20	1.000	405.5	7.15e-20	1.000	406.0	7.19e-20	1.000
406.5	7.32e-20	1.000	407.0	7.58e-20	1.000	407.5	7.88e-20	1.000	408.0	7.97e-20	1.000	408.5	7.91e-20	1.000
409.0	8.11e-20	1.000	409.5	8.41e-20	1.000	410.0	8.53e-20	1.000	410.5	8.59e-20	1.000	411.0	8.60e-20	1.000
411.5	8.80e-20	1.000	412.0	9.04e-20	1.000	412.5	9.45e-20	1.000	413.0	9.34e-20	1.000	413.5	9.37e-20	1.000
414.0	9.63e-20	1.000	414.5	9.71e-20	1.000	415.0	9.70e-20	1.000	415.5	9.65e-20	1.000	416.0	9.69e-20	1.000
416.5	9.89e-20	1.000	417.0	1.00e-19	1.000	417.5	1.02e-19	1.000	418.0	1.00e-19	1.000	418.5	1.02e-19	1.000
419.0	1.01e-19	1.000	419.5	1.01e-19	1.000	420.0	1.03e-19	1.000	420.5	1.01e-19	1.000	421.0	1.04e-19	1.000
421.5	1.05e-19	1.000	422.0	1.06e-19	1.000	422.5	1.04e-19	1.000	423.0	1.05e-19	1.000	423.5	1.05e-19	1.000
424.0	1.01e-19	1.000	424.5	1.01e-19	1.000	425.0	1.05e-19	1.000	425.5	1.03e-19	1.000	426.0	1.02e-19	1.000
426.5	1.01e-19	1.000	427.0	9.77e-20	1.000	427.5	9.81e-20	1.000	428.0	1.00e-19	1.000	428.5	1.02e-19	1.000
429.0	9.89e-20	1.000	429.5	9.85e-20	1.000	430.0	1.04e-19	1.000	430.5	1.08e-19	1.000	431.0	1.05e-19	1.000
431.5	1.02e-19	1.000	432.0	9.64e-20	1.000	432.5	1.01e-19	1.000	433.0	1.06e-19	1.000	433.5	1.09e-19	1.000
434.0	1.04e-19	1.000	434.5	1.03e-19	1.000	435.0	1.07e-19	1.000	435.5	1.16e-19	1.000	436.0	1.09e-19	1.000
436.5	1.11e-19	1.000	437.0	9.81e-20	1.000	437.5	9.71e-20	1.000	438.0	1.06e-19	1.000	438.5	1.16e-19	1.000
439.0	1.08e-19	1.000	439.5	1.05e-19	1.000	440.0	9.70e-20	1.000	440.5	1.01e-19	1.000	441.0	1.04e-19	1.000
441.5	1.07e-19	1.000	442.0	1.02e-19	1.000	442.5	9.68e-20	1.000	443.0	1.00e-19	1.000	443.5	1.14e-19	1.000
444.0	1.13e-19	1.000	444.5	1.03e-19	1.000	445.0	9.74e-20	1.000	445.5	8.46e-20	1.000	446.0	8.70e-20	1.000
446.5	9.97e-20	1.000	447.0	1.01e-19	1.000	447.5	9.15e-20	1.000	448.0	9.41e-20	1.000	448.5	8.99e-20	1.000
449.0	1.10e-19	1.000	449.5	9.12e-20	1.000	450.0	8.56e-20	1.000	450.5	8.28e-20	1.000	451.0	6.15e-20	1.000
451.5	5.56e-20	1.000	452.0	6.47e-20	1.000	452.5	7.27e-20	1.000	453.0	5.75e-20	1.000	453.5	5.08e-20	1.000
454.0	4.38e-20	1.000	454.5	3.81e-20	1.000	455.0	3.61e-20	1.000	455.5	3.61e-20	1.000	456.0	3.13e-20	1.000
456.5	2.72e-20	1.000	457.0	2.44e-20	1.000	457.5	2.22e-20	1.000	458.0	1.82e-20	1.000	458.5	1.43e-20	1.000
459.0	1.32e-20	1.000	459.5	1.05e-20	1.000	460.0	8.95e-21	1.000	460.5	8.90e-21	1.000	461.0	7.94e-21	1.000
461.5	7.04e-21	1.000	462.0	6.46e-21	1.000	462.5	5.63e-21	1.000	463.0	4.78e-21	1.000	463.5	3.94e-21	1.000
464.0	3.26e-21	1.000	464.5	2.97e-21	1.000	465.0	2.65e-21	1.000	465.5	2.46e-21	1.000	466.0	2.27e-21	1.000
466.5	2.08e-21	1.000	467.0	1.86e-21	1.000	467.5	1.76e-21	1.000	468.0	1.60e-21	1.000	468.5	1.44e-21	1.000
469.0	1.34e-21	1.000	469.5	1.20e-21	1.000	470.0	1.07e-21	1.000	470.5	1.02e-21	1.000	471.0	9.92e-22	1.000
471.5	9.97e-22	1.000	472.0	8.87e-22	1.000	472.5	8.27e-22	1.000	473.0	7.76e-22	1.000	473.5	7.15e-22	1.000
474.0	6.71e-22	1.000	474.5	6.67e-22	1.000	475.0	6.10e-22	1.000	475.5	6.17e-22	1.000	476.0	5.54e-22	1.000
476.5	5.22e-22	1.000	477.0	5.10e-22	1.000	477.5	5.17e-22	1.000	478.0	4.80e-22	1.000	478.5	4.71e-22	1.000
479.0	4.60e-22	1.000	479.5	4.35e-22	1.000	480.0	3.90e-22	1.000	480.5	3.71e-22	1.000	481.0	3.62e-22	1.000
481.5	3.52e-22	1.000	482.0	3.05e-22	1.000	482.5	3.05e-22	1.000	483.0	2.86e-22	1.000	483.5	2.53e-22	1.000
484.0	2.75e-22	1.000	484.5	2.59e-22	1.000	485.0	2.47e-22	1.000	485.5	2.36e-22	1.000	486.0	2.12e-22	1.000
486.5	1.89e-22	1.000	487.0	1.93e-22	1.000	487.5	1.86e-22	1.000	488.0	1.82e-22	1.000	488.5	1.75e-22	1.000
489.0	1.74e-22	1.000	489.5	1.72e-22	1.000	490.0	1.66e-22	1.000	490.5	1.75e-22	1.000	491.0	1.54e-22	1.000
491.5	1.74e-22	1.000	492.0	1.63e-22	1.000	492.5	1.53e-22	1.000	493.0	1.52e-22	1.000	493.5	5.85e-23	1.000
494.0	0.00e+00	1.000												

Table A-4. Chamber wall effect and background characterization parameters used in the environmental chamber model simulations for mechanism evaluation.

Cham.	Set [a]	Value	Discussion
<u>RN-I (ppb)</u>			
DTC	18	0.066	Ratio of the rate of wall + hv -> HONO to the NO ₂ photolysis rate. Average of value of RS-I which gave best fits to n-butane - NO _x chamber experiments carried out in this chamber. The initial HONO was optimized at the same time. If a temperature dependence is shown, it was derived from the temperature dependence of the RN-I values that best fit characterization data in outdoor chamber experiments, with the same activation energy used in all cases. If a temperature dependence is not shown, then the temperature variation for experiments in this set is small compared to the run-to-run variability in the best fit RN-I values. Note that the radical source in Sets 3, 12, 13, and 16 runs was anomalously high. Any dependence of apparent radical source on initial NO _x levels in Teflon bag chambers was found to be much less than the run-to-run variability.
CTC	9	0.097	Same procedure as for the DTC. The runs in Set 9 had slightly higher radical source than most other CTC experiments, so a slightly higher radical source parameter is used for those runs.
	≤8,10	0.064	
<u>HONO-F (unitless)</u>			
DTC	18	0.8%	Ratio of the initial HONO concentration to the measured initial NO ₂ . [The initial NO ₂ in the experiment is reduced by a factor of 1 - (HONO-F)]. Unless the characterization data indicate otherwise, it is assumed that the initial HONO is introduced with the NO ₂ injection, so it is assumed to be proportional to the initial NO ₂ concentration. Average of value of initial HONO to initial NO ₂ which gave best fits to n-butane - NO _x chamber experiments carried out in this chamber. The RN-I parameter was optimized at the same time.
CTC	All	0.08	Same procedure as for CTC
<u>E-NO₂/K₁ (ppb)</u>			
All Teflon Bag Chambers		0	Ratio of rate of NO ₂ offgasing from the walls to the NO ₂ photolysis rate. The NO _x offgasing caused by representing the radical source by HONO offgasing appears to be sufficient for accounting for NO _x offgasing effects in most cases. RN-I parameters adjusted to fit experiments sensitive to the radical source are consistent with NO _x offgasing rates adjusted to fit pure air or aldehyde - air runs, to within the uncertainty and variability.
<u>K(NO₂W) (min⁻¹)</u>			
All Teflon Bag Chambers		1.6e-4	Rate of unimolecular loss (or hydrolysis) of NO ₂ to the walls. Based on dark NO ₂ decay and HONO formation measured in the ETC by Pitts et al. (1984). Assumed to be the same in all Teflon bag chambers, regardless of volume.
<u>YHONO</u>			
All Teflon Bag Chambers		0.2	Yield of HONO in the unimolecular reaction (hydrolysis) of NO ₂ on the walls. Based on dark NO ₂ decay and HONO formation measured in the ETC by Pitts et al. (1984). Assumed to be the same in all Teflon bag chambers, regardless of volume.
<u>K(O₃W) (min⁻¹)</u>			
DTC	All	1.5e-4	Unimolecular loss rate of O ₃ to the walls. Based on results of O ₃ decay in Teflon bag chambers experiments as discussed by Carter et al (1995c).
CTC	All	8.5e-5	Based on results of O ₃ decay experiments in this chamber

Table A-4 (continued)

Cham.	Set [a]	Value	Discussion
<u>k(N26I) (min⁻¹)</u>			Rate constant for N2O5 -> 2 Wall-NOx . This represents the humidity-independent portion of the wall loss of N ₂ O ₅ , or the intercept of plots of rates of N ₂ O ₅ loss against humidity.
All Teflon Bag Chambers		2.8e-3	Based on N ₂ O ₅ decay rate measurements made by Tuazon et al (1983) for the ETC. Assumed to be independent of chamber size (Carter et al, 1995c).
<u>k(N26S) (ppm⁻¹ min⁻¹)</u>			Rate constant for N2O5 + H2O -> 2 Wall-NOx . This represents the humidity dependent portion of the wall loss of N ₂ O ₅ , or the slope of plots of rates of N ₂ O ₅ loss against humidity.
All Teflon Bag Chambers		1.1e-6	Based on N ₂ O ₅ decay rate measurements made by Tuazon et al (1983) for the ETC. Assumed to be independent of chamber size (Carter et al, 1995c).
<u>k(XSHC) (min⁻¹)</u>			Rate constant for OH -> HO2 . This represents the effects of reaction of OH with reactive VOCs in the background air or offgased from the chamber walls. This parameter does not significantly affect model simulations of experiments other than pure air runs.
All Teflon Bag Chambers		250	Estimated from modeling several pure air in the ITC (Carter et al, 1996d), and also consistent with simulations of pure air runs in the ETC (Carter et al, 1997a).
<u>H2O (ppm)</u>			Default water vapor concentration for runs where no humidity data are available.
DTC CTC	all	1.0e+3	Experiments in this chamber were carried out using dried purified air. The limited humidity data for such runs indicate that the humidity was less than 5%, probably no more than ~2.5%, and possibly much less than that. The default value corresponds to ~2.5 - 3% RH for the conditions of most experiments.

[a] Set refers to the characterization set, which refers to the group of experiments assumed to have the same run conditions and represented using the same chamber-dependent parameters. See Carter et al (1995) for more discussion. All DTC experiments in this program were in DTC characterization set 18. Run CTC255 and the earlier characterization runs for this program are in set 9, and all the other CTC runs for this program are in set 10.